Dynamic regulation of Rho GTPase networks and correlation with effector pathways

Inaugural-Dissertation

zur

Erlangung des Doktorgrades

Dr. rer. nat.

der Fakultät für Biologie

an der

Universität Duisburg-Essen

vorgelegt von

Melanie Gräßl

aus Essen

November 2015

Die der vorliegenden Arbeit zugrunde liegenden Experimente wurden in der Abteilung für Molekulare Zellbiologie der Universität Duisburg-Essen und in der Abteilung für Chemische Biologie der TU Dortmund durchgeführt.

1. Gutachter: Prof. Dr. Perihan Nalbant

2. Gutachter: Prof. Dr. Michael Ehrmann

Vorsitzender des Prüfungsausschusses: Prof. Dr. Dominik Boos

Tag der mündlichen Prüfung: 04.03.2016

DOI: 10.17185/duepublico/41005
URN: urn:nbn:de:hbz:464-20200527-085617-9

TABLE OF CONTENTS

List of Figures

List of Tables

Abbreviation Index

A	ampere
approx	approximately
Arp2/3	actin-related-protein 2/3
ADP	adenosine diphosphate
AOTF	acousto optic tunable filter
ATP	adenosine triphosphate
AU	arbitrary unit
bp	base pairs
BSA	*Bovine* serum albumin
°C	degrees Celsius
c	centi
Cas9	Caspase 9
CCD	charge-coupled device
CMV	*cytomegalovirus*
CRISPR	clustered (regularly interspaced) short palindromic repeats
CytoD	Cytochalasin D
Da	Dalton
DAAM	dishevelled-associated activators of morphogenesis
DAD	diaphanous autoregulation domain
DAPI	4',6-diamidino-2-phenylindole
Dia	diaphanous
DIC	differential interference contrast
DMEM	Dulbecco's modified eagle's medium
DMSO	dimethyl sulfoxide
DPBS	Dulbecco's phosphate-buffered saline
DRF	diaphanous-related formins
DTE	dithioerythritol
E.	*Escherichia*
e.g.	exempli gratia
EB	elution buffer
ECL	entry-level peroxidase substrate for enhanced chemiluminescence
EDTA	ethylene diamine tetraacetic acid
EGFP	enhanced green fluorescent protein
EMCCD	electron multiplying charge-coupled device
FAK	focal adhesion kinase
FBP	formin-binding protein
FCS	fetal calf serum
FH	formin homology
FHOD	formin-homology domain
FML	formin-like proteins
GAP	GTPase-activating protein
GBD	GTPase-binding domain
GDI	GTP-dissociation inhibitor
GDP	guanosine diphosphate
GEF	GTP-exchange factor
GTP	guanosine triphosphate
HRP	horseradish peroxidase
LatA	Latrunculin A
LUT	look up table
h	hour(s)
HBSS	Hank's Balanced Salt Solution

HDR	homology-directed repair
HEPES	4-(2-hydroxyethyl)-1-piperazineethanesulfonic acid
k	kilo
KO	knockout
l	liter
LB	Luria-Bertani
m	meter
m	milli
M	molar
µ	micro
MAPK	Mitogen-activated protein kinase
min	minute(s)
Myo9b	Myosin9b
N	number of cells
n	nano
NA	numerical aperture
NMHC	non-muscle myosin heavy chain
NTP	nucleoside 5-triphosphates
OD	optical density
osc	oscillation(s)
Pa	pascal
PAGE	polyacrylamide gel electrophoresis
PBS	phosphate-buffered saline
Pi	inorganic phosphate
PIP2	phosphatidylinositol (4,5)-bisphosphate
PIP3	phosphatidylinositol 1,4,5-triphosphate
PMT	photo multiplier
PVDF	polyvinylidene difluoride
r	mean crosscorrelation coefficient
rpm	revolutions per minute
RBD	Rho-binding-domain
RFP	red fluorescent protein
RIPA	radioimmunoprecipitation assay buffer
ROCK	Rho-associated protein kinase
RT	room temperature
s	second(s)
SDS	sodium dodecyl sulfate
s.e.	standard error
s.e.m.	standard error of the mean
ss	steady state
TAE	Tris, acetic acid, EDTA
TBS	Tris-buffered saline
TEMED	tetramethylethylenediamine
TIRF	total internal reflection fluorescence
Tris	Tris(hydroxymethyl) aminomethane
TSS	transformation & storage solution
U	enzyme unit
V	volt
VASP	Vasodilator-stimulated phosphoprotein
v/v	volume solution per volume solution
wt	wild-type
w/v	mass solute per volume solution

Zusammenfassung

Zellen erkunden ihre Umgebung und sind in der Lage auf extrazelluläre Signale mit der Aktivierung spezifischer Signalwege zu reagieren. In eukaryotischen Zellen bildet das Aktin Zytoskelett die Grundlage für dynamische Zellprozesse, da es durch aktive Umstrukturierungen rasche Veränderungen der Zellmorphologie ermöglicht. Insbesondere das Zusammenspiel zwischen Aktin-basierten Ausstülpungen der Plasmamembran und Myosin-assoziierten, kontraktilen Stressfasern steht in direktem Zusammenhang mit der zellulären Mechanotransduktion in Prozessen wie der Zelladhäsion, Proliferation oder Differenzierung. Die präzise räumliche und zeitliche Koordination dieser Signalwege ist jedoch nicht vollständig erforscht. In den letzten Jahren wurden Studien zu Aktivator-Inhibitor Signalnetzwerken, bestehend aus einer signalverstärkenden und einer verzögerten, inhibierenden Rückkopplung, in verschiedenen Zellentypen veröffentlicht, die auf ihre Relevanz für dynamische Zellprozesse hindeuten. In dieser Arbeit wurde erstmalig ein anregbares Signalnetzwerk identifiziert, das Oszillationen lokaler Rho Aktivität in U2OS Zellen hervorruft. Diese wurden mittels TIRF Mikroskopie und Kreuzkorrelationsanalysen eines gering-exprimierten Rho Aktivitätssensor und fluoreszenzmarkierter Regulator- und Effektor-Proteinen charakterisiert. Zusätzlich wurden RNAi und pharmakologische Wirkstoffe eingesetzt, um die Rolle der einzelnen Netzwerkkomponenten zu entschlüsseln. Rho Aktivitätsoszillationen korrelierten stark mit intrazellulären Oszillationen von Aktin, Myosin-IIa und dem Stressfaser-assoziiertem Formin FHOD1. Dabei traten Myosin-IIa Oszillationen deutlich verzögert zu Rho Oszillationen auf, die zudem durch die Inhibition von ROCK oder Myosin-IIa stark verringert wurden. Die Depletion von FHOD1 hingegen, hatte keinen Einfluss auf Oszillationen von Rho oder Myosin-IIa, aber auf Aktin Oszillationen. FHOD1 hat demzufolge keine regulatorische Funktion in dem beschriebenen Netzwerk, während Myosin-IIa Rho Oszillationen über eine zeitverzögerte Rückkopplung inhibiert. Kreuzkorrelations-, Expressions- und Depletionsstudien deuten darauf hin, dass diese Rückkopplung durch zwei RhoGAPs, ARHGAP18 und Myosin9b, vermittelt wird. Insgesamt wurde ein Aktivator-Inhibitor Netzwerk identifiziert, das Rho Aktivitätsoszillationen generiert und sich selbst verstärkt, indem es Aktivatoren (GEFs) rekrutiert, und inhibiert, indem es Myosin-IIa und verschiedenen GAPs aktiviert. Experimente mit elastischen Oberflächen verschiedener Härtegrade lieferten zudem Hinweise, dass die von Rho und Actomyosin vermittelten Signaloszillationen zur Mechanotransduktion beitragen und somit an zellulären Prozessen wie der Migration oder Zell-Ausbreitung beteiligt sind.

Summary

Cells can explore their environment and respond to different extracellular signals by activating distinct intracellular pathways. In eukaryotic cells, the actin cytoskeleton builds the foundation for dynamic cell behavior as it is able to reorganize rapidly to drive cell shape changes. As a counterbalance to actin based protrusions, myosin-decorated actin stress fibers that are able to generate cellular contractility have been linked to cellular mechanosensing in multiple processes such as cell adhesion, proliferation and differentiation. However, how these signaling pathways are coordinated precisely in space and time is not fully understood. During the last years, excitable activator-inhibitor signal networks that comprise signal self-amplification and delayed inhibitory feedback loops have been reported in different types of eukaryotic cells, implicating their relevance in dynamic cell behavior. In this work, a novel excitable signal network generating Rho activity oscillations was identified and characterized in detail. TIRF microscopy and low-expression constructs such as a domain based Rho activity sensor, fluorescently tagged regulatory proteins and well established effectors were used to characterize signal oscillations and to perform crosscorrelation analyses. In addition, RNAi based depletion and pharmacological manipulations were applied to further characterize the role of potential network components. Rho activity oscillations strongly correlated with subcellular oscillations of actin, myosin-IIa and the stress fiber associated formin FHOD1. Interestingly, myosin-IIa oscillations were significantly time-delayed as compared to Rho activation and inhibition of ROCK and myosin-II, respectively, lead to substantially perturbed Rho activity dynamics. In contrast, FHOD1 depletion did not affect Rho and myosin-IIa, but only actin oscillations. Thus, while FHOD1 seems not to play a regulatory role in the Rho based excitable network, myosin-IIa activity might facilitate a negative feedback to control time-delayed Rho inhibition. Based on crosscorrelation analysis, overexpression and siRNA-depletion, two RhoGAPs, ARHGAP18 and Myosin9b, are proposed to mediate this time delayed inhibition of Rho by myosin-II. Overall, we have identified an excitable activator-inhibitor network generating Rho activity oscillations and propose that the GTPase self-amplifies its activity by recruiting GEF activators and controls its own inhibition by myosin-II dependent time-delayed activation of multiple RhoGAPs. Using elastomeric surfaces with different rigidities we further provide evidence that Rho and acto-myosin based signal oscillations play a critical role in mechanosensing and thus contribute to exploratory processes such as cell spreading and durotaxis.

1. Introduction

1.1 Excitable behavior in cells

1.1.1 Oscillatory signal dynamics and wave propagation regulate numerous cellular processes

Oscillatory behavior is a widespread dynamic phenomena in cell biology, resulting from the interplay of multiple cellular components. It arises from the collective dynamic behavior that is known as self-organization, causing the emergence of spatio-temporal patterns (reviewed by Kruse and Jülicher, 2005). Cellular oscillations can be mediated by chemical, mechanical or genetic networks. For instance, hair cells in the hearing organs of vertebrates can amplify mechanical stimuli (Hudspeth, 1997), while genetic oscillators include circadian clocks and cell cycle oscillators (Dunlap, 1999; Tyson et al, 2001). The oscillatory behavior of biochemical networks often relies on oscillations of second messenger molecules such as cyclic ATP, calcium or phosphatidylinositol 1,4,5-triphosphate (PIP3). In particular, calcium oscillations or waves are known for almost 30 years (Woods et al, 1986) and have been reported in a vast array of cell types and organisms (Jaffe, 1991). They are thought to control various cellular processes such as neuronal differentiation, exocytosis, embryonic development, cell proliferation, apoptosis and motility (reviewed by Clapham, 2007; Gu and Spitzer, 1995; Orrenius et al, 2003; Malmersjö et al, 2013). On the molecular level, oscillations of second messengers have been shown to regulate these processes via multiple signaling pathways. For example, downstream of calcium waves the mitogen-activated protein (MAP) kinase pathway, controls egg fertilization (see Figure 1.1a; Miyazaki et al, 1993; Stricker, 1999; Kumano et al, 2001). The activation of MAP kinase and other calcium effectors, like NFAT (nuclear factor of activated T-cells), NF-κB (nuclear factor 'kappa-light-chain-enhancer' of activated B-cells), CaMKII (Calcium/calmodulin-dependent protein kinase II), and calpain was recently shown to depend on the frequency and duration of calcium oscillation (Smedler and Uhlén, 2014). Upstream, calcium oscillations can be regulated by PIP3, a second messenger that is activated by phospholipase C (PLC) and stimulates the release of calcium upon binding to the PIP3 receptor (reviewed by Berridge, 2009). In cardiac myocytes taken from rats, propagating IP_3-dependent calcium waves can be observed (see Figure 1.1b) that originate from transient calcium sparks and are related to heart failure and ventricular arrhythmias (Chen et al, 2011; reviewed by Hohendanner et al, 2014). In migratory fibroblasts, IP3 oscillations were found to mediate self-amplification of calcium signals via a positive feedback loop leading to robust calcium oscillations (Harootunian et al, 1991).

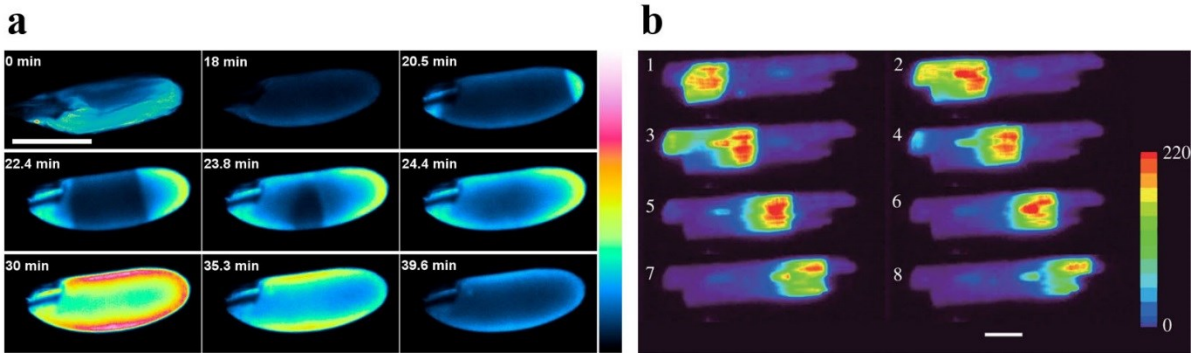

Figure 1.1: Calcium waves in a fertilized *Drosophila* oocyte and in a rat cardiac myocyte.

(a) Fluorescence images of Ca^{2+} flux in *Drosophila* oocytes. After *in vitro* fertilization at t = 0 min, the oocyte swells gradually before a rise of calcium signal at both poles emerges (20.5 min) that extends towards the cell center, until reaching a maximal signal intensity throughout the whole cell periphery (30 min). Afterwards, the calcium signal gradually decreases, before returning to basal level (39.6 min). Scale bar: 200 µm; calcium intensity is depicted in false-colors, calibration bar is shown on the right. (This Figure was modified after Kaneuchi et al, 2015). **(b)** Confocal images of a calcium wave propagating from the boundary of a cardiac myocyte throughout the cell (Sprague Dawley® rat). Time interval between images: 0.1 s; scale bar: 20 µm. Calibration bar depicts fluorescence intensity in AU. (This Figure was taken from Chen et al 2011.)

However, PIP3 oscillations can emerge independently of calcium oscillations. For instance, in insulin-secreting β-cells PIP3 oscillations were triggered by pulsatile release of insulin after stimulation with glucose (Hagren and Tengholm, 2006).

In the slime mold *Dictyostelium discoideum*, the PIP3 oscillations induced by extracellular oscillations of ATP are known for a long time as regulatory mechanism during chemotaxis and aggregation (Tyson and Murray, 1989; Europe-Finner et al, 1989), a phase of their life cycle in which the amoebae communicate with each other. Later studies revealed an additional function of PIP3 oscillations in phagocytosis (Gerisch et al, 2009). This search for food is also mediated by propagating actin waves, which are further discussed in section 1.2.2, see Figure 1.6.

1.1.2 Excitable dynamics of cellular wave-generating systems

Excitability describes the phenomenon where a system (here the activity state of a protein) has two modes of returning to its equilibrium state or steady state (ss) after stimulation. For subthreshold perturbations the return is monotonic, while perturbations beyond a certain threshold elicit a response in that state variable (intensity peak) much larger than the perturbation, before returning to the steady state (Murray, 2011). The most common way of obtaining excitability in biological systems is the combination of a fast positive feedback, coupled to a slow negative feedback loop (see Figure 1.1.2a). Feedback occurs if, based on a signal cascade forming a circuit, the output of a system is routed back as input (reviewed by Allard and Mogilner, 2013). Some of the parameters of an excitable system display a stable steady state in which the stimulation of the first component A, does not affect the activity of a

second component B. If this steady state is disturbed by external factors, different types of dynamic behavior can occur (see Figure 1.2b). First, excitable behavior, which is triggered by a stimulation that is large enough to move the state of A across a threshold, resulting in a transient excitation of B. Second, oscillations of B emerge if the steady state of component A is entirely increased above threshold. Lastly, bistable behavior can be observed, if the component A can switch to a second stable steady state (reviewed by Allard and Mogilner, 2013). The occurrence of travelling waves depends additionally on the spatial coupling between the local dynamics of neighboring areas. Whereas traveling wave pulses are found in excitable systems, travelling wave fronts require bistability (Rinzel and Terman, 1982; Elphick et al, 1997).

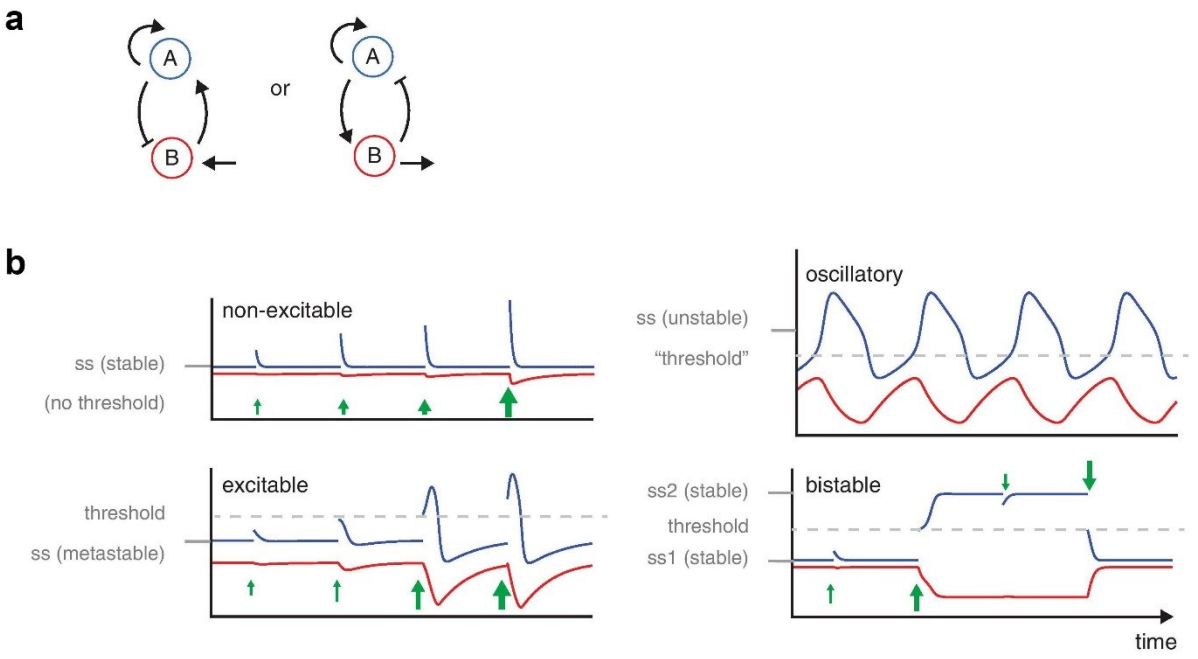

Figure 1.2: Different dynamic behavior of biochemical networks consisting of a positive and a temporal delayed, negative feedback loops.

(a) In a biochemical networks consisting of a fast positive and a slow negative feedback loop, component A can either activate or inhibit component B. **(b)** The behavior of A and B is indicated by blue and red curves; ss: steady state values of component A. External stimulations are depicted as green arrows. An increase of A above a critical threshold (dashed lines) in a non-excitable system will relax by returning to the steady state without affecting component B. As opposed to an excitable system, in which an excitation of A is coupled to a transient excitation of B. If the stimulation of A increases its steady state above threshold, the system becomes intrinsically oscillatory. In case of a second steady state for component A, the stimulation can cause the switch to this alternative steady state, a behavior designated as bistable behavior (this Figure was modified from Allard and Mogilner, 2013).

In systems with spatial coupling of intrinsic oscillatory behavior, under certain conditions, sequences of wave pulses (also called wave trains) can occur that can transition to synchronized oscillations (Murray, 2007; Fall et al, 2010).

This simplified description for excitability provides a framework that needs to be extended, as real biological signal networks are much more complex and wave propagation is thought to

require additional network components that are spatially coupled (for recent mathematical models of excitable networks see reviews from Iglesias and Devreotes, 2012; Gelens et al, 2014).

1.2 Dynamic reorganization of the actin cytoskeleton underlies oscillatory cell behavior

Since the first live-cell studies of migrating fibroblast, oscillatory cycles of membrane protrusion and retraction at the leading edge (lamellipodium) have been observed as a common feature of migrating and spreading eukaryotic cells (see Figure 1.3) (Abercrombie et al, 1970; Giannone et al, 2003; Burnette et al, 2011; Ryan et al, 2012).

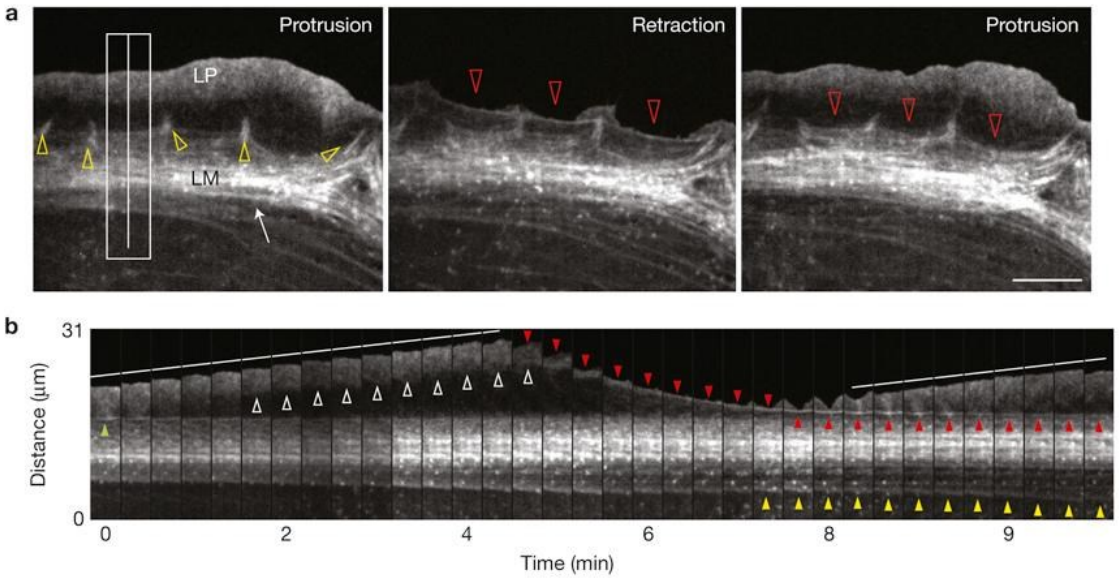

Figure 1.3: Cycles of membrane protrusion and retraction at the leading edge in PtK1 cells.

(a) Individual frames of a time-lapse measurement with actin–mRFP, during the transition from membrane protrusion (left panel) to retraction (mid panel) and back to protrusion (right panel). LP denotes the lamellipodium; white arrow highlights actin arcs in the lamella (LM). Yellow arrowheads indicate actin filaments anchored by focal adhesions. Red arrowheads illustrate a newly formed actin arc. Scale bar: 10 µm. **(b)** Montage of the area indicated by white box in **a**. Depicted is the formation of an actin arc (red arrowheads) between two protrusion cycles (white lines); the zone of actin polymerization is highlighted by white arrowheads. The actin arc formed during the previous retraction cycle is indicated in the first frame by a green arrowhead; yellow arrowheads mark the loss of actin arcs (this Figure was taken from Burnette et al, 2011).

The actin meshwork underlying those protrusion and retraction cycles is in itself highly dynamic and provides a structural framework during cell shape changes, driving cell behavior such as migration and division (Hall, 1998). The dynamic properties of cellular actin structures are based on the ability of actin subunits to convert rapidly between a monomeric, unbound state and their filamentous form, in which the individual subunits are held together by reversible, non-covalent bonds (Wegner, 1976) (see Figure 1.4).

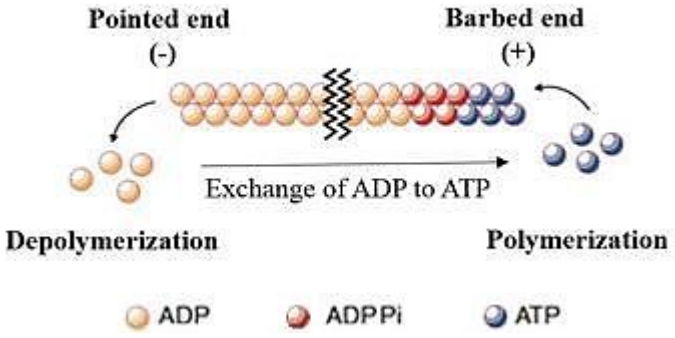

Figure 1.4: Schematic model of actin filament assembly.

ATP-bound actin monomers associate to the barbed (plus) end of actin filaments. Hydrolysis of ATP facilitates actin depolymerization by removing ADP-bound G-actin molecules from the pointed (minus) end of actin filaments. If ADP, bound to the dissociated actin subunits, is replaced by ATP, the actin monomers are able to associate at the barbed end again (this Figure was modified from Littlefield and Fowler 2002).

During F-actin assembly, ATP-actin is added at the barbed end of the growing filament, leading to its elongation, if the polymerization rate is higher than the dissociation rate of ADP-actin at the pointed end. Filament elongation is facilitated by profilin that binds to monomeric actin and catalyzes the exchange of ADP to ATP (Carlsson et al, 1977). Furthermore profilin guides ATP-bound actin monomers towards the barbed end of the filament, where it quickly dissociates and is able to bind and recruit new actin subunits (Goldschmidt-Clermont et al, 1991; Pantaloni und Carlier, 1993). The shrinkage of actin filaments, on the other hand, happens if the dissociation rate of ADP-actin exceeds the association rate of ATP-actin at the barbed end. This is aided by F-actin severing proteins, such as cofilin, promoting the loss of actin monomers from the pointed end (McGough et al, 1997; Le und Carlier, 2008). The process of "actin treadmilling" occurs when the polymerization and depolymerization rates are balanced (Wegner, 1976). The transition between actin monomers and filamentous actin, as well as their organization in three-dimensional arrays, is precisely regulated by a large number of actin regulators and signaling molecules (reviewed by Campellone and Welch, 2010), enabling the formation of various different actin-based structures in eukaryotic cells (reviewed by Ridley, 2011).

1.2.1 Actin based protrusions

At the leading edge of a migrating cell, the formation of a thin protrusive structure, the lamellipodium, can be observed, which is driven by coordinated actin-polymerization (Pollard and Borisy, 2003). Within those structures, two types of actin networks are found, due to two different modes of filament nucleation. The nucleation and elongation of the barbed end by formins (such as mDia1, see section 1.3.2.2) promotes the formation of straight filaments (Li and Higgs, 2003; Moseley et al, 2004), while the actin-related-protein 2/3 (Arp2/3) nucleates new filaments at the sides of preexisting filaments, producing a branched network, see Figure 1.5 (Sagot et al, 2002; Ponti et al, 2004).

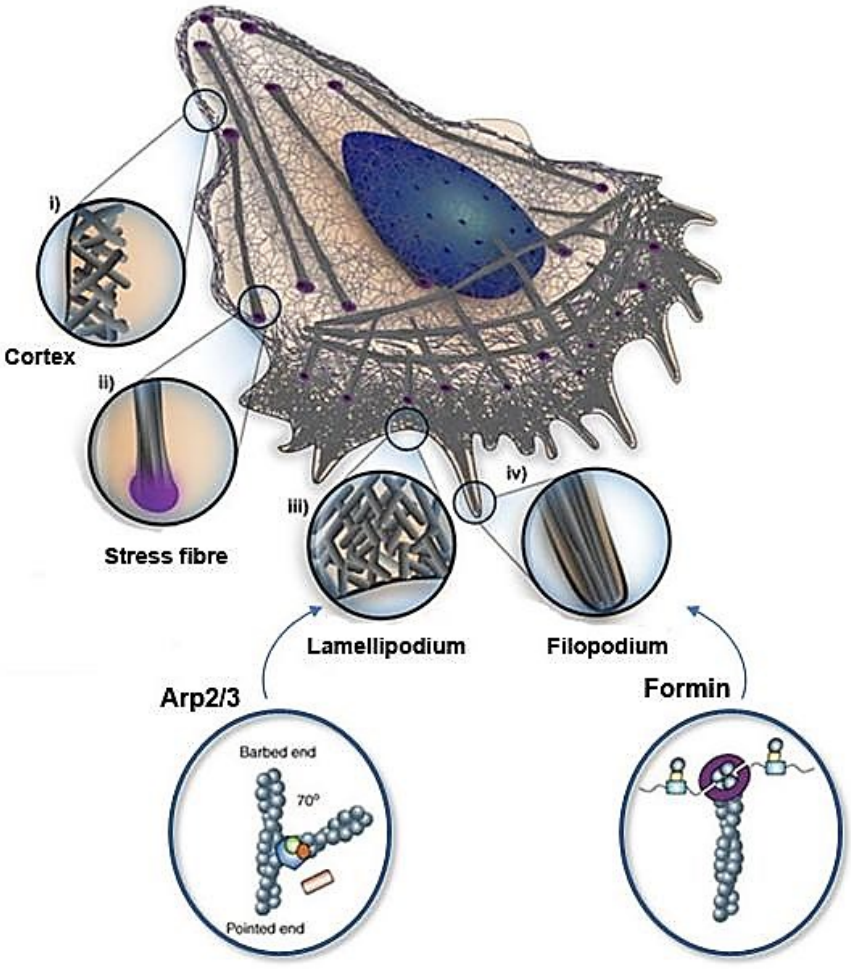

Figure 1.5: The variety of cytoskeletal actin structures is based on different modes of actin nucleation

Schematic model of a cell with different actin-based structures: *i)* the cell cortex; *ii)* a contractile stress fiber; *iii)* the lamellipodium; and *iv)* a filopodia. The Arp2/3 complex nucleates actin filaments at sides of existing filaments generating branched network and increasing the number of free barbed end. Formins create long, unbranched filaments that can be crosslinked into bundles. (These Figures were modified from Blanchoin et al, 2014 and Kerkhoff, 2006.)

1.2.2 Propagating waves of actin polymerization

Dense assemblies of Arp2/3 dependent actin filaments are not limited to the leading edge of migrating cells. In *Dictyostelium* for instance, they can also be found at the substrate-attached surface, in the form of traveling waves and transient foci (Bretschneider et al, 2004). Studies revealed that those propagating actin waves form distinct intracellular areas. These areas differ in actin organization and correlate not only with Arp2/3, but also with the contractility generating motor protein, myosin, as well as PIP3 signaling, see Figure 1.6 (Schroth-Diez et al, 2009; Gerisch et al, 2010).

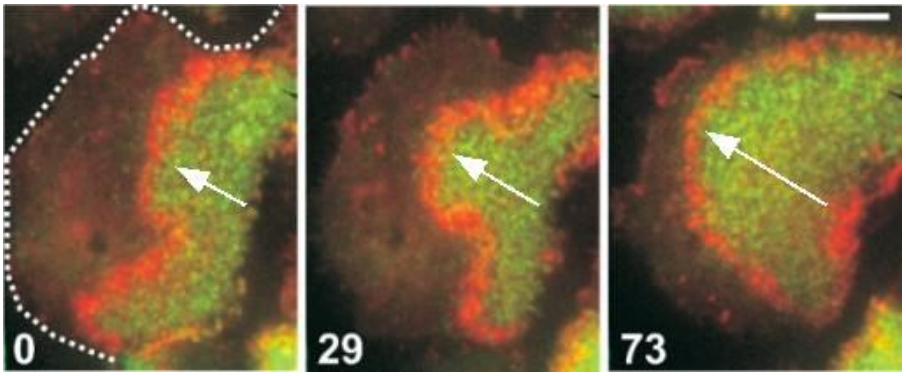

Figure 1.6: Actin waves at the border of PIP3-rich areas in a *Dictyostelium discoideum* cell.

Individual frames of TIRF time-lapse measurement of a propagating F-actin wave (marked by mRFP-LimEΔ, illustrated in red) at the border of a PIP3-rich area (visualized by PHcrac-GFP, depicted in green) of the plasma membrane. During wave propagation, the cell shape remains almost constant; indicated by a dotted line in the first frame. White arrows illustrate wave propagation. Time after first frame is displayed in seconds. Scale bar: 5 µm. (This Figure was modified from Gerisch, 2010).

Actin waves have been described for migrating, spreading as well as for stationary cell types (Weiner et al, 2007; Dubin-Thaler et al, 2012; Ryan et al, 2012). The physiological relevance of actin waves was found to comprise cell polarity and motility, but also vesicle secretion and cell division (Ozbudak et al, 2005; Weiner et al, 2007; Wollman and Meyer, 2012; Mitsushima et al, 2010). Additionally, traveling actin waves have been shown to generate force that is thought to propel the plasma membrane forward (Bretschneider et al, 2009). In the fruit fly *Drosophila*, actin oscillations correlate with oscillations of PIP3, and so do calcium and PIP3 oscillations in mast cells that drive vesicle secretion and endocytosis (Gerisch, 2010; Wollman and Meyer, 2012). Robust travelling waves of filamentous actin were also observed in fish epithelial keratocytes (Barnhart et al, 2011). Those were reported to travel along the leading edge of migrating cells and are thought to self-organize via actin, myosin and focal adhesions (Barnhart et al, 2011). In mouse fibroblasts, local oscillations of protrusion and retraction at the cell border are associated with propagating actin waves, myosin light chain kinase and α-actinin activity (Giannone et al, 2004 and 2007). Furthermore, Weiner et al reported actin and Arp2/3

waves in human neutrophils that correlate with waves of an upstream regulator of Arp2/3, as well as calcium waves. There, waves of Hem-1 (a component of the Scar/WAVE complex) stimulate actin assembly, which in turn removes Hem-1 from the plasma membrane potentially (Weiner et al, 2007). A current study performed in the osteosarcoma cell line U2OS, reported calcium-independent F-actin waves that are related to Arp2/3 driven actin-polymerization and the formation of focal adhesions (Case and Waterman, 2011).

1.2.3 Myosin driven contractile actin structures counterbalance cell protrusions

Acto-myosin decorated stress fibers and the cortical actin meshwork are critical structural elements, counterbalancing cellular protrusions and driving global cell shape changes (Giannone et al, 2004; Vicente-Manzanares et al, 2009). At the molecular level, cell contractility arises from the interplay between myosin-II motor proteins, filamentous actin and actin crosslinking proteins such as α-actinin or filamin A (Bendix et al, 2008; Koenderink et al, 2009). Myosin-II molecules form a hexamer comprised of two heavy chains (MHCs) and four light chains, of which two are regulatory light chains (MRLCs) (see Figure 1.7; reviewed by Sellers, 2000).

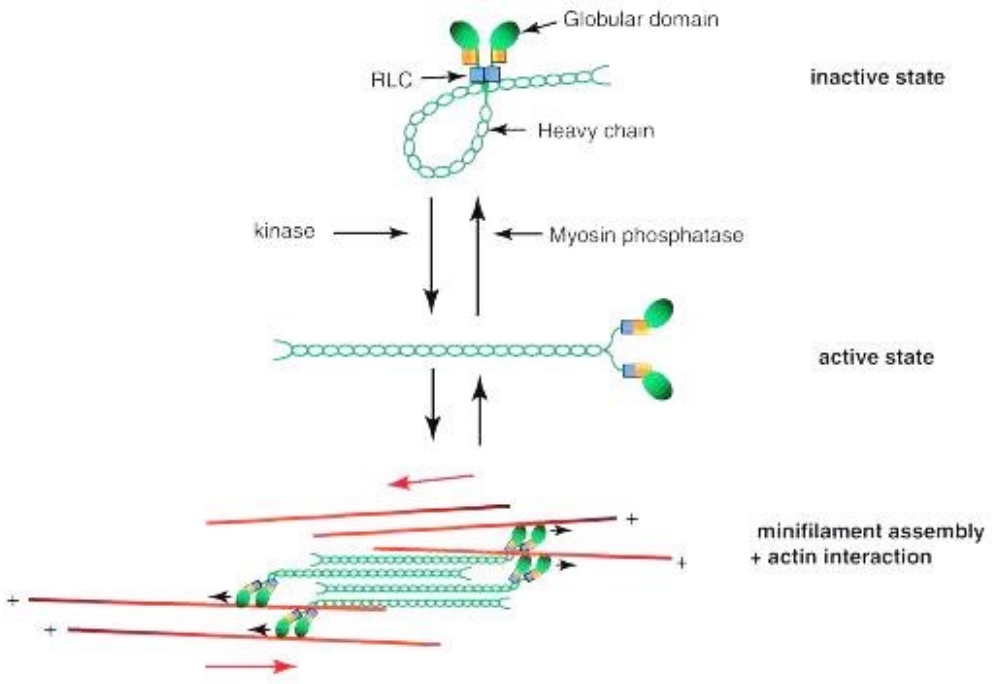

Figure 1.7: Myosin-II activation and minifilament assembly.

The inactive, auto-inhibited state of myosin-II is released upon phosphorylation of its RLC (regulatory light chain) by kinases, such as Rho-associated protein kinase (ROCK) (top). Active myosin-II proteins associate with actin filaments and assemble into minifilaments (bottom). Black arrows represent the walking direction of the motor proteins, red arrows display the direction of sliding actin filaments (this Figure was modified from Levayer and Lecuit, 2012).

To transfer myosin-II into its active state, two highly conserved residues (T18 and S19) within the MRLCs can be phosphorylated by multiple kinases (reviewed by Matsumura, 2005). In its active state, the auto-inhibitory head-to-tail interaction of MHCs is released, allowing the binding of actin filaments and enabling myosin motor activity (Craig et al, 1983; Jung et al, 2008). This motor activity is coupled to a cyclic binding and release of actin filaments and is provided by the globular domain at the N-terminus of myosin-II (designated as "head") that comprise actin and ATP binding sites (Rayment et al, 1993). Rapid succession of ATP hydrolysis and replacement by ATP supplies the mechanical energy needed to displace actin filaments ("powerstroke") (Huxley, 1974). Myosin motor activity alone is not sufficient to create contractility, single myosin-II proteins are unipolar and barely processive (Finer et al, 1994). *In vitro*, myosin-II proteins accumulate to bipolar minifilaments, varying in number of active hexamers from a few dozen in non-muscle cells, to hundreds of myosin heads forming thick filaments of skeletal muscle myosin (Niederman and Pollard, 1975; Skubiszak and Kowalczyk, 2002). These minifilaments translocate actin filaments mostly towards their barbed (plus) end, pulling them towards each other if the actin filaments are of opposite polarity (antiparallel), which forms the molecular basis for cellular contractility (reviewed by Levayer and Lecuit, 2012, see Figure1.7, bottom).

1.2.4 Formation of contractile stress fibers

Three stress fiber types have been described for mammalian cells (reviewed in Small et al, 1998). Transversal actin arcs, dorsal and ventral fibers differ not only in their subcellular localization and attachment to focal adhesions (shown in Figure 1.8), but also in the mechanisms of their assembly (Hotulainen and Lappalainen, 2006).

Dorsal stress fibers are attached to a focal adhesion with one end, while arcs rise towards the dorsal surface (Heath and Dunn, 1978). Dorsal fibers are driven by actin-polymerization at focal adhesions at the leading edge providing a structural template for adhesion maturation (Hotulainen and Lappalainen, 2006; Small et al, 1998; Oakes et al, 2012). Myosin incorporation into dorsal fibers was thought to be restricted to intersections of dorsal stress fibers with transverse actin arcs (Hotulainen and Lappalainen, 2006; Tojkander et al, 2011) until we and others recently discovered that myosin also localizes to the distal ends overlapping with focal adhesions (Schulze et al, 2014, Pasapera et al, 2015).

Ventral stress fibers are contractile bundles of actin that are attached to focal adhesions at each end and display, as transversal arcs, the periodic patterns of alternating myosin-II and α-actinin

(Burridge, 1986; Hotulainen and Lappalainen, 2006). This type of stress fibers promotes rear establishment and the formation of a front-to-rear polarity axis during cell migration (Ang et al, 2010; Vicente-Manzanares et al, 2008). Traction force microscopy could recently confirm that ventral stress fibers are under higher mechanical tension, then any other stress fiber type (Soiné et al, 2015). They are thought to mature by direct fusion of two dorsal stress fibers (Small et al, 1998) or by conjunction of two dorsal stress fibers with a transversal arc (Hotulainen and Lappalainen, 2006). However, a third mechanism of assembly seems likely, since the depletion of dorsal stress fibers in U2OS cells does not reduce the number of ventral stress fibers (Kovac et al, 2013; reviewed in Vallenius, 2013).

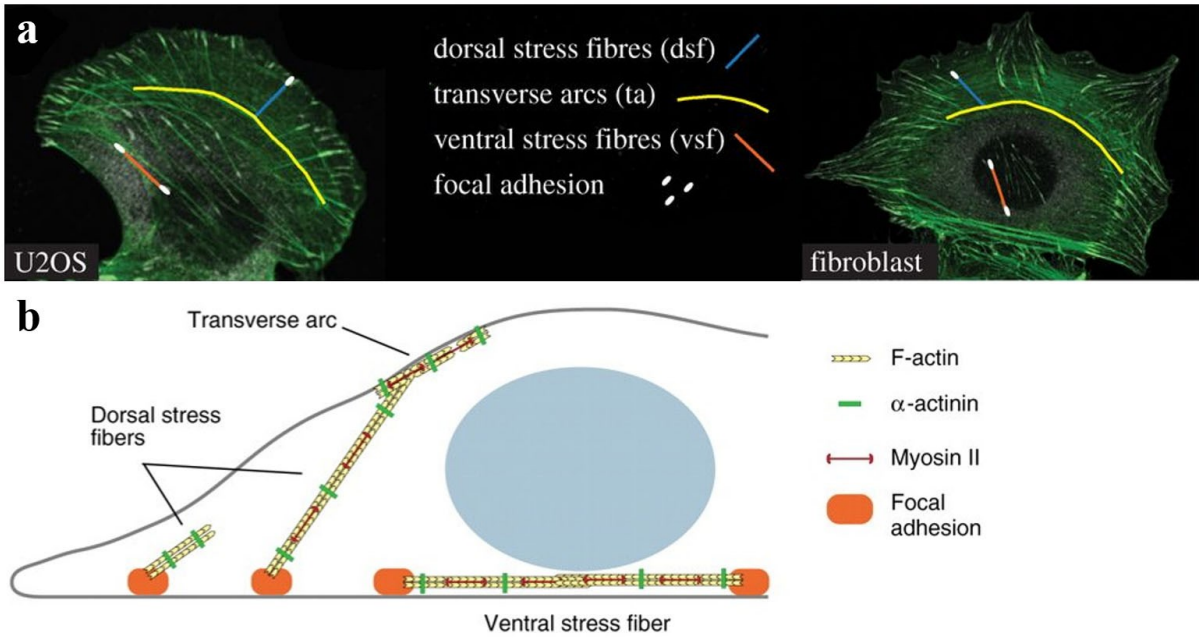

Figure 1.8: Three different types of stress fibers in mammalian cells

(a) F-actin (depicted in green) and vinculin (illustrated in grey) co-stained in a migrating U2OS cell (left panel) and a fibroblast (right panel) that recently spread on fibronectin. Actin stress fiber subtypes and attached adhesions are highlighted color coded. (This Figure was taken from Vallenius, 2013.) **(b)** Schematic model of stress fiber subtypes, their cellular localization and proposed molecular composition. (This Figure was taken from Pellegrin and Mellor, 2007.)

Transversal arcs are arc-shaped actin bundles that are formed just behind the leading edge. They move centripetally and were shown to disassemble in front of the nucleus (Heath, 1983). Transversal arcs are not attached to focal adhesions, but display a periodic distribution of myosin and α-actinin (Lazarides und Burridge, 1975; Hotulainen und Lappalainen, 2006).

Together, the different types of stress fibers built tension-bearing structures that, in turn, are able to generate the cellular force, necessary to drive dynamic changes of cellular morphology during migration. Also, periodic generation of contractile forces likely forms an additional layer to control oscillatory behavior such as during cell protrusion/retraction cycles in the leading

edge (Giannone et al, 2003). However, in contrast to polymerization mediated actin waves (section 1.2.2) oscillations of actin mediated contractility have not been reported so far.

1.3 Rho GTPase signaling controls actin dynamics

The family of Rho GTPases belongs to the Ras superfamily of small GTPases and consists of more than 20 GTP-binding proteins in mammals. Rho proteins regulate a variety of physiological processes such as gene expression, cell division and cell migration (see also section 1.4; Rajakylä and Vartiainen, 2014; Narumiya and Yasuda, 2006; Sadok and Marshall, 2014). Most members act as molecular switches, cycling between an inactive GDP-bound state and an active state bound to GTP (reviewed by Vetter and Wittinghofer, 2001; Hakoshima et al, 2003; Jaffe and Hall, 2005). The switch between the two activity states is positively regulated by guanine nucleotide-exchange factors (GEFs), and negatively controlled by their intrinsic GTPase activity, as well as GTPase activating proteins (GAPs) and guanine nucleotide-dissociation inhibitors (GDIs) (see Figure 1.9; Hall, 1998 and 2012; Heasman and Ridley, 2008; Cherfils and Zeghouf, 2013). All Rho GTPases also share an isoprenylation site at their C-termini allowing their insertion into cellular membranes, which is key prerequisite for their correct localization and cellular function (Michaelson et al, 2001).

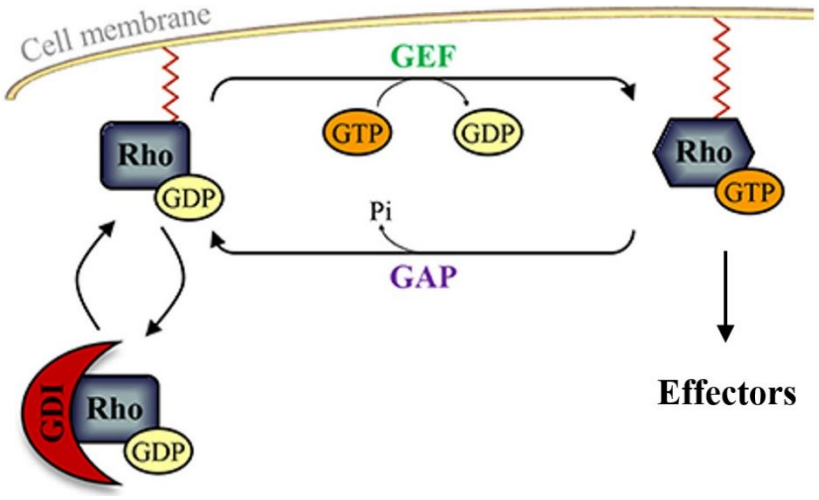

Figure 1.9: The GTPase cycle enables Rho GTPases to act as molecular switches.

Rho GTPases in their inactive state are bound to GDP and can be kept in this form via association with a guanine nucleotide dissociation inhibitor (GDI). Rho proteins are activated by the exchange of GDP to GTP that is mediated by guanine nucleotide-exchange factors (GEFs). In their active form, Rho GTPases interact with multiple downstream effectors, regulating a broad range of cellular processes. Inactivation of Rho proteins is achieved by hydrolysis of an inorganic phosphate (Pi) from the associated GTP, which is facilitated by GTPase-activating proteins (GAPs). (This Figure was modified from Azzarelli et al, 2015).

In their active state, Rho GTPases can interact with an array of downstream signaling molecules, so called effectors, mediating a broad spectrum of different signaling processes.
The best studied Rho GTPases are Rac1, Cdc42 and RhoA. Classically, Cdc42 is thought to be associated with filopodia formation, while Rac1 promotes the protrusion of lamellipodia and RhoA regulates cell contraction via formation of stress fibers and focal adhesions (Ridley and Hall, 1992; Nobes and Hall, 1995). Interestingly, crosscorrelation analysis of activity dynamics of all three Rho GTPases showed coordinated activation patterns during protrusion/retraction cycles in the leading edge of migrating cells (Machacek et al, 2009). In particular, RhoA has emerged as a critical regulator during this process, as aberrant leading edge activity of the GTPase has been linked to perturbed protrusion dynamics (Nalbant et al, 2009).
Selected cytoskeleton associated regulators and relevant downstream effectors of RhoA involved in actin polymerization and cytoskeletal contractility are discussed in detail below.

1.3.1 Selected upstream regulatory proteins controlling spatio-temporal RhoA activity

Guanine nucleotide exchange factors (GEFs):

In order to transfer from its inactive GDP-bound state to its active state bound to GTP, RhoGTPases have to release GDP, which is a very slow, energetically unfavorable process that is accelerated by GEFs to yield efficient activation levels in cells (Vetter and Wittinghofer, 2001; reviewed by Cherfils and Chardin, 1999; Bos et al, 2007). GEFs are usually multi-domain proteins that often include protein or lipid interaction domains, suggesting that they can serve as localization signals or as scaffolds for the assembly of protein complexes (reviewes by Bos et al, 2007; Cherfils and Zeghouf, 2013). The majority of GEF proteins are members to the Dbl family, characterized by a Dbl homology (DH) domain (Dbl: oncogene first identified in a B-cell lymphoma) and a pleckstrin homology (PH) domain (reviewed by Zheng, 2001). Some GEFs, such as Vav2, can catalyze nucleotide exchange of different Rho GTPases (Abe et al, 2000). Others display a specific activity for only one GTPase, such as ITSN-1 for Cdc42 (Hussain et al, 2001).

GEF-H1: GEF-H1 is a member of the Dbl family of GEFs that was found to associate with the Rho GTPases RhoA, RhoB and RhoC (Ren et al, 1998; Krendel et al, 2002). However, later studies attested its specific activity for RhoA (Birkenfeld et al, 2007; Chang et al, 2008) that is regulated by the association of GEF-H1 with microtubules, inhibiting its activity (Krendel et al, 2002). GEF-H1 is activated upon release from the microtubules, which can be caused by nocodazole-induced microtubule depolymerization (Chang et al, 2008), as well as microtubule destabilization in response to changes in the stiffness of the extracellular matrix (Heck et al,

2012). The physiological relevance of GEF-H1 was revealed by siRNA-mediated downregulation, demonstrating its significance for cleavage furrow formation in cytokinesis (Birkenfeld et al, 2007) and for leading edge integrity during cell migration (Nalbant et al, 2009).

GTPase activating proteins (GAPs):

GAPs catalyze the transition between the GTP- and the GDP-bound state, inactivating the Rho GTPase and counterbalancing GEFs (reviewed by Cherfils and Zeghouf, 2013). As GEFs, most RhoGAPs are large multi-domain proteins, containing not only a GAP domain, but several other functional domains such as SH3 (SRC homology 3 domain), PH (pleckstrin homology) or myosin motor activity domains, by which they can integrate other signaling pathways (see Figure 1.10; reviewed by Tcherkezian and Lamarche-Vane, 2007; van Buul et al, 2014).

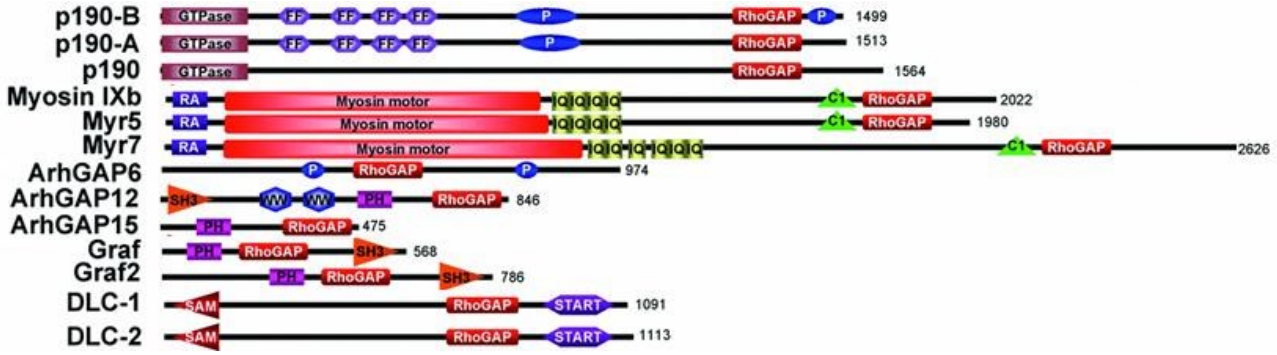

Figure 1.10: Multidomain structure of RhoGAPs.

RhoGAPs can contain a multitude of different functional domains, enabling a crosstalk between Rho GTPases and other signaling pathways. Domain abbreviations are as follows: C1, cysteine-rich phorbol ester binding; IQ, calmodulin-binding motif; FF, two signature phenylalanine residues; P, proline-rich; PH, pleckstrin homology; RA, Ras association domain; SAM, sterile alpha motif; SH3, SRC homology 3 domain; START, StAR (steroidogenic acute regulatory)-related lipid transfer; WW, two signature tryptophan residues. (This Figure was modified from Tcherkezian and Lamarche-Vane, 2007).

p190RhoGAP: Among the first GAPs, identified in human was p190RhoGAP that was shown to interact with p120RasGAP in a Src-kinase dependent manner (Ellis et al, 1990; Roof et al, 1998). Later studies revealed a second related RhoGAP, designated as p190B, to be conserved in mammals, while in *Drosophila* only one p190RhoGAP was found (Burbelo et al, 1995; Chakravarty et al, 2001; Billuart, 2001). Along a C-terminal RhoGAP domain, members of this superfamily contain an N-terminal GTPase domain and four consecutive FF domains (each composed of two phenylalanines), as well as a prolin-rich region (P) (see Figure 1.10). Multiple GTPases have been suggested as effectors of p190GAP. While *in vitro* studies suggest GAP activity towards Rac1, Cdc42 and most prominently RhoA, studies with Swiss 3T3 fibroblasts expressing p190-A constructs attend GAP activity exclusively towards RhoA (Settleman et al, 1992; Burbelo et al, 1995; Ridley et al, 1993; Haskell et al, 2001). In addition, p190RhoGAP

has been shown to directly inactivate the Ras pathway via the association with p120RasGAP, thus controlling cell proliferation (Moran et al, 1991; Shen et al, 2008). Upstream of RhoA, p190GAP was reported to inhibit cell migration, spreading and cancer cell invasion (Arthur and Burridge, 2001; Kusama et al, 2006).

Myo9b: The mammalian class IX myosins, Myo9a (myr7) and Myo9b (myr5) are found to be unconventional myosins as they combine a Rho-specific GAP as well as a motor activity (Chieregatti et al, 1998; Reinhard et al, 1995; Müller et al, 1997). Beside, class IX myosins are single-headed, but still exhibit the processive movement along actin filaments that is characteristic for double-headed myosins (Post et al, 2002; Nishikawa et al, 2006). This is achieved by an additional actin-binding site in the head domain acting as an actin tether to keep the actin filament attached during movement (Kambara and Ikebe, 2006; Struchholz et al, 2009; Elfrink et al, 2014). Additionally, Myo9a and Myo9b contain multiple "IQ" sites (binding myosin light chains) and a C1 (Zn^{2+} binding) motif close to the RhoGAP domain (see Figure1.10) (Reinhard et al, 1995; Wirth et al, 1996). Both isomers localize to the leading edge of migrating cells, whereas Myo9a is accumulated in nascent adhesions, while Myo9b is found in regions containing dynamic actin filaments (Omelchenko and Hall, 2012; van den Boom et al, 2007; Xu et al, 2014). Studies with Myo9b-deficient mice and macrophages revealed its key role as negative regulator of Rho during cell motility, the formation of protrusions and to control cell shape changes (Hanley et al, 2010; Bähler et al, 2011). However, the dynamics of this spatio-temporal control of Rho and the mechanism by which Myo9b activity is regulated and how this is linked to extracellular signals is still unknown.

ARHGAP18: This RhoGAP, formerly known as MacGAP or SENEX, was found to be crucial for the survival of endothelial cells (Li et al, 2008; Coleman et al, 2010). Maeda and colleagues reported ARHGAP18-mediated inactivation of RhoA during remodeling of the actin cytoskeleton in response to integrin signaling, thus controlling cellular shape changes. Furthermore it was reported to localize to the leading edge of spreading and migrating cells (Maeda et al, 2011). On the other hand, a recent study indicates that ARHGAP18 acts specifically on RhoC in a ROCK dependent manner during vascular morphogenesis, destabilizing cell junctions (Chang et al, 2014). Based on sequence similarities, Arhgap18 is closely related to Arhgap6, Arhgap11, Arhgap28, Arhgap40, DLC1, DLC2 and DLC3 (Yeung et al, 2014), although its detailed domain structure is still not identified.

1.3.2 Selected downstream effectors of RhoA

1.3.2.1 ROCK1/2 mediate stress fiber formation

Members of the ROCK family of serine/threonine kinases (Rho-associated, coiled-coil containing protein kinase) are pivotal effectors of the Rho GTPase RhoA in the reorganization of the actin cytoskeleton (Fujisawa et al, 1996; Leung et al, 1996). The two identified isoforms, ROCK1 (1354 amino acids) and ROCK2 (1388 amino acids) comprise both three major protein domains: a kinase domain, a coiled-coil domain (including the Rho-binding site (RBD)), and a pleckstrin homology (PH) domain (Nakagawa et al, 1996). The latter was later found to be bisected by an internal cysteine-rich zinc finger-like motif domain (CRD), see Figure 1.11 (Wen et al, 2008).

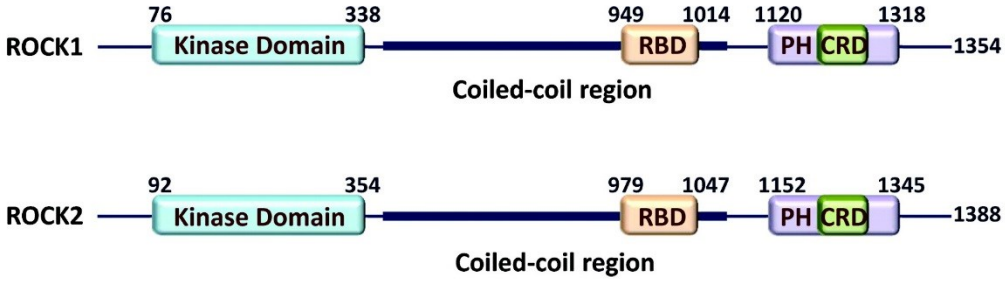

Figure 1.11: Multidomain structure of ROCK kinases.

Domain abbreviations are as follows: RBD, Rho-binding domain; PH, pleckstrin homology; CRD, cysteine-rich zinc finger-like motif domain. Protein domains and their indicated positions were taken from the National Center for Biotechnology Information (NCBI; http://www.ncbi.nlm.nih.gov/protein) for human ROCK1 (NP_005397.1) and ROCK2 (NP_004841.2) (this Figure was taken from Julian and Olsen, 2014).

Furthermore, studies demonstrated a dimerization domain in the N-terminus of the ROCK kinase domains to mediate the formation of head-to-head homodimers (Jacobs et al, 2006; Yamaguchi et al, 2006). The auto-inhibitory properties of ROCK kinases are based on an intramolecular interaction between the kinase domain and the C-terminal PH domain, rendering the kinase inactive (Amano et al, 1999). Active, GTP-bound Rho interacts with the RBD leading to the disruption of the negative regulatory interaction and to the elevation of the kinase specific activity of ROCK (Leung et al, 1996; Ishizaki et al, 1996).

For long, myosin-II has been described as direct effector of ROCK that phosphorylates myosin light chain (MLC) (Totsukawa et al, 2000) (see also section 1.2.3). Notably, ROCK 1/2 can also activate myosin-II by inhibiting myosin phosphatases (reviewed by Riento and Ridley, 2003; Matsumura und Hartshorne, 2008). Furthermore, ROCK kinases were shown to control myosin-II-mediated contractility, as their pharmacological inhibition reduces stress fiber tension significantly (Kumar et al, 2006). Little is known about the subcellular localization of ROCK1. However, it was suggested that the ROCK isoform associates with the plasma membrane (Glyn et al, 2003; Stroeken et al, 2006) and centrosomes (Chevrier et al, 2002; Kanai et al, 2010). Similarly, ROCK2 has been described to localize to cellular membranes and

centrosomes as well (Leung et al, 1995; Ma et al, 2006). In addition, ROCK2 has been shown to associate with actin microfilaments and stress fibers (Katoh et al, 2001; Kawabata et al, 2004) and was found to accumulate at the cleavage furrow, suggesting its role in cytokinesis (Kosako et al, 1999). Interestingly, overexpression of active RhoA was observed to recruit ROCK2 to the cell membrane (Leung et al, 1995; Vandenabeele et al, 2010), indicating that the subcellular localization of the kinase has an influence of on its biological function (reviewed by Julian and Olsen, 2014).

1.3.2.2 Formin effectors downstream of RhoA control actin polymerization and stress fiber formation

The architecture and dynamics of the eukaryotic cytoskeleton is precisely regulated in space and time by a variety of actin binding proteins. Among these are the multigene family of formins, long multi-domain proteins, which are highly conserved in all eukaryotes (Chalkia et al, 2008). Formins are thought to mediate the crosstalk between microtubules and the actin cytoskeleton, and were found to be key regulators of many cytoskeletal processes downstream of Rho GTPases, such as cell division, endocytosis, neurite outgrowth, migration and adhesion (reviewed by Tanaka, 2000; Wallar and Alberts, 2003; Goode and Eck, 2007; Chesarone et al, 2010; Zhang and Wang, 2015). Formins are defined by three common regions, designated as formin homology (FH1, FH2 and FH3) domains (Wallar and Alberts, 2003; Kitayama and Uyeda, 2003; Schönichen and Geyer, 2010).

The diaphanous-related formins (DRFs) constitute a subfamily of formins characterized by additional conserved domains, including a GTPase-binding domain (GBD, N-terminal) and a diaphanous autoregulation domain (DAD, C-terminal) (Alberts, 2001). The latter exhibits dual functions. First, it is able to recruit actin monomers and thus to enhance actin nucleation (Gould et al, 2011). But more importantly, the DAD can interact with the N-terminal FH3 domain, generating an intramolecular, auto-inhibited complex (Alberts, 2001; Li and Higgs, 2005; Wallar et al, 2006). This complex is dissolved by a conformational change in the FH3 domain, which can be triggered by the association of a GTPase with the GBD domain, leaving the DRF in its active state (Watanabe et al, 1999; Alberts, 2001; Li and Higgs, 2003; Lammers et al, 2005). At present, DRFs are subdivided into eight subfamilies, such as DAAM (dishevelled-associated activators of morphogenesis), Dia (diaphanous), FHOD (formin-homology domain proteins) and FMNL (formin-like proteins) (Schönichen and Geyer, 2010; Breitsprecher and Goode, 2013; Kühn and Geyer, 2014).

mDia: For the mammalian diaphanous family of formins (mDia), three isoforms mDia1-3 have been identified (reviewed by Goh and Ahmed, 2012). Interestingly, all mDia isoforms directly interact with members of the Rho family of GTPases, and not with the Rho downstream effector ROCK (Watanabe et al, 1997; Alberts et al, 1998; Yasuda et al, 2004). Both mDia1 and mDia2, which are regulated downstream of RhoA, are known to nucleate and elongate actin filaments (Li and Higgs, 2003; Moseley et al, 2004 and 2006), as well as to form lamellipodia and filopodia at the plasma membrane (Zaoui et al, 2008; Yang et al, 2007; Goh et al, 2011 and 2012). This ability of mDia proteins to induce the assembly of actin filaments is best studied for mDia1 that was shown to be essential for numerous cellular processes, among them cell polarization (Yamana et al, 2006) and migration (Hotulainen and Lappalainen, 2006). In order to modulate actin, two mDia1 proteins dimerize head-to-tail, via their FH2 domains (Harris et al, 2004 and 2006), forming a donut-shaped ring that can lay itself around an actin filament (Xu et al, 2004; Moseley et al, 2004). FH2 domains have two actin-binding-domains, which bind highly affine to the barbed ends of actin filaments (Xu et al, 2004; Sagot et al, 2002). During elongation, the proline-rich FH1 domains deliver monomeric actin (Paul and Pollard, 2008), while the FH2 domains stay attached to the growing filament, stabilizing it and preventing the binding of capping proteins (Zigmond, 2003; Harris et al, 2004; Romero et al, 2004). The step-wise elongation of an actin filament mediated by formins is shown schematically in Figure 1.12.

During formation of stress fibers, thick bundles of such linear actin filaments are prerequisite for the formation of dorsal fibers (reviewed by Naumanen et al, 2008). In agreement with this, mDia1 was shown to promote the growth of dorsal fibers in U2OS cells (Hotulainen and Lappalainen, 2006).

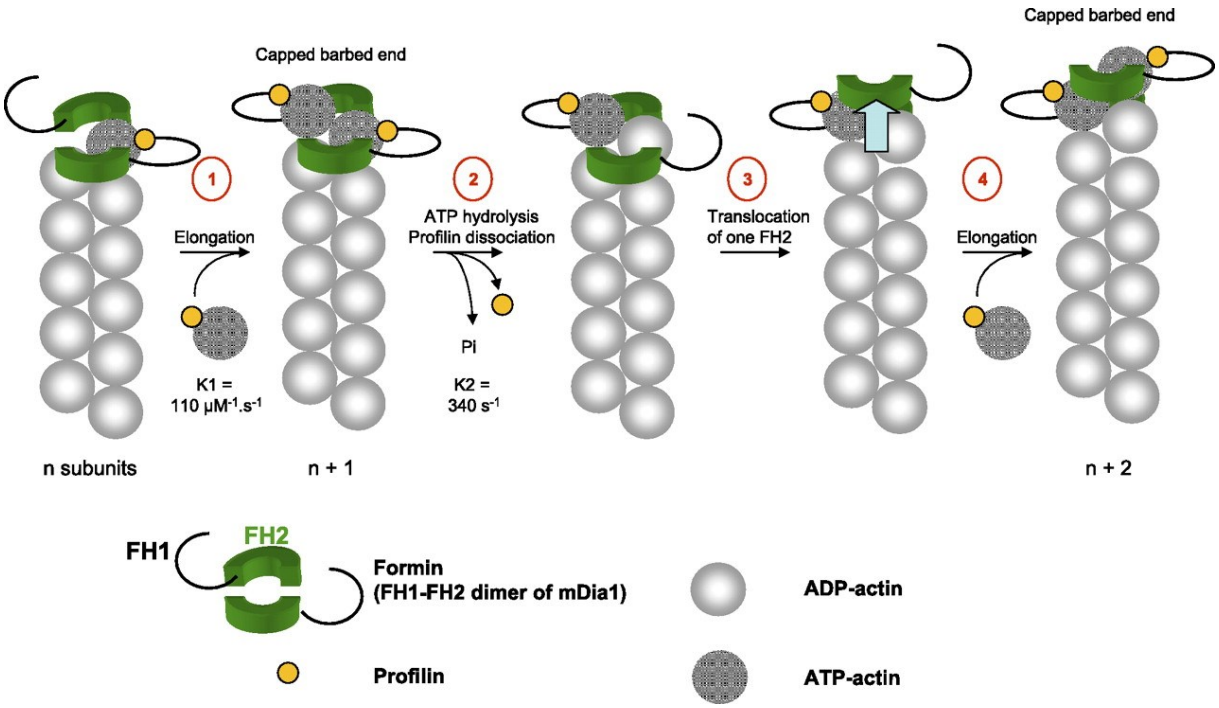

Figure 1.3.2.2.12: Model for processive actin assembly mediated by the FH1 and FH2 domains of mDia1.

1) Formin bound barbed end of an actin filament assembles two profilin-actin subunits, resulting in a capped barbed end. To this end each FH2 domain of the dimer associates with two profilin-actin subunits; one FH2 domain binds to the first and second subunit, the other FH2 domain attaches to the second and third profilin-actin subunit. 2) The dissociation of profilin is initiated by ATP hydrolysis. 3) One of the actin-formin contacts is released and the FH2 domain translocates, uncapping the growing filament. 4) The next profilin-actin subunit is added and bound by the free FH2 actin-binding-domain. (This Figure was modified from Le Clainche and Carlier, 2008.)

FHOD1: The mDia1 related formin FHOD1 has been shown to stimulate stress fiber formation in eukaryotic cells derived from fruit fly (Lammel et al, 2014), mouse (Gasteier et al, 2003) monkey (Schönichen et al, 2013) or human (Schulze et al, 2014). However, in contrast to other DRFs, its activation is not regulated via association of a GTPase to the GBD and to date, the mechanism by which its auto-inhibited state is released remains still elusive (reviewed by Bechthold et al, 2014). Initial studies suggested that Rac1 might activate FHOD1 via a proposed interaction that occurs independently of the activity state of Rac1 (Westendorf, 2001; Gasteier et al, 2003). Furthermore FHOD1 in conjunction with Rac1 was reported to regulate the actin tail formation in *vaccina* virus motility (Alvarez and Agaisse, 2013). Despite the structural identification of a GTPase binding site, in form of an ubiquitin superfold in the GBD of FHOD1, a direct interaction with Rac1 could not be confirmed in later studies (Schönichen et al, 2006; Schulte et al, 2008). Instead Gasteier and colleagues found first evidence that FHOD1 is regulated by the Rho-ROCK pathway (Gasteier et al, 2003 and 2005). Further studies confirmed this finding and identified three targets for ROCK phosphorylation within the C-terminal DAD (S1131, S1137, T1141) that mediate the release of the auto-inhibited state (Schulte et al, 2008; Takeya et al, 2008; Hannemann et al, 2008). Interestingly, phosphorylation by ROCK (Rok)

was found to activate FHOD1 in *Salmonella* invasion, as well as the FHOD Knittrig in *Drosophila*, suggesting this to be a conserved activation mechanism for FHOD1 (Truong et al, 2013; Lammel et al, 2014). In addition to ROCK mediated activation, proteins of the Src-family of kinases, such Src, Yes and Fyn, were suggested to control mRNA levels of FHOD1 and the correct spatial targeting of the formin to focal adhesions (Koka et al, 2005; Iskratch et al, 2013). Figure 1.13 summarizes the different regulators suggested for FHOD1 and provides an overview of its multi-domain structure.

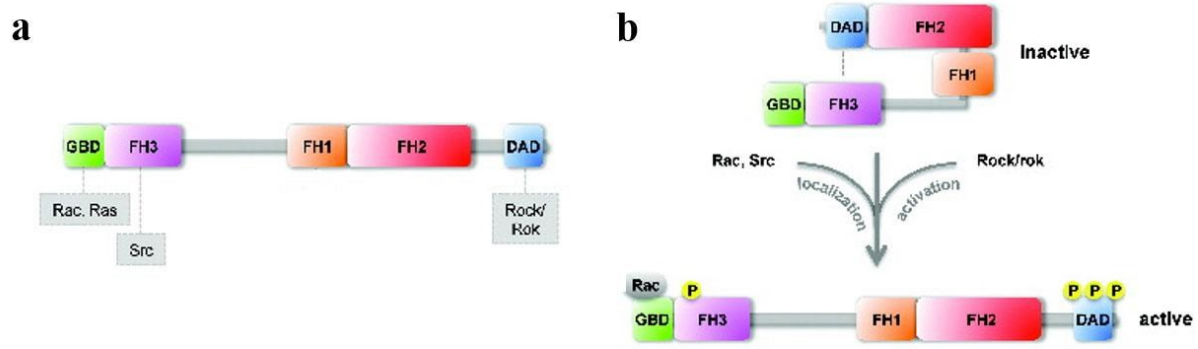

Figure 1.13: Domain architecture of FHOD1, potential regulators and their targeting.

(a) Domain structure of FHOD1 and assumed interactors linked to the FHOD1 domains indicated. GBD: GTPase-binding domain; FH3: Formin homology 3; FH1: Formin homology 1; FH2: Formin homology 2; DAD: Diaphanous autoregulation domain. **(b)** Proposed model of different signaling pathways that were suggested to control the activation and the cellular localization of FHOD proteins sites (these Figures were modified from Bechtold et al, 2014).

As opposed to other related formins, *in vitro* actin polymerization assays performed with purified active FHOD1 implicated a dual function as actin capping and bundling protein, rather than an actin nucleating or polymerizing activity (Schönichen et al, 2013). The expression of FHOD1 is up-regulated during epithelial-mesenchymal transition (Gardberg et al, 2013) and was found to promote cell migration and invasion, when overexpressed in melanoma and breast cancer cells (Koka et al, 2003; Jurmeister et al, 2012). At the same time overexpression of active FHOD1 leads to a phenotype characterized by thick stress fibers throughout the cell (Koka et al, 2003; Gasteier et al, 2003). Accordingly, FHOD1 depletion with siRNAs suppresses stress fiber formation, cell spreading and migration, but also decreases the size of focal adhesions, suggesting a role of FHOD1 in stress fiber formation and focal adhesion maturation (Iskratsch et al, 2013; Schulze et al, 2014). In detail, FHOD1 was shown to promote the formation of transverse arcs and facilitate their maturation to ventral stress fibers, whereas the growth of dorsal stress fibers is inhibited by active FHOD1 (Schulze et al, 2014). These processes were found to be regulated by the Rho/ROCK-pathway, however, the detailed mechanism of its spatio-temporal activation and its precise, dynamic localization is yet unclear.

1.4 Cell fate regulation and environmental mechanosensing by focal adhesions and Rho dependent acto-myosin contractility

Mechanosensing (also referred to as mechanotransduction) describes the ability of cells to perceive changes in extracellular substrate rigidity and respond to those changes. It is essential for numerous physiological and pathological processes, such as stem cell behavior, embryogenesis and cellular morphogenesis (Li et al, 2010; Engler et al, 2006; Lanniel et al, 2011). Recent studies with elastic gel substrates of varying stiffness confirm that the molecular forces at the cell-substrate interface determine the cell-fate of stem cells, as well as the degree of spreading in differentiated cells (Trappmann et al, 2012; Chandra and Lee, 2015; Chowdhury et al, 2015). The incorporation of mechano-chemical signals is therefore thought to be essential for the control of cellular behavior, gene transcription and cell fate (reviewed by Vogel and Sheetz, 2009).

Two main cellular pathways are stimulated by mechanical cues, both including the actin cytoskeleton and depending on active generation of intracellular forces provided by the motor protein myosin-II (Wang et al, 1993; Discher et al, 2005). For one, ion channel activity is altered in response to changes in external force, a process that activates multiple downstream signaling pathways and was shown to depend on cytoskeletal tension (reviewed by Morris, 1990; Janmey and Culloch, 2007). Such mechano- and osmotically sensitive ion channels were shown to transduce physical signals that influence stem cell proliferation and morphogenesis (Fiorio Pla et al, 2005; Tai et al, 2009). On the other hand, the binding between transmembrane adhesion proteins (such as integrins) and the extracellular substrate is governed by focal adhesions that are key regulators of cell migration and mechanosensing (Geiger et al, 2009; Patla et al, 2010; Kanchanawong et al, 2010). In particular, the focal adhesion proteins zyxin, talin and vinculin are well-known to mediate mechanosensing.

Zyxin is a LIM domain protein that is recruited to contracting stress fibers only (Zaidel-Bar et al, 2003) and has been associated with stress fiber repair and force generation (Colombelli et al, 2009). Zyxin contributes to mechanosensing via the recruitment of the actin crosslinking protein α-actinin and the phosphoprotein VASP (Vasodilator-stimulated phosphoprotein) (Smith et al, 2010; Sun and Walcott, 2010), which promotes actin polymerization (Hansen and Mullins, 2010; Winkelman et al, 2014).

Vinculin consists of a head and tail domain, connected by a flexible proline rich linker (Bakolitsa et al, 1999; Borgon et al, 2004). A recent study demonstrated that a mutation within the vinculin tail causes defects in cell adhesion, spreading, migration and the generation of

traction forces (Jannie et al, 2015). Inactive vinculin is auto-inhibited by an interaction between head and tail (Johnson and Craig, 1994) that is released upon binding of talin (Cohen et al, 2006; Chase et al, 2015). In its active state vinculin binds actin via its tail region, stimulating the formation of new actin bundles and modifying existing bundles (Johnson and Craig, 1995; Wen et al, 2009). The recruitment of vinculin to cell adhesion sites is upregulated by force (Riveline et al, 2001; Galbraith et al, 2002) and vinculin-mediated signaling pathways were recently shown to remain active only in cellular areas where tension is maintained (Carisey et al, 2013). Furthermore, the complex of talin and vinculin has been implicated to serve as adjustable force transmission link, translating mechanical force to biochemical signal pathways (Galbraith et al, 2002; Hu et al, 2007). This sensitivity to force is mediated by the rod of talin, which contains elven vinculin-binding sites, which are buried inside helix bundles in the relaxed state of the protein (Papagrigoriou et al, 2004; Gingras et al, 2005; Fillingham et al, 2005). Using atomic force microscopy it could be demonstrated that mechanical stretching of talin, exposes these sites, allowing the binding of several vinculin molecules per talin (Hytönen and Vogel, 2008; del Rio et al, 2009). Figure 1.14 summarizes the molecular components of focal adhesions and demonstrates their spatial distribution relative to the plasma membrane.

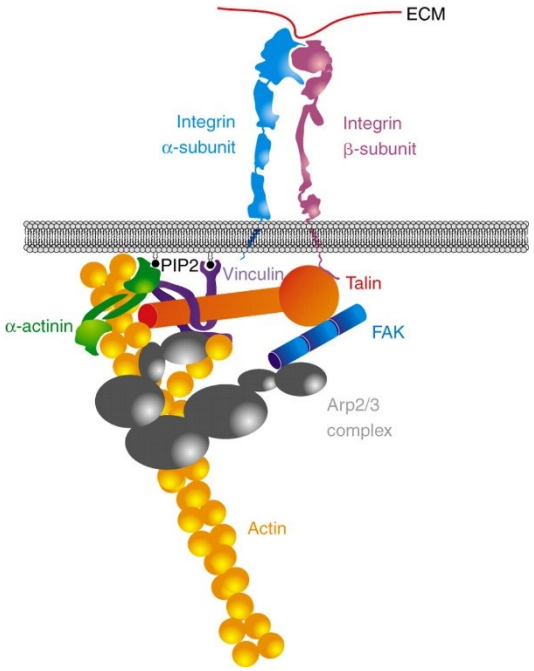

Figure 1.14: Schematic illustration of a focal adhesion complex

The extracellular matrix (ECM, illustrated as red line) is linked to the actin cytoskeleton (represented in yellow) via integrins (α- and β-transmembrane subunits depicted in light blue and pink). Talin is able to bind directly to integrins via its head domain (orange sphere), while its tail domain (orange rod) can associate directly with actin and vinculin (indicated in purple). Vinculin can, in turn, bind to actin and the crosslinker α-actinin (shown as green dimer). Both vinculin and α-actinin are anchored in the plasma membrane and are regulated via phosphatidylinositol (4,5)-bisphosphate (PIP2). Vinculin and the focal adhesion kinase (FAK; depicted in blue) can bind to the actin nucleating complex Arp2/3 (illustrated in grey). (This Figure was taken from Vicente-Manzanares et al, 2009.)

A key role in the control of cell proliferation was also demonstrated for the focal adhesion kinase (FAK), which activates the MAPK/ERK pathway (Schlaepfer et al, 1994; Chen et al, 1994) via phosphorylation of the extracellular signal-regulated kinases 1 and 2 (ERK1/2) (Wang et al, 2001 and 2005). Mitogen-activated protein kinase (MAPK) pathways mediate signal transduction from receptor tyrosine kinases at the cell membrane to the DNA in the cell nucleus, controlling gene transcription and thus, cell survival and differentiation (reviewed by Zhang and Liu, 2002; Junttila et al, 2008). In addition, FAK was shown to phosphorylate paxillin, in response to myosin-II-mediated contractility, thus recruiting vinculin (Pasapera et al, 2010).

Despite the discovery of multiple potential mediators of mechanosensation, such as acto-myosin contractility or focal adhesion proteins, the underlying mechanisms are still poorly understood. In particular, this work contributes to the detailed dissection of spatio-temporal Rho activation and effector signaling, in the context of cellular mechanosensation.

1.5 Purpose of this thesis

The aim of this work was to characterize the irregular cortex activity oscillations of the contractility generating GTPase Rho, in adherent U2OS cells, and to identify signal network components controlling the spatio-temporal dynamics of these activity patterns. To this end, the high spatial resolution of TIRF microscopy was utilized together with fluorescently tagged low-expression constructs to further increase sensitivity of signal detection. In particular, an effector-domain based sensor coupled to mCherry or EGFP was used, for detection of Rho activity. To identify potential network components participating in the generation of Rho activity oscillations, spatio-temporal signal dynamics of multiple upstream regulatory proteins, prominent Rho effectors and the cytoskeletal protein actin were measured to allow temporal crosscorrelation analyses. Furthermore, RNAi based depletion and pharmacological perturbations of upstream regulators and downstream effector proteins were performed to characterize potential feedback interactions with Rho activity. In order to understand the relevance of Rho activity and contractility oscillations for cell shape changes and establishment of polarity, spatio-temporal activity dynamics of Rho and myosin-II were characterized in spreading cells. Furthermore, elastomeric surfaces with different rigidities were deployed to elucidate the potential role of sub-cellular signal oscillations in physiological processes related to mechanosensation.

2. Materials and Methods

2.1 Materials

2.1.1 Equipment and consumables

Table 2.1: Equipment and consumables used for cell culture

Description		Catalogue number/model	Company
Biosafety cabinet		Hera Safe	Thermo Scientific
Cell culture vessels	100 mm dish	83.1802	Sarstedt
	6-well plate	662160	Greiner
	24-well plate	657160	Greiner
	glass-bottom dish	13 mm Ø	MatTek
Centrifuge		5810R	eppendorf
Centrifuge rotor (swing-bucket)		A-4-44 and A-4-81	eppendorf
Cover slips		13 mm Ø, 15 mm thick	Thermo Scientific
Cryo freezing container		Nalgene® Mr. Frosty	Sigma-Aldrich
Cryogenic tube		E309.1	Roth
Hemacytometer		Neubauer improved, 0.1 mm	Hartenstein
Incubator		HEPA Class 100	Thermo Scientific
Steril filters		83.1826.001	Sarstedt
Water bath		Aqualine AL18	Lauda

Table 2.2: Equipment and consumables used for cloning

Description	Catalogue number/model	Company
Biological shaker	MaxQ 4000	Thermo Scientific
Centrifuge	5415 D	eppendorf
Centrifuge rotor (fixed angle)	F-34-6-38	eppendorf
Culture tubes (Bacteria)	Cultubes, 14 ml, EC04.1	Simport
Electrophoresis chamber	MIDI-1 HU10	Roth
incubator	Function Line	Thermo Scientific
Power supply	Power PacTM	BioRad
Spectrophotometer	Nanodrop 100	PeqLab
UV transilluminator (for gels)	Gel Doc 2000 system (integrated CCD camera)	BioRad

Table 2.3 Equipment and consumables used for western blot

Description	Model	Company
10-well comb	Mini-PROTEAN Comb, 10-well, 1.0 mm	BioRad
Chamber for PAGE	Mini- PROTEAN	BioRad
Chamber for blotting	Fastblot B34	Biometra
Cuvette (disposable)	PS Halbmikroküvetten	VWR
Gel casting module	Mini-PROTEAN Tetra Cell	BioRad
Imager (for Western Blots)	Fusion FX7	PeqLab
Rocking shaker	Collection	VWR
Rotator	Tube Rotator	VWR
Spectrophotometer	Genesys 6	Thermo Scientific
Power supply	EV231, EV243 and EV 265	Consort
PVDF membrane	0.45µm; 26.5 cm x 3.75m	Thermo Scientific

Table 2.4 General equipment and consumables

Description		Catalogue number/model	Company
Balances		ABJ 80-4M (Analytical Scale)	Kern
		CB 200-3B (Micro Scale)	Kern
Heating block		TH26	HLC Bio Tech
Micro-centrifuges		Mikro 120	Hettich
		IR	Roth
Parafilm		M	Bemis
pH meter		seven easy pH	Mettler-Toledo
Pipette controller		Automatic-Sarpette, 92189120	Sarstedt
Pipettes		1 mL, 100 µL, 10 µL, 2.5 µl	eppendorf
Serological pipettes	5 ml	86.1253.001	Sarstedt
	10 ml	86.1254.001	Sarstedt
	25 ml	86.1685.001	Sarstedt
Tubes	50 ml	62.554.502	Sarstedt
	15 ml	62.547.254	Sarstedt
	2 ml	72.695	Sarstedt
	1.5 ml	72.704	Sarstedt
	0.5 ml	72.706	Sarstedt
	0.2 ml	AB-0620	Thermo Scientific
Vacuum pumps		KNF laboport	Neolab
		Vacusafe comfort	Integra Biosciences
Vortex mixer		PV-1	Grant-Bio
Water purification system		Milli-Q-System	Millipore

Table 2.5: Microscopical setups

Description	Model/Details	Company
Microscope (widefield)	***Eclipse* Ti-E,** inverted microscope **Camera**: CoolSNAP HQ2, 1394, 14-bit, 220 V **Objectives**: S Plan Fluor EL 20x DIC N1(NA: 0,45); Plan Fluor VC 60x OIL DIC N2 (NA: 1,4) **Lamp**: TI-PS 100W **Filter**: Lambda 10-2 RS232 (Sutter Instruments) **Software**: NIS-Elements, Version:AR 3.2	Nikon
Microscope (TIRF)	**Olympus IX81F-3**, inverted microscope **Camera**: Hamamatsu Image EMCCD-C9100-13 **Objective**: PlanApo 60xOil TIRF (NA = 1.45), **Lasers**: 488 nm: 400 mW Argon ion laser (Melles Griot) 561 nm: 100 mW diode laser (Cell R) **Filters**: Triple bandpass dichroic mirror (405/488/561), Emission filter (HC 520/35 and HC 629/53, AHF) **Software**: Cell R	Olympus
Microscope (TIRF)	***Eclipse* Ti-E**, inverted microscope **Cameras**: Clara Interline CCD camera (Andor Technology) iXon3 897 single photon EMCCD camera (Andor) **Objective**: Apo TIRF 100×1.49 NA oil immersion objective **Laser**: AOTF Laser Combiner (Andor Technology) **Filters**: Dual bandpass dichroic mirror (zt488/561rpc, AHF) CSU Quad Dichroic mirror/emission filter set (405/488/568/647 nm; Semrock) **Software:** Andor IQ Software (Andor Technology)	Nikon
Microscope (confocal)	**TCS SP5 AOBS**, inverted microscope DMI6000B **Objective**: HCX PL APO lambda blue 63x oil UV; NA.1,40 **Lasers**: Argon (488 nm), 405 nm, 561 nm, 633 nm **Detectors**: Photo multiplier (PMTs) GaAsP-Hybrid-Detection system (HyDs) **Software**: LAS AF	Leica

2.1.2 Cell lines and media

Table 2.6: Cell line used for cell culture

Cell line	Species	Disease	Tissue	Morphology	Type
U2OS	Human	Osteosarcoma	Bone	Epithelial	ATCC® HTB-96™

Table 2.7: Cell line used for cloning

Cell line	Species	Genotype	Company
DH5α	*E.coli*	F-, supE44, ΔlacU169, [Φ80lacZΔM15], hsdR17, recA1, endA1, gyrA96, thi-1, (res-, mod+), deoR	Invitrogen

Table 2.8: Media used for human cell culture

Medium	Components
Growth medium	DMEM GlutaMAX™ 10 % (v/v) FCS 50 µg/ml Penicillin 50 µg/ml Streptomycin
Medium for siRNA transfection	DMEM GlutaMAX™ 10 % (v/v) FCS
Imaging medium	1 mM Calcium chloride 10 % (v/v) FCS 10 mM L-Glutamine 10 mM HEPES HBSS (Hank's balanced salt solution) 1 mM Magnesium chloride

All cell culture media were sterile filtered after preparation.

Table 2.9: Media used for bacteria

Medium	Components
LB Agar Plates	1.5 % (w/v) Agar 1 % (w/v) Sodium chloride 1 % (w/v) Tryptone 0.5 % (w/v) Yeast extract pH 7.0
Luria-Bertani (LB)-Medium	1 % (w/v) Sodium chloride 0.25 % (w/v) Sodium hydroxide 1 % (w/v) Tryptone 0.5 % (w/v) Yeast extract pH 7.4
Final concentration of antibiotics:	Ampicillin 100 µg/ mL Kanamycin 30 µg/mL

Medium and agar plates were autoclaved before usage.

2.1.3 Reagents and buffers

Table 2.10: Reagents used for human cell culture

Description	Company
Dulbecco's Modified Eagle Medium (DMEM) GlutaMAX™	Life Technologies
DPBS	Life Technologies
FCS	Life Technologies
HiPerFect	Qiagen
Isopropanol	Roth
Lipofectamine 2000	Life Technologies
OptiMEM	Life Technologies
Penicillin/Streptomycin	Life Technologies
Puromycin	Sigma-Aldrich
Trypsin-EDTA	Life Technologies
VenorGeM (Mycoplasma detection kit)	Minerva Biolabs

Table 2.11: Reagents used for cloning

Description		Company
Agar		Roth
Agarose		Bioenzym
Antarctic Phosphatase		New England Biolabs
Antibiotics	Ampicillin	Roth
	Kanamycin	Roth
Bromphenol blue		Serva
Buffers	CutSmart	New England Biolabs
	T4 DNA Ligase Buffer	New England Biolabs
1kb DNA ladder		BioBudget
dNTP Mix (10 mM each)		Roth
Enzymes	AgeI-HF	New England Biolabs
	EcoRI-HF	New England Biolabs
	T4 DNA Ligase	New England Biolabs
	XhoI	New England Biolabs
	XmaI	New England Biolabs
Ethidium bromide		Roth
Glycerol		AppliChem
Kits	Plasmid Purification Kit	Qiagen
	Gel Extraction Kit	Qiagen
Potassium chloride		Roth
Potassium hydrogen phosphate		Roth
Sodium chloride		Roth
Sodium hydroxide		Roth
Sodium hydrogen phosphate		Roth
Tryptone		BD Biosciences
Yeast extract		Serva

Table 2.12: Reagents used for western blot

Description	Company
Acetic acid	Roth
Acrylamide/ bisacrylamide	Roth
6-Aminohexanoic acid	Roth
Ammonium persulfate	Roth
Bradford protein-assay dye	BioRad
BSA	Sigma-Aldrich
DTE	Roth
ECL (Chemilumineszenz West pico)	Thermo Scientific
EDTA	AppliChem
Methanol	VWR
NP-40	Life Technologies
Nuclease-free water	Qiagen
Ponceau S	Roth
Protease-inhibitor (7 fold)	Roche
Protein ladder (prestained 10 to 180 kDa)	Thermo Scientific
SDS	Roth
Sodium chloride	Roth
Sodium deoxycholate	Life Technologies
Sodium fluoride	Sigma-Aldrich
Sodium orthovanadate	Sigma-Aldrich
Sulfosalicylic acid	Roth
TEMED	Roth
Tris-hydrochloride	AppliChem
Tween 20	Roth

Table 2.13: Reagents used for microscopy

Description	Company
Blebbistatin	Sigma-Aldrich
Calcium chloride	Roth
Collagen (from rat tail, type I)	BD Bioscience
Cytochalasine D	Sigma-Aldrich
DMSO	Roth
FCS	Life Technologies
Formaldehyde solution (37%)	Roth
L-Glutamine	Life Technologies
HBSS (Hank's balanced salt solution)	Life Technologies
HEPES	Life Technologies
Latrunculin A	Life Technologies
Magnesium chloride	Roth
Nocodazole	Sigma-Aldrich
OptiMEM	Life Technologies
Triton® X-100	Roth
Y-27632	Selleck

Table 2.14: Buffers and solutions used for western blot

Buffer/Solution	Components
Anode buffer I	0.3 M Tris-hydrochloride 10 % (v/v) Methanol pH 10.4
Anode buffer II	25 mM Tris-hydrochloride 10 % (v/v) Methanol pH 10.4
Blocking solution	5 % (w/v) BSA in TBS-T
Kathode buffer	40 mM 6-Aminohexanoic acid 25 mM Tris-hydrochloride 10 % (v/v) Methanol pH 9.4
500x Ponceau solution	1 % (v/v) Acetic acid 2 % (w/v) Ponceau S 30 % (w/v) Sulfosalicylic acid 30 % (w/v) Trichloroacetic acid
5x Protein loading dye	0.025 % (w/v) Bromphenol blue 300 mM DTE 50 % (v/v) Glycerol 0.5 mM Tris-hydrochloride pH 6.8
RIPA lysis buffer	1 mM EDTA 1 % (v/v) NP-40 1x Protease-inhibitor cocktail 150 mM Sodium chloride 0.25 % (v/v) Sodium deoxycholate 1 mM Sodium fluoride 1 mM Sodium orthovanadate 50 mM Tris-hydrochloride pH 7.4
SDS-PAGE Buffer	125 mM Glycerol 0.05 % (w/v) SDS 12.5 mM Tris-hydrochloride pH 6.8
SDS stacking gel buffer	1 M Tris-hydrochloride pH 6.8
SDS separating gel buffer	1.5 M Tris-hydrochloride pH 8.8
TBS buffer	137 mM Sodium chloride 20 mM Tris-hydrochloride pH 7.6
TBS-T buffer	TBS Buffer 0.1 % (v/v) Tween 20

All buffers were prepared using deionized water.

Table 2.15: Buffers used for cloning and fixation

Buffer	Components
5x DNA loading dye	0.25 % (w/v) Bromphenol blue 0.325 % (w/v) Xylene cyanol 30 % Glycerol
Elution buffer (EB)	10 mM Tris-Cl pH 8.5
PBS buffer	2.7 mM Potassium chloride 1.8 mM Potassium hydrogen phosphate 137 mM Sodium chloride 10.1 mM Sodium hydrogen phosphate
TAE buffer	40 mM Tris-acetate 5 mM EDTA pH 8.3
TSS buffer	5 % (v/v) DMSO 85 % (v/v) LB-medium 50 mM Magnesium chloride 10% (v/v) PEG6000 (50 % (w/v) solution) pH 6.5

Buffers were prepared with deionized water, TSS buffer was sterile filtrated after preparation.

2.1.4 siRNAs, antibodies and dyes

Table 2.16: siRNAs used for FHOD1 knockdown

Description	Sequence (5´->3´)	Company
siFHOD1 #2	CAGCGAGAGGAGCATCTACAA	Qiagen
siFHOD1 #5	AGGGTCAACGCTATCTTGGAA	Qiagen
siFHOD1 #6	CCCGCCGTGTTGCCATGCTAA	Qiagen
siFHOD1 #7	CCCGTGCACCCAGGCTCTCTA	Qiagen

Table 2.17: Primary antibodies (used for western blot and staining)

Specificity	Organism	Dilution	Company
anti-FHOD1	mouse	1 : 200	Santa Cruz Biotechnology
anti-Paxillin	mouse	1 : 500	BD Transduction Laboratories
anti-Tublin	mouse	1 : 20000	Sigma-Aldrich

Table 2.18: Secondary antibodies (used for western blot and staining)

Specificity	Conjugate	Dilution	Company
Goat-anti-mouse IgG	HRP	1 : 10000	Santa Cruz Biotechnology
Goat-anti-mouse IgG	Alexa Fluor 633	1 : 1000	Life Technologies

Table 2.19: Dyes used for staining fixed cell

Description	Specificity	Dilution	Company
DAPI	DNA	1 : 2000	Sigma-Aldrich
Rhodamine-phalloidin	F-actin	1 : 1000	Life Technologies
Alexa488-phalloidin	F-actin	1 : 1000	Life Technologies

2.1.5 DNA plasmids

Table 2.20: DNA plasmids used for cloning and transfections

Name	Description	Source
delCMV-EGFP-C1	EGFP low expression	This thesis
pEGFP-C1	EGFP expression	Clontech Laboratories
mCherry-C1	mCherry expression	Clontech Laboratories
delCMV-mCherry-RBD	mCherry labeled Rho activity sensor	Abram Calderon (University of Pennsilvania) (Graessl et al, submitted)
delCMV-EGFP-RBD	EGFP labeled Rho activity sensor	Abram Calderon (University of Pennsilvania) (Graessl et al, submitted)
delCMV-EGFP-FHOD1	EGFP labeled FHOD1 (low expression)	Matthias Geyer (CAESAR, Bonn) (Schönichen et al, 2013)
mKate-paxillin	mKate labeled paxillin	Eli Zamir (MPI Dortmund) (Hoffmann et al, 2014)
delCMV-EGFP-actin	EGFP labeled actin (low expression)	Naoki Watanabe (Tohoku University, Japan) (Watanabe und Mitchison, 2002)
delCMV-mCherry-actin	mCherry labeled actin (low expression)	This thesis
EGFP-NMHCIIA	EGFP labeled myosin-IIa heavy chain	Addgene Plasmid 11347 (Wei und Adelstein, 2000)
mCherry-NMHCIIA	mCherry labeled myosin-IIa heavy chain	Addgene Plasmid 35687 (Dulyaninova et al, 2007)
EGFP-ARHGAP18 wt	EGFP labeled ARHGAP18 wildtype	Takeshi Senga (Nagoya University) (Maeda et al, 2011)
EGFP-ARHGAP18 R365A	EGFP labeled ARHGAP18 mutant, lacking GAP activity	Takeshi Senga (Nagoya University) (Maeda et al, 2011)
EGFP-p190RhoGAP	EGFP labeled p190RhoGAP wildtype	Keith Burridge (UNC, Chapel Hill) (Maddox and Burridge, 2003)

Table 2.20: DNA plasmids used for cloning and transfections (continued)

Name	Description	Source
EGFP-p190RhoGAP DN	EGFP labeled p190RhoGAP mutant, lacking GAP activity	Keith Burridge (UNC, Chapel Hill) (Maddox and Burridge, 2003)
EGFP-Myo9b	EGFP labeled Myosin9b wildtype	Martin Bähler (University of Münster) (van den Boom et al, 2007)
ArhGAP28 wt-V5	ARHGAP28 wildtype	Karl Kadler (University of Manchester) (Yeung et al, 2014)
ArhGAP28 R425A-V5	ARHGAP28 mutant, lacking GAP activity	Karl Kadler (University of Manchester) (Yeung et al, 2014)
EGFP-ARHGAP28 wt-V5	EGFP labelled ARHGAP28 wildtype	This thesis
EGFP-ARHGAP28 R425A-V5	EGFP labelled ARHGAP28 mutant, lacking GAP activity	This thesis
CRISPR/Cas9 ARHGAP18 KO	CRISPR/Cas9 ARHGAP18 knock-out plasmid	Santa Cruz Biotechnology
CRISPR/Cas9 ARHGAP18 HDR	RFP labeled CRISPR/Cas9 plasmid, mediating puromycin resistance	Santa Cruz Biotechnology
CRISPR/Cas9 Control	CRISPR/Cas9 Control plasmid, lacking knock-out sequence	Santa Cruz Biotechnology

2.2 Methods

2.2.1 Molecular biological methods

2.2.1.1 Determination of DNA concentrations

The DNA concentration of plasmid preparations and their purity can be spectrophotometrically documented, due to the light absorption of nucleic acids that is caused by heterocyclic ring structures. The optical density (OD) of a watery solution containing 50 µg/ml double-stranded DNA at 260 nm is defined as 1. The absorption maxima of proteins is at 280 nm, thus the quotient OD_{260}/OD_{280} indicates the ratio between nucleic acids and proteins and therefore the purity of the DNA solution. A pure DNA solution has an OD_{260}/OD_{280} of 1.8. All spectrophotometrically measurements were performed with a Nanodrop spectrophotometer (ND-100, PeqLab) using pure solvent (water or EB) as reference.

2.2.1.2 Hydrolysis of plasmid DNA with endonucleases

Restriction with endonucleases is an important analytical method to characterize and isolate DNA segments. Furthermore it is a fundamental approach enabling the cloning of new plasmids, as further discussed in section 2.1.1.1. Restriction endonucleases recognize and bind to specific double-stranded DNA sequences. Afterwards they catalyze hydrolysis, preferably within these palindromic sequences at a defined points of intersection, creating DNA fragments with blunt or sticky ends. Here, restriction enzymes from New England Biolabs were used for molecular cloning (see section 2.1.1.1) or analytical double digestion. Thereto two different endonucleases were used simultaneously (double digestion), as indicated by the manufacturer. The resulting DNA fragments were separated via gel electrophoresis (see section 2.2.1.3).

2.2.1.3 DNA gel electrophoresis

After restriction with endonucleases, DNA fragments can be separated based on their size via gel electrophoresis. Thereto, an electric field is applied, moving the negatively charged DNA fragments through a matrix of agarose towards an anode, whereby the migration velocity is inversely proportional to the logarithmic length of the individual fragments. Depending on the size of the DNA segments, gels containing 0.5-2 % of agarose were used. For this purpose the required amount of agarose was dissolved in TAE buffer by heating. After a short cool-down period (~50°C), ethidium bromide was added (0.05 % (v/v)) and the mixture was poured into a gel electrophoresis chamber (MIDI-1 HU10, Roth). When the gel was solid, the chamber was filled with TAE buffer and loading dye in a ratio of 1:6 was added to the DNA samples, which were placed into the pockets of the agarose gel along with 5 µl of 1 kb DNA ladder (BioBudget). The separation was performed at 100 V for approx. 1 h, afterwards the DNA marked with ethidium bromide was visualized under UV-light (312 nm) and documented.

2.2.1.4 Cloning of GFP-fused ARHGAP28 plasmids and delCMV-mCherry-actin

To construct a mCherry-fused actin plasmid and two ARHGAP28 plasmids containing EGFP, new DNA plasmids were cloned via restriction, gel purification and ligation, see Figure 2.1.

Figure 2.1: Schematic illustration of molecular cloning via restriction and ligation
Holding vector (A) and endpoint vector (B) are cut by specific endonucleases at unique recognition sites. Afterwards the backbone fragment (A) and the insert fragment (B) are isolated by gel purification and the insert is ligated into the new backbone. (This Figure was modified from [1]).

[1] Rebecca Tirabassi, *Foundations of Molecular Cloning-Past, Present and Future*
[Online Publication:] URL: https://www.neb.com/tools-and-resources/feature-articles/foundations-of-molecular-cloning-past-present-and-future [download: 10/06/2015, 14:58]

For this purpose different DNA plasmids were incubated with 5 U of each of the two restriction enzyme per µg DNA for 2 h (double digestion, see section 2.1.1.1). Table 2.21 summarizes the cloning strategies applied, Table 2..22 demonstrates exemplary conditions used for digestion.

Table 2.21: Cloning strategies

New Plasmid	Backbone fragment	Insert fragment
delCMV-mCherry-actin	Double digestion (AgeI/XhoI) of delCMV-EGFP-actin	Double digestion (AgeI/XhoI) of mCherry-C1
EGFP-ARHGAP28 wt-V5	Double digestion (EcoRI/XmaI) of pEGFP-C1	Double digestion (EcoRI/AgeI) of ArhGAP28 wt-V5
EGFP-ARHGAP28 R425A-V5	Double digestion (EcoRI/XmaI) of pEGFP-C1	Double digestion (EcoRI/AgeI) of ArhGAP28 R425A -V5

Table 2.22: Example of double digestion conditions

Component	Volume	Initial concentration	Final quantity
AgeI	3 µl	10,000 U/ml	30 U
XhoI	1.5 µl	20,000 U/ml	30 U
CutSmart buffer	5 µl	10 fold	1 fold
pDNA (mCherry-C1)	6 µl	500 ng/µl	3 µg
Nuclease-free water	33.5 µl	-	up to 50 µl total reaction volume

After the plasmid DNA holding the insert, as well as the plasmid DNA designated as backbone were cut by endonucleases, 1 µl (5 U) of Antarctic Phosphatase (New England Biolabs) was added to the restriction solution containing the backbone fragment, followed by 1 h incubation at 37°C. This step removes the 5' phosphates of restricted DNA fragments, preventing self-ligation and hence minimizing the vector background. Afterwards both restricted fragments were isolated with gel electrophoresis (see section 0), purified with a gel extraction kit (Qiagen) and eluted in 30 µl nuclease-free water. These eluates were ligated at RT for 1 h with T4 DNA Ligase (New England Biolabs), using the conditions shown in Table 2.23.

Table 2.23: Exemplary conditions used for ligation

Component	Volume	Initial concentration	Final quantity
Backbone fragment (5077 bp)	1.5 µl	x	y
Insert fragment (734 bp)	10.5 µl	x / (5077bp/734bp)	y
T4 Ligase buffer	2 µl	10 fold	1 fold
T4 Ligase	1 µl	400,000 U/ml	400 U
Nuclease-free water	4 µl	-	up to 20 µl total reaction volume

The ligated DNA solutions were used to transform competent *E. coli* cells, as described in section 2.2.1.6.

2.2.1.5 Preparation of heat-shock competent *E.coli*

The preparation of heat-shock competent *E. coli* cells was done according to Chung et al. (Chung et al, 1989). Thereto 4 ml of antibiotic-free LB-medium were inoculated with 10 µl bacterial suspension (DH5α, Invitrogen) and incubated shaking for 14-16 h (37°C; 180 rpm). The next day this overnight culture was used in turn to inoculate 400 ml warm LB-medium, which were incubated shaking (180 rpm) until an OD_{600} of 0.5 was reached. At this point the bacterial suspension was incubated for at least 20 min on ice and sedimented by centrifugation (10 min, 4000 rpm, 4°C), before resuspension in 15 ml ice cold TSS buffer. Finally, the suspension of competent bacterial cells was portioned in 200 µl aliquots, shock frosted in liquid nitrogen and stored at -80°C.

2.2.1.6 Bacterial (re-)transformation using heat-shock

To transform the competent *E.coli* cells derived previously (see section 2.2.1.1) with plasmid DNA, aliquots of the bacterial suspension were thawed on ice, before 1 or 7 µl DNA were added for retransformations of plasmid or transformations of cloned DNA. After an incubation on ice for at least 30 min, the heat-shock was administered for 90 s at 42°C, followed by another incubation on ice for 90 s. Afterwards 800 µl of antibiotic-free LB-medium were added to each tube, which were then incubated shaking (180 rpm) at 37 °C for 60-90 min. The bacterial cells were sedimented by centrifugation (3 min, 13000 rpm) and 800 µl of the supernatant were discarded, while the remaining media was used to resuspend the pelleted *E.coli* cells. The resulting suspension was plated on LB Agar plates containing the corresponding and incubated overnight at 37°C. For storage, the plates covered with bacterial colonies were kept at 4°C for no longer than three weeks.

2.2.1.7 Preparation of bacterial glycerol stocks

In order to conserve the cloned DNA plasmids in bacterial glycerol stocks, 4 ml LB-medium (containing the respective antibiotic) were inoculated with a single bacterial colony obtained from transformation and incubated overnight shaking (37°C; 180 rpm). The next day 500 µl of the overnight culture were mixed with 500 µl glycerol (50 % (v/v)) and stored at -80°C.

2.2.1.8 Isolation of plasmid DNA from *E.coli*

To purify small amounts of plasmid DNA from bacterial overnight cultures, the QIAprep Spin Miniprep Kit (Qiagen) or the GenElute Plasmid Miniprep Kit (Sigma-Aldrich) were used as indicated by the manufacturer. Isolation of DNA on a larger scale, was performed with the QIAprep Spin Maxiprep Endofree Kit (Qiagen).

2.2.2 Biochemical methods

2.2.2.1 Protein extraction from cultured cells

To extract proteins from adherent eukaryotic cells, RIPA buffer (originally developed for radioimmunoprecipitation assays) was utilized in combination with a protease-inhibitor cocktail (see Table 2.14). To this end, cells cultured on 10 cm dishes [6-well plates] were washed with 10 ml [1 ml] ice cold PBS buffer, before 300 µl [75 µl] of RIPA buffer were added to each dish [well]. The cells were scraped off using sterile, kinked pipette tips, the lysates were placed in cold tubes and centrifuged for 15 min at 4°C (14000 rpm). The sediment containing cell debris and unbroken cells was discarded, while the supernatant was placed in a fresh, cold tube and the concentration of total protein was determined (see section 2.2.2.2), followed by SDS-PAGE, western blot and immunodetection, see sections 402.2.2.3 and 2.2.2.4 .

2.2.2.2 Determination of protein concentration

The concentration of the isolated protein lysates was ascertained by the Bradford method (Bradford, 1976), which is based on the shift in maximal absorbance of Coomassie Brilliant Blue G250. If the sulfonic acid groups of the dye bind to basic amino acids (mainly arginine, lysine and histidine) of proteins, its maximal absorbance is shifted from 470 nm to 595 nm. This color change of the dye from red to blue is measurable via the level of absorbance at 595 nm. By comparison to a standard curve, generated with samples of defined protein concentration, concentrations of proteins can be determined. Thereto Bradford-solution (BioRad) was diluted 1:5 in water and 1 ml of this assay buffer was mixed with 5 µl of five BSA solutions of varying concentrations (0.4; 0.8; 1.2; 1.6; 2.0 µg/µl in Tris-HCl Buffer) each, as well as 5 µl of fresh cell lysate. All samples were prepared as duplicates and incubated for 5 min at RT, before the absorbance at 595 nm was documented with a spectrophotometer (Thermo Scientific).

2.2.2.3 SDS-PAGE

Continuous SDS-polyacrylamide gel electrophoresis, developed by Laemmli, is a widely-used technique to separate proteins according to their molecular weight (Laemmli, 1970). SDS (sodium dodecyl sulfate) plays a key role in this method, since it denaturizes the proteins and masks their electrical charges, generating micelles with a constant negative charge / mass ratio. The polyacrylamide gel hinders those micelles to move towards the anode if an electric field is applied, resulting in drift velocities inversely proportional to the molecular weight of the proteins. Here, polyacrylamide gels containing 5 % acrylamide-bisacrylamide mix (30 %) were used for stacking and 10 % gels for separating the proteins, see Table 2.24.

Table 2.24: Components of stacking and separating gels for SDS-PAGE

Component	10 % Separating gel (5 ml)	5 % Stacking gel (4 ml)
acrylamide-bisacrylamide (30%)	1.6 ml	0.67
SDS	0.05 ml	0.04 ml
APS (10 %)	0.05 ml	0.04 ml
TEMED	0.004 ml	0.004 ml
Stacking gel Buffer	-	0.5 ml
Separating gel Buffer	1.25 ml	-
Nuclease-free water	2 ml	2.7 ml

The separating gels were prepared first and layered with isopropanol to create an even boundary between stacking and separating gel. After the separating gel was polymerized, the isopropanol was discarded and the stacking gel mixture was added along with a 10-well comb (1 mm, BioRad). The cell lysates of known concentration derived earlier (see section 2.2.2.1) were denaturized with 5 fold protein loading dye for 10 min at 95°C. Of each cell lysate 100 µl were placed in the prepared gels, along with 5 µl prestained protein ladder (10 to 180 kDa, Thermo Scientific) and run at 40 mA constant current per gel, for approx. 1 h.

2.2.2.4 Western blot and immunodetection

Western blotting is a common method to identify and quantify specific proteins from complex mixtures of proteins, such as cell lysates. The proteins are separated by size (see section 2.2.2.3) and immobilized on a polyvinylidene difluoride (PVDF) membrane utilizing a semidry blotting chamber (Biometra). For this purpose, the separations gels were isolated and incubated in cathode buffer for 15 min. The PVDF membrane was activated with methanol for 30 s and washed with water for 30 s, before incubation in anode buffer II for 5 min. Gel, membrane and

six Whatman filter papers were stacked from anode to cathode of the blotting chamber, in the following order:
- Two filter papers soaked in anode buffer I
- One filter paper soaked in anode buffer II
- PVDF membrane incubated in anode buffer I
- Gel incubated in cathode buffer
- Three filter papers soaked in cathode buffer

The proteins were transferred at 20 V for 50 min, which was verified by staining the membrane with Ponceau S solution (Roth).

In order to precisely identify the immobilized proteins, primary antibodies were used that bind specifically to the target proteins (Tubulin or FHOD1). The secondary antibodies bind to the Fc region of immunoglobulins, specific for the organisms from which the primary antibody originated. Additionally the secondary antibodies are fused to horseradish peroxidase (HRP), enabling an enzyme-based quantification of the target proteins. To prevent unspecific binding of the antibodies, the PVDF membrane was incubated with blocking solution (5 % milk powder or 5 % BSA in TBS-T buffer) at RT for 1 h. Afterwards the membrane was immunostained (overnight, 4°C) with the primary antibody diluted in blocking solution (see Table 2.17 for dilution factors). The next day, unbound antibody was washed off by three incubation steps with TBS-T for 10 min, before the membrane was placed in blocking solution, containing the secondary antibody (see Table 2.18). After 1 h incubation at RT the secondary antibody was washed off with TBS-T again, whereat the last of the three washing steps (10 min, RT) was performed with TBS, to prevent an impairment of the detection reagent by the Tween enclosed in the TBS-T buffer. As detection reagent entry-level peroxidase substrate for enhanced chemiluminescence (ECL, SuperSignal West Pico, Thermo Scientific) was used for 5 min at RT. This substrate enables a quantitative detection of HRP activity, which was documented on a Fusion FX7 system and analyzed densitometrically using Bio1D software (PeqLab).

2.2.3 Cell biological methods and microscopy

All experiments were performed with the human osteosarcoma cell line U2OS that was derived from a sarcoma of the tibia in 1964 and is widely used for studies of the actin cytoskeleton. Compared to other osteosarcoma cell lines, they have the lowest number of chromosomal variations and are less aggressive than for instance Saos-2 (Sarcoma osteogenetic) cells (Niforou et al, 2008). Their epithelial morphology combines migratory behavior with a

pronounced stress fibers network, composed of all three stress fiber types described for mammalian cells (reviewed in Small et al, 1998).

All cell cultural methods involving direct handling of living cells were performed under sterile conditions in a biosafety cabinet (Thermo Scientific). U2OS cells were cultured at constant temperature (37°C), carbon dioxide concentration (5 %) and high humidity (90-95 %) in a CO_2-incubator (Thermo Scientific). At regular intervals, the cells were examined microscopically for bacterial contaminations, an infection with *mycoplasma* was excluded by periodic testing (VenorGeM, Minerva Biolabs).

2.2.3.1 Subculture of adherent cells

Working stocks of U2OS cells were cultured in polystyrene dishes, suitable for sensitive adherent cells (35 x 10 mm, Cell+, Sarstedt). Every three to four days, when a confluency of 80-90 % was reached, the cells were seeded into fresh growth medium (see Table 2.8). Thereto aliquots of growth media, PBS and trypsin were warmed up in a water bath (37°C), before the adherent cells were washed with 10 ml PBS and incubated with 2 ml of trypsin at 37°C. After 5 min the cells were examined with a light microscope and incubated for another 2-5 min, if some cells still remained attached to the surface. When all cells were brought into suspension, trypsin was inactivated by addition of 8 ml warm growth medium and clustered cells were split up by pipetting up and down several times. The number of cells in the suspension was determined using a counting chamber (Improved Neubauer, depth 0.1 mm, Hartenstein) and 3-4 $x10^5$ cells were added to a new dish, filled with 10 ml fresh growth medium. This procedure was repeated up to passage twenty, before a new, low-passage cell stock of U2OS cells was thawed and cultivated (see next section).

2.2.3.2 Cryopreservation of cells

To conserve cells during long-term storage, they are frozen at -150°C, inhibiting enzymatic or chemical activity that could damage the cells. The major problem in cryopreservation is reaching low temperatures without the formation of intercellular ice crystals, which is solved by DMSO addition and the usage of a cryo freezing container that cools down the cells very slowly, with a rate of 1°C / h. In detail, e.g. ten dishes with U2OS cells of 70 % confluency were washed and trypsinized as described in section 2.2.3.1, before addition of 4 ml growth media per dish and sedimentation by centrifugation (5 min, 1000 rpm). The supernatant was discarded and the cell pellet was resuspended in 8 ml freezing medium (growth medium, containing 5 % DMSO). The resulting cell suspension was aliquoted in cryogenic tubes (Roth),

which were placed in an isopropanol-filled cryo freezing container (Sigma-Aldrich) and frozen overnight at -80°C. The next day the tubes were transferred into a -150°C freezer for long-term storage.

To put stored U2OS cells into culture, aliquots were transported on ice and incubated in a water bath (37°) just until the cell suspension was thawed. At this point, the cells were transferred into 14 ml of warm growth medium and centrifuged for 5 min at 1000 rpm. The DMSO-containing supernatant was discarded, while the pelleted cells were resuspended in 5 ml warm growth medium and placed into a 10-cm dish filled with 5 ml warm growth medium, which was cultured at 37°C.

2.2.3.3 Transient transfection with siRNAs and plasmid DNAs

The transient transfection with siRNAs was performed 72 h prior to live-cell imaging and western blot using the Fast-Forward transfection reagent HiPerFect (Qiagen). This method is constituted by simultaneous cell seeding and transfection. To this end, transfection solutions were prepared, consisting of 8 µl HiPerFect and up to 100 µl OptiMEM (Life Technologies) per well, mixed with 10 nM FHOD1 or non-targeting siRNA and incubated for 10 min at RT. During that time, U2OS cells were trypsinized (as described in section 2.2.3.1) and 1.5 $x10^5$ cells were seeded in 2 ml antibiotic-free growth medium per well of a 6-well plate. Of the transfection solutions 100 µl were trickled carefully on each well, before the plates were incubated at 37°C. After 24 h the cells were plated in fresh growth medium on collagen-coated glass bottom dishes (MatTek Corporation) for live-cell imaging, or on 6-well dishes for western blot.

The transfection with plasmid DNAs was done 15-24 h before imaging and western blot, thus 48 h after siRNA transfection and 24 h after plating on collagen-coated glass bottom dishes. The transfection solutions were prepared by incubating 3 µl Lipofectamine 2000 (Life Technologies) in 97 µl OptiMEM per dish for 5 min at RT. Afterwards, 100 µl DNA solution (150-1000 ng DNA in 100 µl OptiMEM) were added and the mixture was incubated for 20 min at RT. Fresh growth medium was filled in the dishes and 200 µl of the transfection solution was trickled carefully on each dish. The transfected cells were incubated at 37°C overnight, before the medium was exchanged against fresh growth medium or imaging medium, see also section 2.2.3.5.

2.2.3.4 Stable transfection with CRISPR/Cas9 plasmids

The adaption of clustered, regularly interspaced, short palindromic repeats (CRISPRs), found in Archaea and bacteria, to generate RNA-guided nucleases has become a widespread approach for targeted genome editing (Sander and Joung, 2014; reviewed by Jeffry and Keith, 2014). This new technique enables sequence-specific targeting of CRISPR-associated (Cas) nuclease that induce a double-stranded break (DSB) in the target DNA, leading to specific gene knockout (KO) (Jinek et al, 2012; Gasiunas et al, 2012). To create a stable KO-cell line it is crucial to select transfected cells with antibiotics, which is achieved by the insertion of a Homology-Directed-Repair (HDR) plasmid into the cleavage site of the CRISPR/Cas9 plasmids (Ran et al, 2013). Besides a resistance for puromycin, this plasmid mediates the expression of a red fluorescent protein (RFP), allowing to control the transfection state microscopically. In this thesis the CRISPR/Cas9-system was used to generate a stable U2OS cell line, lacking ARHGAP18. For this purpose, a dose response curve (kill curve) for puromycin was established for U2OS cells, to determine the optimal dosage for the later selection of transfected cells. Thereto 2 x10^5 cells were plated in each well of a 6-well plate and incubated at 37°C for 24 h. The next day different concentrations of puromycin (0.1-1.2 µg/µl) were added to the wells and the cell viability was monitored over the next four days. Thus a puromycin concentration of 1 µg/µl was defined for initial selection.

The transfection of cells with CRISPR/Cas9 plasmids (Santa Cruz Biotechnology) was performed as described in section 2.2.3.3 with 1 µg CRISPR/Cas9 ARHGAP18 KO plasmid and 1 µg CRISPR/Cas9 ARHGAP18 HDR plasmid per well, followed by 24 h incubation at 37°C and initial selection with puromycin for three days. Afterwards the cells were transferred into growth medium with 0.1 µg/µl puromycin to maintain selection pressure and examined via confocal microscopy and live-cell TIRF studies.

2.2.3.5 Sample preparation for live-cell imaging and drug treatments

For live-cell experiments glass bottom dishes and elastomeric substrates were coated with collagen type I, to create an ideal environment for U2OS cell that is suitable for high resolution microscopy. To it, a solution of 1% (v/v) collagen (from rat tail, type I, BD Bioscience) in PBS was pipetted on top of the glass or elastomeric surfaces within the dishes, which where incubated for 1-2 h at 37°C or overnight at 4°C. The abundant collagen was washed off with 3x 1 ml PBS and 1.5 x 10^5 U2OS cells were plated in 2 ml growth medium on each dish. After an incubation at 37°C for 24-30 h, the cells were transfected with Lipofectamine 2000, as described in section 2.2.3.3.

In order to study dynamic oscillations in spreading cells, the transfer to glass bottom dishes was carried out 30 min before live-cell imaging. To this end, U2OS cells with a confluency of 80 % were plated on 6-well plates (1.5 x10^5 cells per well) 48 h prior to imaging and transfected the next day using Lipofectamine 2000, see section 2.2.3.3. Immediately before imaging, the transfected U2OS cells were washes with 1 ml warm PBS and incubated with 200 µl trypsin for 5 min. When all cells were detached, the trypsin was inactivated with 800 µl imaging medium (see Table 2.8) and 500 µl of the cell suspension was pipetted on a collagen-coated glass bottom dish filled with 1.5 ml imaging medium.

To examine the effect of Rho and acto-myosin activity levels on oscillatory behavior, several activating and inhibiting drugs (or their solvent as control) were applied before or during microscopic measurements. For the latter, cells were imaged in 2 ml imaging medium (pre), before the drug was added in 1 ml warm imaging medium. Table 2.25 displays the respective final concentrations and incubation times preceding a second TIRF measurement (post).

Table 2.25: Conditions used for drug treatments

Drug	Final concentration	Incubation period
Blebbistatin	50 µM	60 min
Cytochalasin D	2 µM	15 min
Latrunculin A	0.6 µM	25 min
Nocodazole	30 µM	30-90 min
Y-27632	50 µM	30 min

2.2.3.6 Live-cell TIRF and spinning disc microscopy

Total internal reflection fluorescence (TIRF) microscopy takes advantage of the electromagnetic field (also called evanescent wave) formed, when the incident angle of the exciting laser is chosen in a way that all light is internally reflected at a solid-liquid interface, see Figure 2.2. The evanescent wave has a defined depth, penetrating only approx. 100 nm into the sample, which can be used to illuminate cells contacting the surface, as first suggested by Ambrose in 1956 (Ambrose, 1956). In the 1980s, Axelrod and colleagues applied this idea to visualize cell-substrate contacts and study biological molecules (Axelrod, 1981; Axelrod et al, 1984). Today, TIRF microscopy is a widely used method to visualize fluorescent molecules close to the membrane with high spatial resolution and low phototoxicity, as well as minimal background signal (reviewed by Axelrod, 2008; Fish, 2009).

Some TIRF experiments of cells plated on glass bottom dishes and spinning disc measurements of cells on elastomeric substrates were obtained on a Nikon *Eclipse* T*i*-E, inverted microscope

equipped with an Apo TIRF 100×1.49 NA oil immersion objective, a Clara Interline CCD camera (Andor Technology) and an iXon3 897 single photon EMCCD camera (Andor). For the excitation of GFP and RFP, laser light with wavelengths of 488 or 561 nm was emitted by an AOTF Laser Combiner (Andor Technology) and filtered by a dual bandpass dichroic mirror (zt488/561rpc, AHF) for TIRF imaging, and a CSU Quad Dichroic mirror/emission filter set (405/488/568/647 nm; Semrock) for widefield imaging. Multiple positions were imaged at the same time (up to 40 frames with a frame rate of 3/min) or single cell measurements were performed (up to 300 frames with a frame rate of 20/min) under the control of Andor IQ Software (Andor Technology).

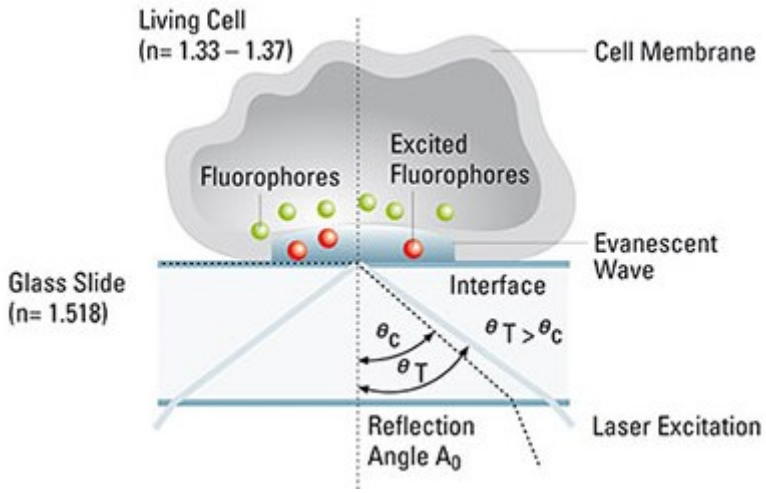

Figure 2.2 Principles of total internal reflection fluorescence (TIRF) microscopy.

Schematic drawing of TIRF illuminating a fluorescent labelled cell. The laser excitation is set at an angle such that the complete laser light is reflected at the oil-glass interface. This total internal reflection causes the appearance of an evanescent wave, passing through the cell with a penetration depth of approx. 100 nm, enabling the monitoring of membrane-based cellular processes. (This Figure was modified from the Leica brochure [2].

Both microscopic set ups comprise temperature-controlled incubation chambers, ensuring that all live-cell studies were carried out at a constant temperature of 37°C.

2.2.3.7 Sample preparation for the imaging of fixed cells

U2OS cells plated on elastomeric substrates and ARHGAP18-KO cells, derived with the CRISPR/Cas9-system (section 2.2.3.4), were fixed and subjected to morphological analysis. For this purpose, the actin cytoskeleton was stained with rhodamine-fused phalloidin, a phallotoxin that is found in the death cap mushroom (*Amanita phalloides*) and binds reversibly to filamentous actin. To visualize focal adhesions, the associated adapter protein paxillin was fluorescent labelled via immunostaining. Thereto, transfected U2OS cells were plated on

[2] Leica AM TIRF MC, *Visualize Life's Secrets with True MultiColor TIRF*
[Online Publication:] URL: http://www.leica-microsystems.com/fileadmin/downloads/Leica%20AM%20-TIRF% 20MC/Brochures/Leica_AM_TIRF_MC-Brochure_EN.pdf [download: 10/06/2015, 17:12]

elastomeric surfaces, as described in section 2.2.3.5 or on 24-well plates, containing collagen-coated coverslips (4 x10^4 cells per well). After a 24 h incubation period, the cells were fixed with formaldehyde solution (4 % (v/v) in PBS) for 20 min at 37°C, all following incubation steps were performed at RT. The formaldehyde was washed off with 3x 1 ml PBS for 5 min, before the cell membranes were permeabilized with Triton X-100 (0.2 % (v/v) in PBS) for 10 min and washed with 3x 1 ml PBS for 5 min again. The following staining was executed in a wet chamber in the dark, to minimize evaporation and photobleaching. To saturate nonspecific binding sites, elastomeric surfaces and coverslips were incubated with blocking solution (2 % (w/v) BSA in PBS) for 1 h. Afterwards the primary antibody (anti-paxillin, see Table 2.17*: Primary antibodies (used for western blot and staining)*) was applied for 1 h and washed off with 3x 1 ml PBS for 5 min. The secondary antibody, fused to Alexa 633 (see Table 2.18), was administered along with rhodamine- or Alexa488-phalloidin (1/1000 in 2 % (w/v) BSA in PBS) and DAPI (1/5000 in 2 % (w/v) BSA in PBS) for 1h. After three final washing steps with PBS for 5 min the surfaces and coverslips were mounted on glass slides and stored at RT, overnight in the dark. The next day, the samples were examined via confocal microscopy, sealed and stored at 4°C.

Confocal microscopy of fixed cells

Confocal laser scanning microscopy (CLSM) is a widely used high resolution imaging technique, allowing the recording of in-focus images from selected cell layers. The enhanced contrast is achieved by the suppression of stray light, emitted over or under the layer in focus. This is accomplished by a laser beam scanning the sample point-by-point and a detector that is focusing the emitted light via a variable pinhole aperture. A key feature of confocal microscopy is the visualization of three dimensional samples by recording Z-sequences of optical slices (image stacks) that can be reconstructed using maximum intensity projections. During this thesis, CLSM was conducted on a Leica TCS SP5 system equipped with a 63 ×1.45 NA oil immersion objective and two detector system (Photo multiplier and GaAsP-Hybrid-Detection system). Four lasers differing in excitation wavelength (405 mm (diode), 488 nm (Argon), 561 nm (DPSS) and 633 nm (helium-neon)) were used to illuminate the different fluorophores sequentially. The range of detection was set to 410-440 nm for DAPI, 495-540 nm for GFP, 570-625 nm for RFP and 640-720 nm for imaging Alexa-633. Image stacks comprising entire cells were acquired with an interval of 210 nm using LAS AF software (Leica). Maximum intensity projections were derived with ImageJ.

2.2.4 Data analyses

Imaging data was analyzed using Matlab R2015b and ImageJ 1.49 (http://imagej.nih.gov/ij/) running on Java 1.8 (64-bit). Statistical analysis and generation of graphs were performed using GraphPad Prism 5 software. All Figures were prepared with Adobe Photoshop CC2014. The analysis of the radial intensity distribution (section 2.2.4.3) was designed by Leif Dehmelt (MPI Dortmund / CCB, TU Dortmund). The analyses of oscillatory behavior (section 2.2.4.1 and 2.2.4.2) were developed in collaboration with Dr. Leif Dehmelt (MPI Dortmund / CCB, TU Dortmund) and Dr. Tomáš Mazel (Charles University, Prag).

2.2.4.1 Temporal crosscorrelation analyses

Temporal crosscorrelation functions were derived from image sequences obtained with a frame rate of 20/min and a 2x2 binning. To further eliminate the influence of noise, image x-y resolution was reduced by a factor of 15-20 via the averaging command in ImageJ. Afterwards, the Pearson crosscorrelation coefficient between time-shifted corresponding images was calculated pixel-wise, using custom Matlab scripts.

2.2.4.2 Analyses of oscillation amplitude, peak frequency and peak width

Image sequences were recorded with a frame rate of 3/min or 20/min and 2x2 binning. Using ImageJ, individual cells were isolated from these images, thresholded, masked and corrected for background intensity. Afterwards, image x-y resolution was scaled down by a factor of 15-20, to reduce noise. To avoid false measurements originating from fluctuations of cell protrusions, peripheral pixels were removed via a binary erode filter with a neighborhood count of 1. Global intensity fluctuation were excluded from the analyses by dividing each frame by the average background-corrected intensity. The remaining pixels were evaluated regarding their temporal intensity changes, to assess the local fluctuations associated with irregular oscillations. For this purpose, image series with a frame rate of 20/min were analyzed with a walking average of 7 frames and thus, the standard deviation of the intensity in each pixel over time was calculated. If the intensity at the given time-point differed by at least 1 % of the average intensity from the following and preceding intensity, a time-point was measured as a peak. To determine oscillation frequency, only peaks that were above 10% of the average intensity were included. As peak height, the difference between the intensity of a peak and the average intensity of the following and preceding minima was measured. The peak width, or duration, was determined as the time difference between two intensity minima.

2.2.4.3 Radial intensity distribution

The radial intensity distribution was analyzed from all 150 frames of each image series (frame rate 20/min), as described in Mohl et al, 2012. Accordingly, the centroid of each cell was determined for each frame using the built-in ImageJ function. The polar coordinate transformation was performed with an external ImageJ plugin (http://rsb.info.nih.gov/ij/plugins/polar-transformer.html). The resulting polar transformed images were interpolated to reach a constant radius. Finally, the average intensity distribution, relative to the cell centroid was calculated for all angles and frames via a custom-built ImageJ macro.

2.2.4.4 Morphological analyses

To assess morphological changes caused by depletion of ARHGAP18 or culture on elastomeric surfaces, fixed cells were imaged at a confocal microscope and analyzed with ImageJ. In detail, each cell was outlined manually and the cell area was measured using the built-in ImageJ function. The ImageJ plugin Shape descriptor (http://www.gcsca.net/IJ/Shapes.html) was applied to determine the circularity of the outlined cells. The circularity is thereby defined as 4π x area / perimeter^2. Consequently, a value of 1.0 would represent a perfect circle. As the value approaches 0.0, the cell shape becomes increasingly elongated.

2.2.4.5 Statistical analyses

For statistical evaluation, one-tailed t-tests were performed for data sets derived from the same cells (e.g. pre and post drug treatment), while two tailed-t-tests were used to analyze data sets from different cells. To verify that the temporal delays derived from crosscorrelation analyses are indeed unequal zero, one-sample t-tests were applied. P-values of t-tests are indicated by stars (*: $P<0.05$; **: $P<0.01$; ***: $P<0.001$; ****: $P<0.0001$). Mean values are denoted ± s.e.m. if the corresponding data sets comprised more than ten values, otherwise mean values are given ± s.e.. In all scatter dot plots mean values are illustrated by red lines.

3. Results

In the recent years a growing number of studies reported the emergence of travelling actin waves and excitable actin dynamics in both stationary and migrating cells (reviewed in Allard and Mogilner, 2013). Oscillatory behavior is also described for other proteins, such as the Arp2/3 activator Hem-1 or the formin-binding-protein FBP17 (Weiner et al, 2007; Wu et al, 2013). In this thesis, subcellular activity oscillations of the small GTPase Rho are reported in U2OS cells for the first time. Furthermore, the regulation of these oscillations via an excitable network consisting of multiple components is elucidated. For this, a Rho activity sensor for living cells developed by Abram Calderon (University of Pennsilvania) was used, comprising a fluorescent protein and the GTPase binding domain of the Rho effector Rhotekin (amino acids 8-89) (Graessl et al, submitted). This domain binds specifically to endogenous, active RhoA and RhoC, but only weakly to RhoB (Reid et al, 1996). The expression of the Rho activity sensor is under the control of a truncated CMV promotor (delCMV; Watanabe and Mitchison, 2002) in order to maintain a low expression level, minimizing the disruption of endogenous cellular processes. As Rho GTPases are localized to the plasma membrane, live-cell activity studies in U2OS cells were performed using Total Internal Reflection Fluorescence (TIRF) microscopy.

3.1 Environmental mechanosensation is mediated by Rho activity and acto-myosin oscillations

RhoA and its downstream effector Rho-kinase promote the formation of cortical acto-myosin structures, by phosphorylation of the actin motor protein myosin-II to generate contractile forces (Chen et al, 2002; Straight et al, 2003). Furthermore active RhoA was found to localize to the leading edge of migrating cells (Pertz et al, 2006), where it can induce membrane ruffling by recruitment of the formin mDia1 (Kurokawa and Matsuda, 2005). Cellular contractility and coordinated cellular protrusions are both critical elements during dynamic behaviors such as cell motility and spreading (Cai et al, 2010; Aratyn-Schaus et al, 2011).

3.1.1 Irregular oscillations of Rho activity and myosin-IIa localization in spreading U2OS cells

To investigate the subcellular dynamics of Rho activity and myosin-IIa localization at the cortex of spreading U2OS cells, live-cell TIRF microscopy was performed. For this, cells were transfected with pEGFP-NMHCIIa and the Rho activity sensor delCMV-mCherry-RBD (Rho-Binding-Domain), trypsinized and plated on collagen-coated glass-bottom dishes (MatTek) 30-60 min prior to time-lapse imaging.

Both, Rho activity (depicted as ImageJ Fire Look-Up-Table (LUT)) as well as the localization of non-muscle myosin heavy chain IIa could be observed at the plasma membrane (Figure 3.1.1a). In particular, near the cell center both fluorescent signals were found to oscillatory behavior (Figure 3.1.1b, black arrows). Interestingly, local Rho activity oscillations seem to precede a local increase in myosin-IIa intensity, see Figure 3.1.1c.

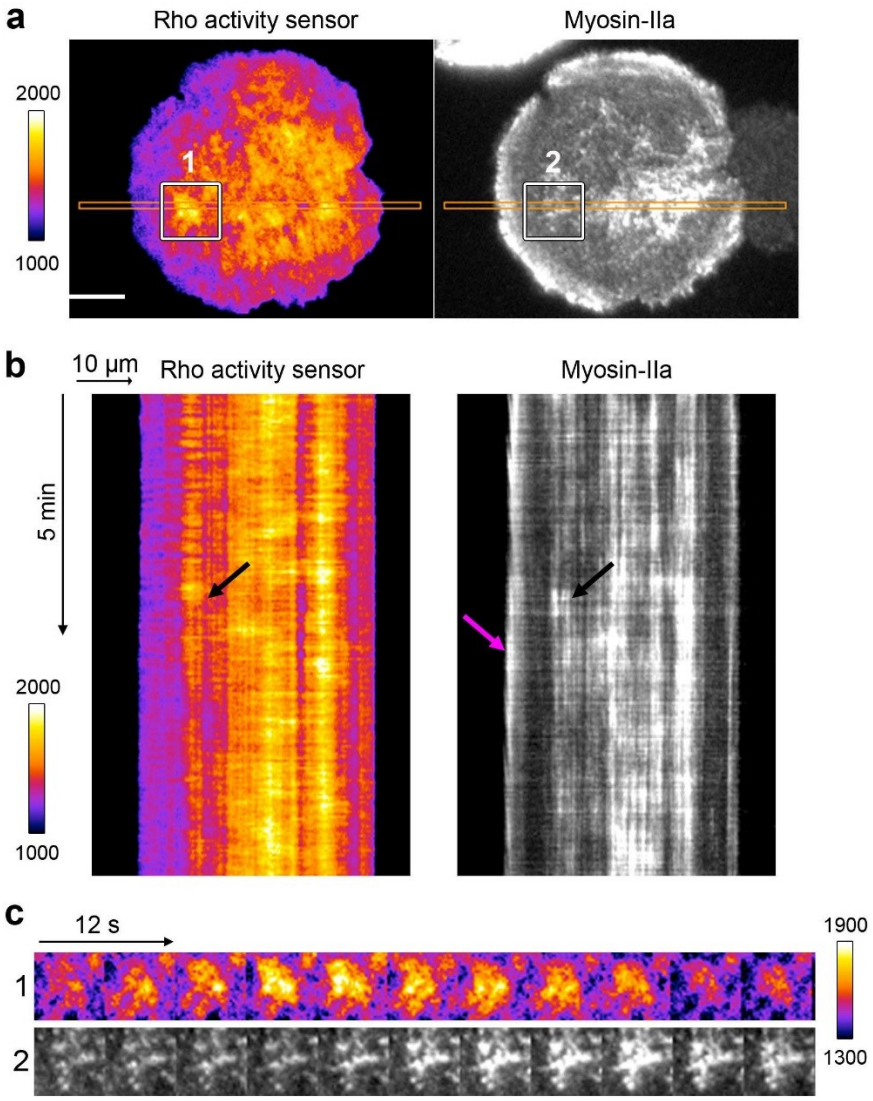

Figure 3.1.1: Irregular oscillations of Rho activity and myosin-IIa during cell spreading.

(a) Individual frames of a TIRF time-lapse micrograph of the Rho activity sensor (delCMV-mCherry-RBD, illustrated by ImageJ Fire Look-Up Table (LUT) and myosin-IIa (EGFP-NMHCIIa) intensity in a representative spreading U2OS cell (plated 30-60 min before imaging). **(b)** Kymographs display the signal dynamics of the areas indicated in **a** over-time (orange rectangles). **(c)** Enlarged regions indicated by white boxes in **a**. Scale bar: 10µm; calibration bars depict intensity in AU; frame rate: 20/min. N > 20 cells from three experiments.

In contrast to this prominent central localization, myosin-IIa localized additionally to the periphery of spreading cells (Figure 3.1.1b, pink arrow). To verify this observation, an ImageJ macro developed in collaboration with Dr. Leif Dehmelt (MPI Dortmund / CCB, TU Dortmund; see section 2.2.4.3) was used. For the analysis, first, polar transformations of signal distribution in N > 24 individual cells were generated. To this end, the center of the cells was determined via ImageJ, before the images were interpolated to reach a constant radius. Then, mean radial intensity plots were produced by calculating average Z-stack projections of these polar transformations. As a control for false positive signal accumulations, delCMV-EGFP-C1 construct was used.

Whereas the EGFP signal was found equally distributed throughout the cells, strong myosin-IIa accumulations were evident in the cell periphery (Figure 3.1.2a, right panel and b). In contrast, no pronounced Rho activity was detected in those regions (Figure 3.1.2a, mid panel and b).

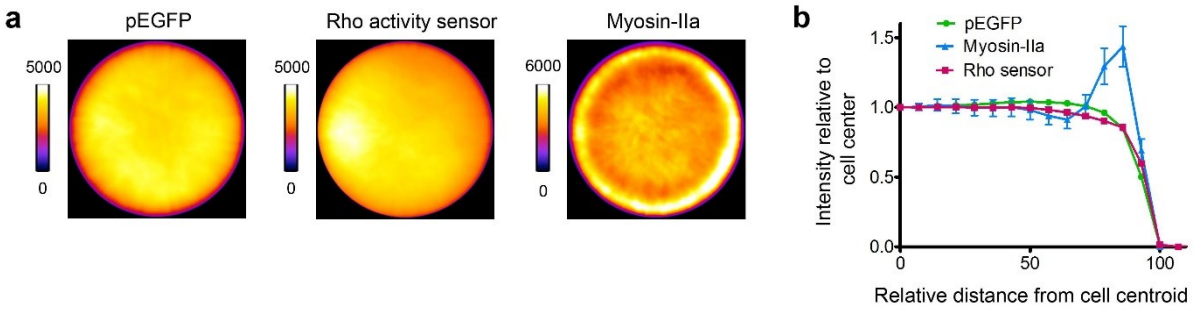

Figure 3.1.2: Radial intensity distribution during cell spreading: Myosin-IIa localizes to the cell center and periphery.

Average images of average intensity Z-projections of polar centroid transformations derived from fluorescence signals in spreading U2OS cells. N = 27 cells for delCMV-EGFP-C1 (right panel), N = 51 cells for delCMV-mCherry-RBD (mid panel) and N = 24 cells for EGFP-NMHCIIa (left panel) from 3 experiments. Signals are depicted as Fire LUT; calibration bars indicate intensity in AU (150 frames, frame rate: 20/min). **(b)** Plots displaying the mean intensities in relation to the distance from the centroid of the cells from **a**. Error bars show s.e.m..

The high correlation of Rho activity and myosin-IIa localization in the center of the cell, but not at the periphery, was further substantiated by crosscorrelation analyses of Rho activity and myosin-IIa localization in central and peripheral regions, respectively (Figure 3.1.3). For this purpose spreading U2OS cells of round shape were selected and their radius from the center to the periphery was measured in ImageJ. Afterwards the area within a circle of half the measured radius was defined as central region, the outside area as peripheral region.

In agreement with the results shown in the radial intensity analysis (Figure 3.1.2), crosscorrelation plots in Figure 3.1.3 reveal that the maximal mean crosscorrelation coefficient (r) of Rho and myosin-IIa is substantially high near the cell center (r =0.59 ± 0.05 s.e.m.) but relatively low and with large variability in the cell periphery (r =0.11 ± 0.16 s.e.m.). The significant difference in the crosscorrelation coefficients of subcellular activities suggests differential dynamic regulation of myosin-IIa downstream of Rho activity that might be linked to distinct cytoskeletal dynamics in those regions.

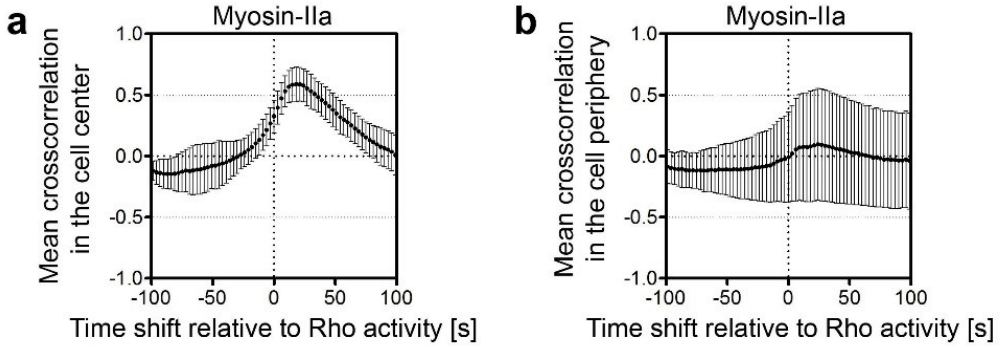

Figure 3.1.3: Crosscorrelation of Rho and myosin-IIa in the cell center but not the cell periphery.

(a-b) Mean temporal crosscorrelation of N = 5 U2OS cells from 3 experiments expressing EGFP-NMHCIIa and delCMV-mCherry-RBD. Error bars: 95% confidence interval. **(a)** Mean crosscorrelation between myosin-IIa and Rho intensity signals in the cell center or **(b)** the cell periphery.

3.1.2 Rho activity oscillations in stationary cells

Irregular oscillations of Rho activity in the cell center might relate to long term processes such as cell shape changes or mechanosensing. Thus, Rho activity was measured in stationary U2OS cells that were plated 48 h prior to imaging and transfected with the activity sensor delCMV-mCherry-RBD (see Figure 3.1.4). As a control, pEGFP-C1 was transfected as a measure for false positive TIRF signals such as due to plasma membrane dynamics.

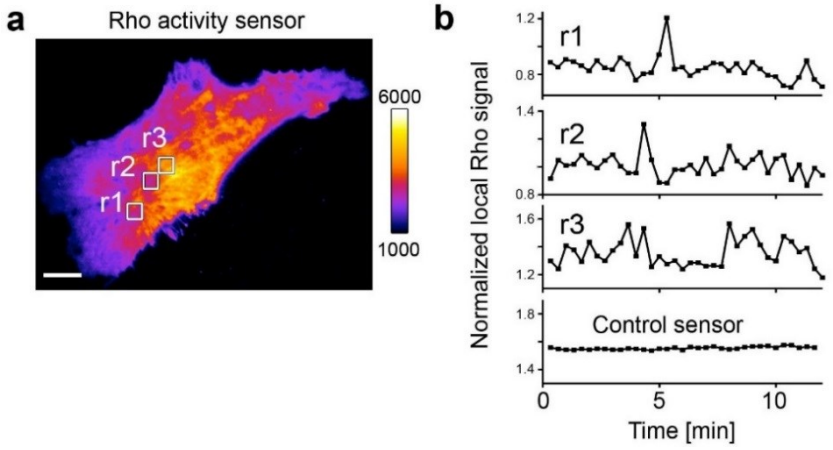

Figure 3.1.4: Irregular oscillations of active Rho in stationary U2OS cells.

(a) TIRF image of a resting cell, plated 48 h prior to imaging and transfected with the Rho activity sensor (delCMV-mCherry-RBD, depicted as Fire LUT). Scale bar: 10µm; calibration bar indicates intensities in AU. **(b)** Local Rho activity dynamics within areas marked by white boxes in **a,** normalized to background intensity. No oscillations are observed in cells expressing a control sensor (pEGFP-C1); N > 30 cells from three experiments.

Similar to spreading cells, Rho activity oscillations were observed in multiple subcellular central regions. In contrast, no oscillations were detected in cells expressing the control sensor (Figure 3.1.4b, bottom), demonstrating that mere dynamics of the plasma membrane is not sufficient to cause fluorescence oscillations.

3.1.3 Irregular oscillations of active Rho correlate with local actin dynamics

To further characterize the nature of the observed Rho activity oscillations in stationary cells, we investigated if those coincide with the dynamic actin reorganization at the cellular cortex. Cells were transfected with the Rho activity sensor along with delCMV-EGFP-actin to visualize spatio-temporal actin dynamics.

First observations revealed coinciding Rho activity and actin signal increase and decrease over time (Figure 3.1.5a). Measuring regional intensity profiles over time further confirmed the observed temporal correlation of signal dynamics in the two channels (Figure 3.1.5b).

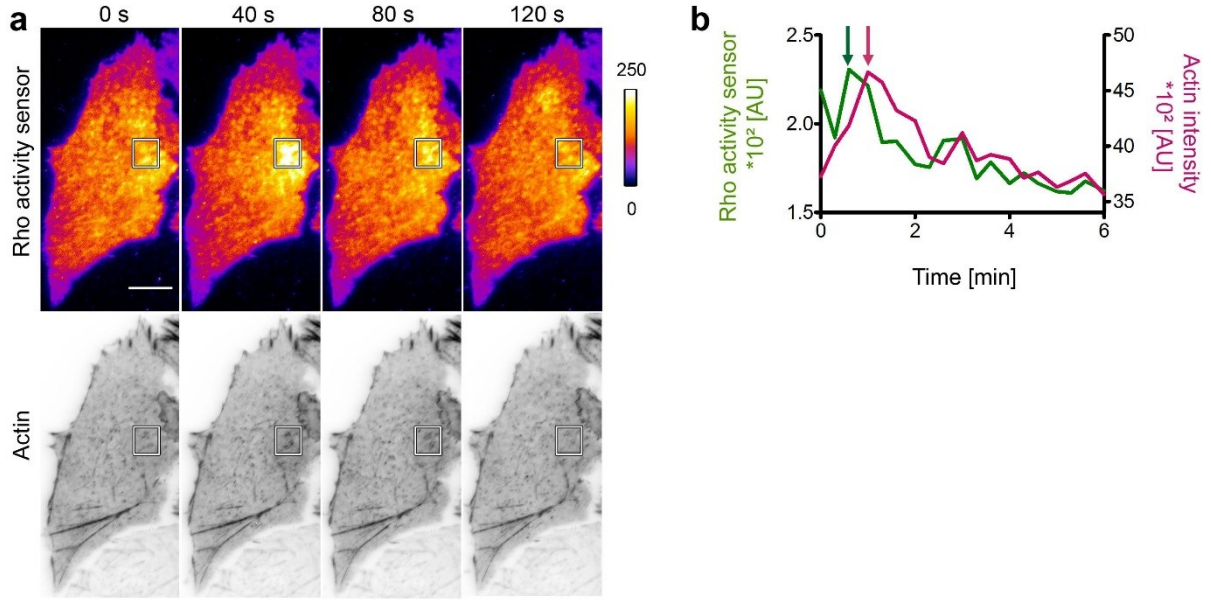

Figure 3.1.5: Correlation of actin localization and Rho activity in stationary U2OS cells.

(a) Individual TIRF time-lapse frames of a U2OS cell expressing the Rho sensor mCherry-RBD (top panels, depicted as Fire LUT) and delCMV-EGFF-actin (bottom, depicted as inverse LUT). Frame rate: 20/min; scale bar: 10µm; calibration bar indicates intensities in AU. **(b)** Intensity measurements within boxes marked in **a**, arrows indicate temporal delay**.** N > 20 cells from three experiments.

Based on the intensity profiles, it appeared that peak Rho activity precedes actin (delCMV-EGFF-actin) enrichment in the observed regions (Figure 3.1.5b, arrows). This temporal delay

of actin intensity oscillations was further characterized by crosscorrelation analyses, which is discussed in chapter (3.1.5).

Previously, several types of actin based oscillations or waves have been reported in various eukaryotic cell types (reviewed in Allard and Mogilner, 2012). In U2OS cells, only so called ventral actin waves (see section 1.2.1) are known so far (Case and Waterman, 2011). Ventral waves emerge by a mechanism dependent of Rac1 and seem to be regulated by Arp2/3 driven actin-polymerization and are relatively slow (1.61 ± 1.06 µm/min) with a lifetime > 1 min (Case and Waterman, 2011).

Here, we have observed that those actin waves described by Case and Waterman are indeed distinct from the irregular Rho activity oscillations depicted in Figure 3.1.5. In particular, irregular actin oscillations appear more diffuse and transient (Figure 3.1.6, duration 1 min) as compared to ventral waves (Figure 3.1.6, duration > 4 min). Interestingly, both types of actin dynamics can emerge simultaneously in the same U2OS cell, suggesting the co-existence of multiple signal networks in U2OS cells that can distinctly regulate dynamic organization of the cortical actin meshwork (Figure 3.1.6).

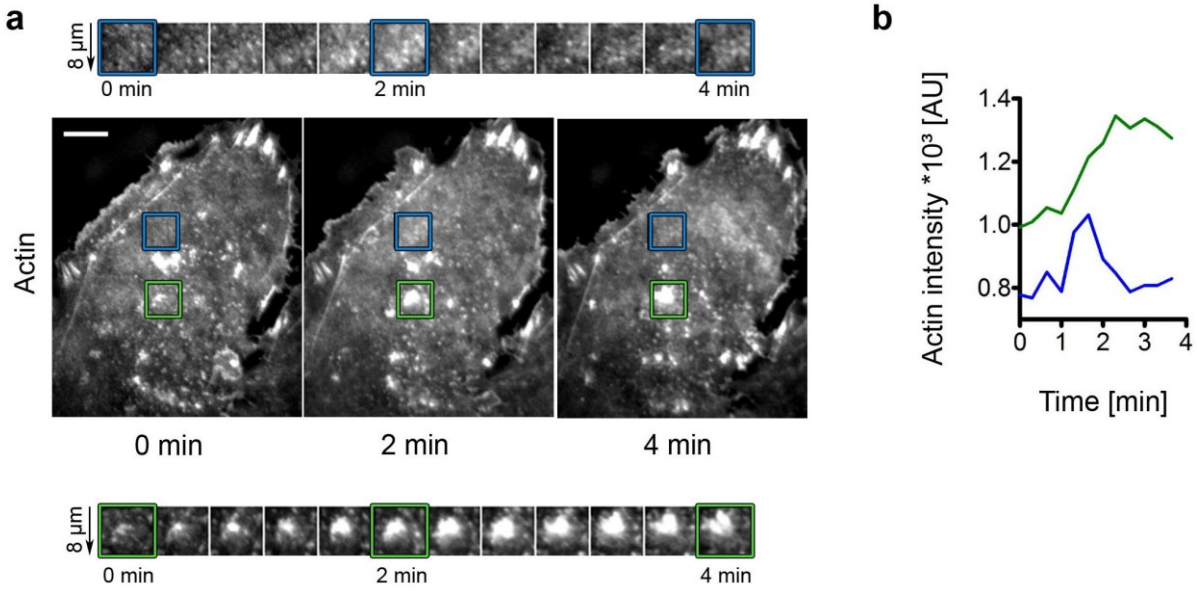

Figure 3.1.6: Ventral actin waves and irregular actin oscillations can occur concurrently in the same U2OS cell.

(a) Individual TIRF time-lapse frames of a U2OS cell expressing delCMV-EGFF-actin (frame rate: 20/min; scale bar: 10 µm). Upper panels: Enlarged images of a representative irregular actin oscillation depicted by the blue boxes (duration approx. 1 min). Lower panels: Enlarged images of a ventral F-actin wave depicted by the green boxes; duration > 4 min). **(b)** Intensity measurements within blue and green boxes marked in **a**. Green line represents the slow increase of intensity during the emergence of a ventral wave, the change of intensity caused by an irregular actin oscillation is illustrated in blue.

3.1.4 Irregular oscillations of Rho activity and actin cortex localization are enhanced by global Rho activation

The microtubule associated guanine nucleotide exchange factor GEF-H1 has been shown to be activated upon its release from microtubules, which can be caused by the microtubule-depolymerizing drug nocodazole. Global release of GEF-H1 by this treatment was shown to activate RhoA globally, leading to robust formation of stress fiber (Chang et al, 2008). In order to assess how global activation of RhoA might affect the local oscillations of the GTPase, Rho activity oscillations were measured in U2OS cells upon nocodazole treatment.

As displayed in Figure 3.1.7, the drug induced a significantly elevated emergence of transient intensity peaks, suggesting an oscillatory behavior (see Figure 3.1.7c). Notably, this peaks occurred not evenly throughout the cell, but localized to subcellular regions, as demonstrated in Figure 3.1.7b). This effect of nocodazole was confirmed by Johannes Koch by quantification of the baseline intensity and peak amplitude of N = 43 U2OS cell from three experiments (data not shown).

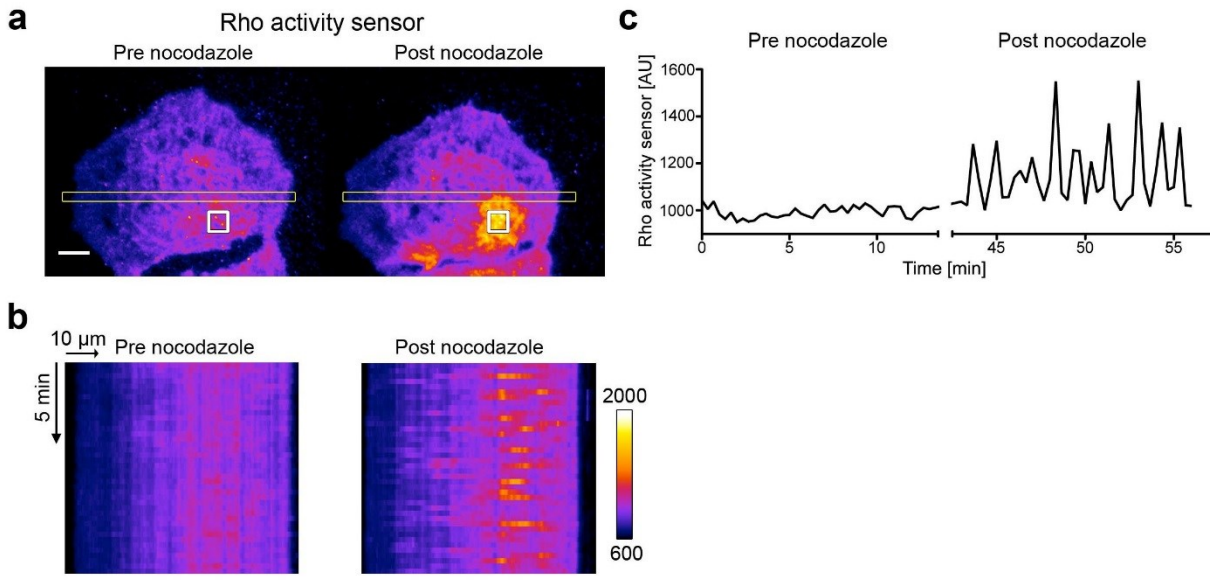

Figure 3.1.7: Global Rho activation enhances local activity oscillations.

(a-c) TIRF measurements of Rho activity in U2OS cells before and after stimulation via nocodazole-induced microtubule depolymerization (30 µM, 45 min). **(a)** TIRF images depicting Rho activity pre and post nocodazole treatment. The intensity of the Rho activity sensor (delCMV-mCherry-RBD) is illustrated as Fire LUT, the calibration bar indicates AU. Scale bar 10 µm; frame rate 3/min. **(b)** Kymographs corresponding to the regions labeled in **a** (orange rectangles). **(c)** Rho activity signal within the white boxes in **a**.

To investigate, if nocodazole induced enhanced Rho activity oscillations were translated into enhanced actin oscillations, cells were transfected with delCMV-mCherry-actin and the control construct delCMV-EGFP-C1, respectively and studied via time-lapse TIRF microscopy before and after treatment with nocodazole (30 µM, 45 min). Figure 3.1.8a-b illustrates a

representative cell and the corresponding intensity plot for actin and EGFP-C1 expression. Before nocodazole treatment, only seldom weak EGFP-actin oscillations were detected that were reminiscent of random signal fluctuations. In cells expressing EGFP control only, signal fluctuations were barely visible (Figure 3.1.8b, pre nocodazole). Nocodazole treatment strongly enhanced signal oscillations of EGFP-actin, whereas dynamics and intensity of EGFP alone was not altered (Figure 3.1.8b, post nocodazole). To better characterize the oscillations, amplitude and frequency was quantified as follows (see also section 2.2.4.2):

- **Peak amplitude [%]**: Difference in intensity between a maximum and the preceding and following minima, expressed in percent above average intensity.
- **Oscillation frequency [oscillations/min]**: Number of intensity peaks per minute that are above 10% of the average intensity.

Both, the amplitude and frequency of actin oscillations was significantly increased upon nocodazole treatment (Figure 3.1.8a-b). The peak amplitude of EGFP control intensity (delCMV-EGFP-C1) remained below 4 %, both before and after nocodazole treatment (Figure 3.1.8c). Thus, no oscillations were counted in the frequency analysis (Figure 3.1.8d). This verifies the independency of oscillations on plasma membrane movement and substantiates the finding that actin oscillations emerge downstream of active Rho.

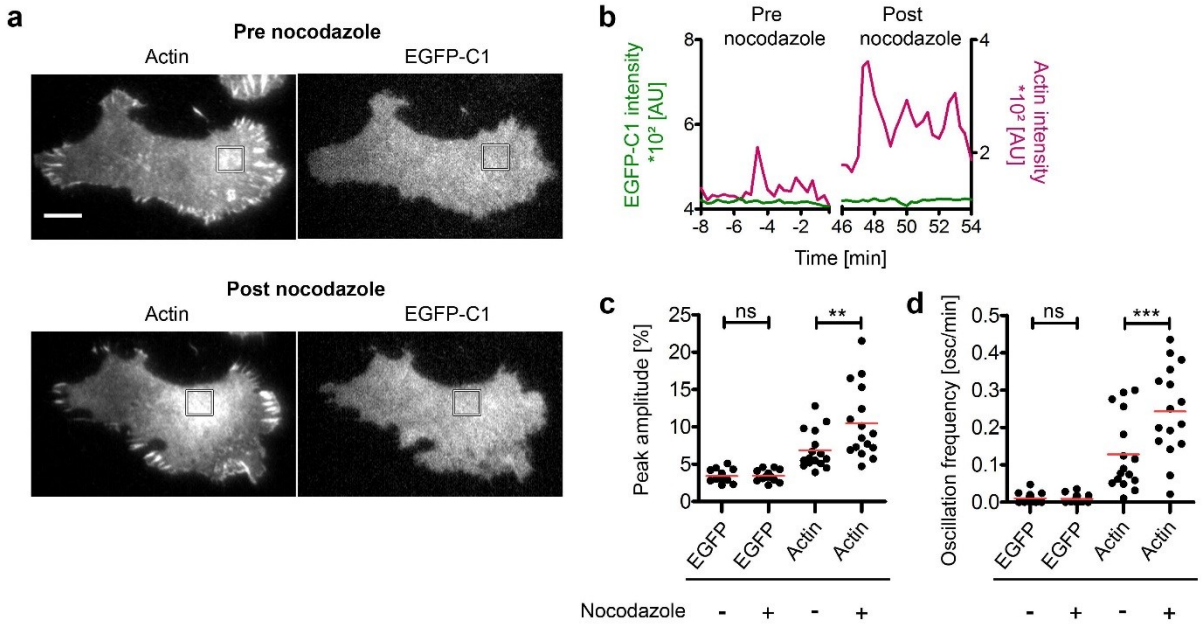

Figure 3.1.8: Global Rho activation enhances amplitude and frequency of actin cortex oscillations.

(a) Individual TIRF images of a representative U2OS cell expressing delCMV-mCherry-actin and delCMV-EGFP-C1, before and after nocodazole treatment (30µM, 45min). **(b)** Intensity plots of the regions marked in **a** (white boxes). **(c)** Peak amplitude (in percent of mean intensity) and **(d)** oscillation frequency (in oscillations per

minute) before and after treatment with nocodazole, N = 16 cells from 3 experiments. Red lines indicate mean; ***: P<0.001; **: P<0.01, ns: not significant in Paired t-test. Frame rate: 3/min. Scale bar: 10µm.

3.1.5 Crosscorrelation analysis reveals temporal delay between Rho activity and actin oscillations

As demonstrated by the fluorescence intensity plots in Figure 3.1.5b, a time shift between Rho activity maxima and actin intensity peaks was observed in unstimulated cells. The robust nature of Rho activity oscillations that were generated after nocodazole-induced microtubule-depolymerization, was used to quantify the time-shift observed between actin oscillations with respect to Rho activity. For this purpose, U2OS cells were transfected with the Rho sensor delCMV-mCherry-RBD, as well as delCMV-EGFP-actin and treated with 30 µM nocodazole 45-90 min before examination via time-lapse TIRF microscopy. For best possible temporal resolution, a frame rate of 20 frames per minute was set. Figure 3.1.9a-b show a representative cell and the corresponding intensity plots of Rho activity and actin oscillations. The crosscorrelation between these two dynamic patterns was quantified with the help of custom Matlab scripts, developed by Dr. Leif Dehmelt (MPI Dortmund / CCB, TU Dortmund) and Dr. Tomáš Mazel (Charles University, Prag) (see section 2.2.4.1). This pixel based whole cell analysis revealed a high maximal crosscorrelation between Rho activity and actin oscillations with a crosscorrelation coefficient of $r = 0.58 \pm 0.04$ s.e.m. (Figure 3.1.9c). Furthermore, the time point of maximal crosscorrelation for each cell was determined and those values were plotted in a frequency distribution graph, revealing a significant temporal delay of actin peak signals relative to Rho activity ($\Delta t = 11.0$ s $\pm$ 1.1 s.e.m.) (Figure 3.1.9d).

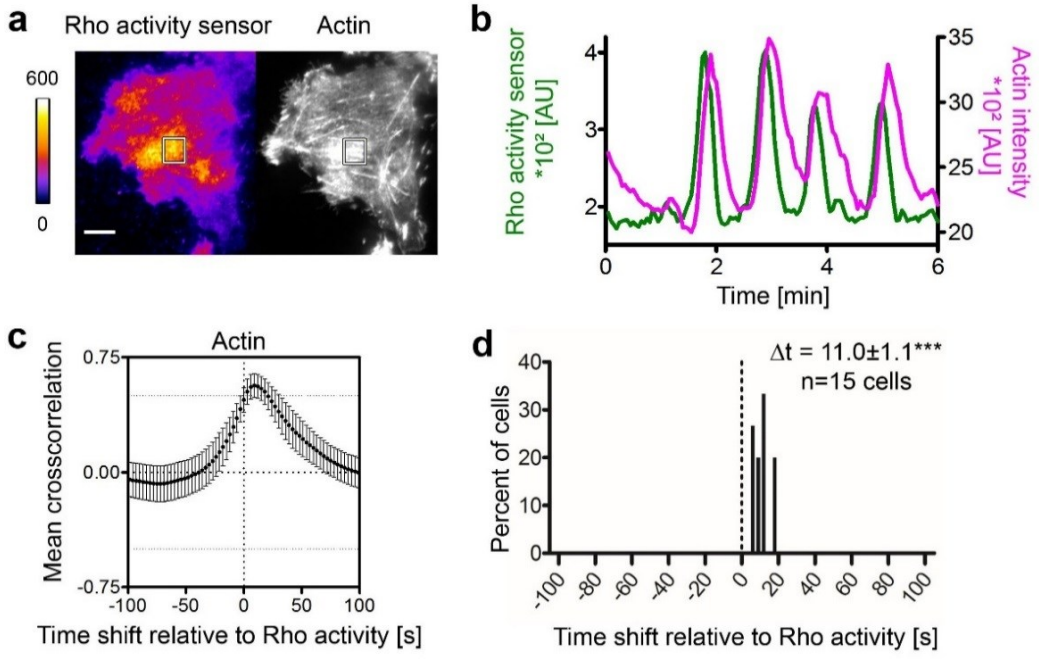

Figure 3.1.9: Quantification of the time-shift between local Rho activity and actin oscillations.

Temporal crosscorrelation analysis of U2OS cells transfected with the Rho activity sensor delCMV-mCherry-RBD (depicted as Fire LUT) and delCMV-EGFP-actin, recorded 45-90 min after nocodazole treatment (30 µM). **(a)** Individual frames of Rho activity and actin time-lapse TIRF measurements. The calibration bar indicates AU. **(b)** Intensity plots of regions marked by white boxes in **a**. **(c)** Mean temporal crosscorrelation function of Rho activity and actin (N = 15 cells from four experiments). Error bars show 95% confidence interval. **(d)** Percent of cells with given time shifts at the point of maximal crosscorrelation relative to Rho activation, derived from **c** (***: P<0.001 in one-sample t test; ±s.e.m.). Frame rate: 20/min, scale bar: 10µm.

3.1.6 Crosscorrelation analysis reveals a temporal delay between Rho activity and myosin-IIa oscillations

The shift in maximal crosscorrelation observed for spreading cells (section 3.1.1, Figure 3.1.3), suggested a time delay of myosin-IIa oscillations relative to RhoA activity. To quantify this delay more precisely, U2OS cells expressing the Rho activity sensor together with EGFP coupled myosin-IIa (pEGFP-NMHCIIa) were treated with nocodazole and the temporal crosscorrelation between the signals was calculated as described for actin (section 3.1.5). Significant crosscorrelation was measured (r = 0.42 ± 0.03 s.e.m.), albeit with a slightly lower crosscorrelation coefficient, compared to actin oscillations (Figure 3.1.9c). Maximal myosin-IIa cortex association was significantly delayed relative to Rho activity (Δt = 39.5 s ± 2.4 s.e.m.) (Figure 3.1.10). Interestingly, this is significantly higher, as compared to the time-shift between Rho activity and actin oscillations determined in section 3.1.5, suggesting a substantial delay of myosin-IIa cortex enrichment relative to actin localization.

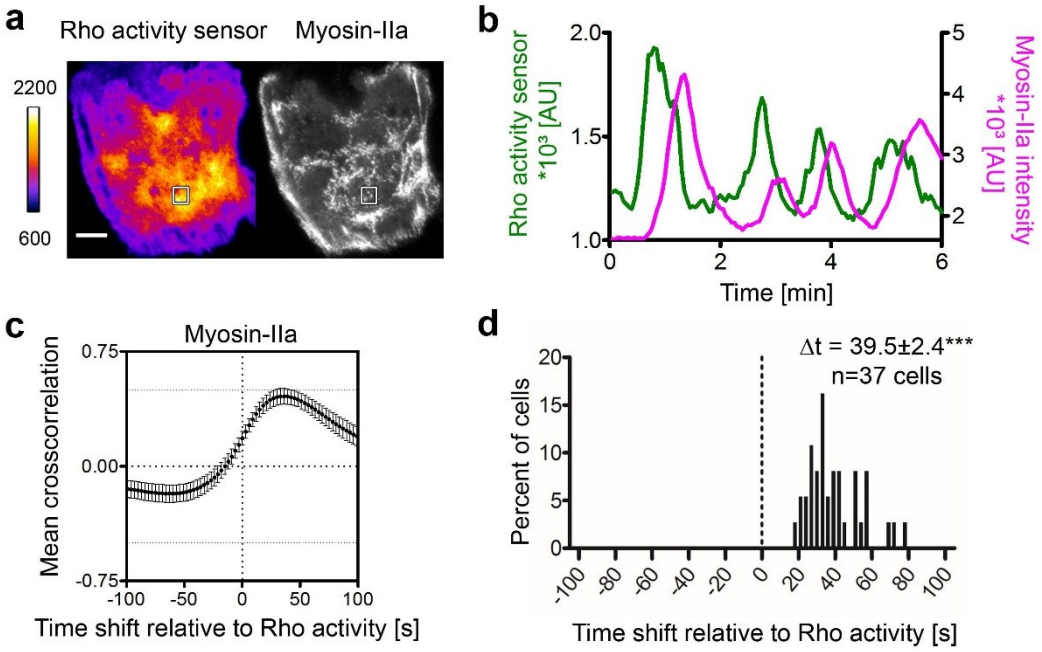

Figure 3.1.10: Quantification of the time-shift between local Rho activity and transient myosin-IIa accumulations.

Temporal crosscorrelation analysis of U2OS cells transfected with the Rho activity sensor delCMV-mCherry-RBD (depicted as Fire LUT) and EGFP-NMHCIIa, 45-90 min after nocodazole treatment (30 µM). **(a)** Individual frames of Rho activity and myosin-IIa time-lapse TIRF micrographs, the calibration bar indicates AU. **(b)** Intensity plots of regions marked by white boxes in **a**. **(c)** Mean temporal crosscorrelation function of Rho activity and myosin-IIa (N = 37 cells from three experiments). Error bars show 95% confidence interval. **(d)** Percent of cells with given time shifts at the point of maximal crosscorrelation relative to Rho activation, derived from **c** (***: P<0.001 in one-sample t test; ±s.e.m.). Frame rate: 20/min, scale bar: 10µm.

As control, the temporal crosscorrelation of Rho activity and exogenously expressed EGFP was quantified (N = 31 cells from three experiments). For this, U2OS cells were transfected with the Rho activity sensor delCMV-mCherry-RBD and pEGFP-C1 and treated with nocodazole (30 µM, 45-90 min). Similar to previous measurements, TIRF imaging was performed using high frame rate (20 frames per minute).

The measurements, presented in Figure 3.1.11, revealed a substantially low mean crosscorrelation value for EGFP and Rho activity (r = 0.20 ± 0.03 s.e.m.) as compared to actin or myosin-IIa. Furthermore, EGFP crosscorrelation maxima were not significantly delayed relative to Rho activity (Δt is undistinguishable from zero) (Figure 3.1.11c-d), further suggesting that simultaneous oscillations of Rho activity and actin cortex association are not due to unspecific reasons as simple colocalization or plasma membrane movements.

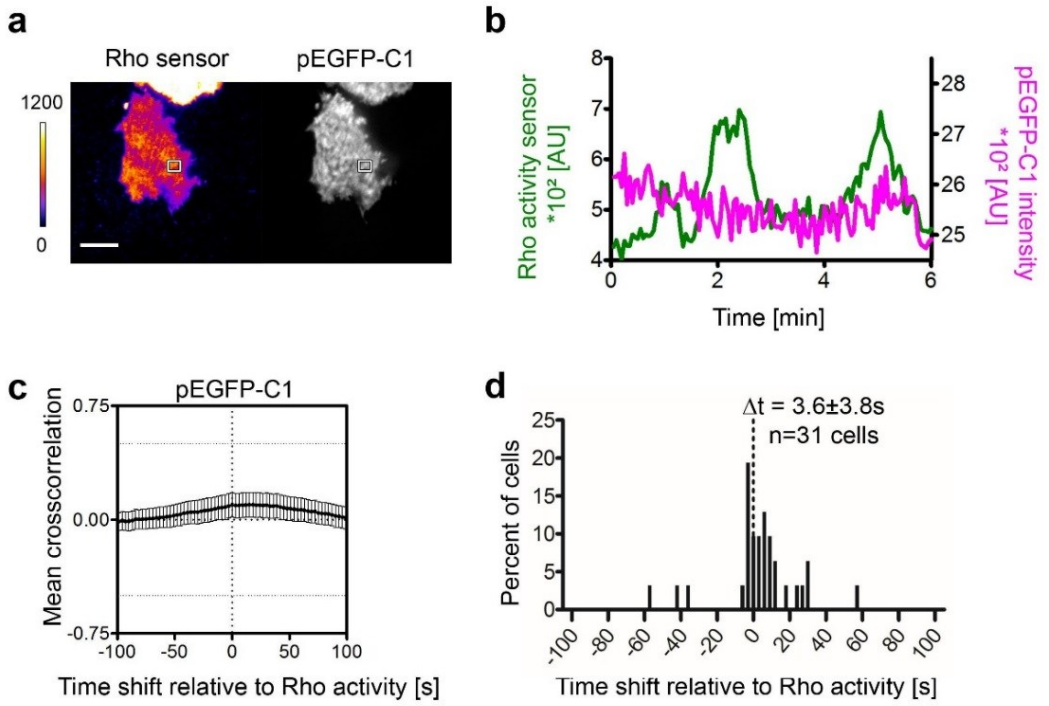

Figure 3.1.11: Quantification of the temporal crosscorrelation between local Rho activity and control EGFP intensity.

Temporal crosscorrelation analysis of U2OS cells transfected with the Rho activity sensor delCMV-mCherry-RBD and pEGFP, 45-90 min after nocodazole treatment (30 µM). **(a)** Individual frames of Rho activity (depicted as Fire LUT, the calibration bar indicates AU) and EGFP time-lapse TIRF micrographs. **(b)** Intensity plots of

regions marked by white boxes in **a**. **(c)** Mean temporal crosscorrelation function of Rho activity and cytosolic expressed EGFP (N = 31 cells from three experiments). Error bars show 95% confidence interval. **(d)** Percent of cells with given time shifts at the point of maximal crosscorrelation relative to Rho activation, derived from **c**. Frame rate: 20/min, scale bar: 10µm.

3.1.7 Substrate elasticity modulates the frequency of myosin-IIa intensity oscillations and cell morphology

As published in Schulze et al, 2014, endogenous myosin-IIa localizes to contractile stress fibers and focal adhesions of U2OS cells. Recent studies show that the association of myosin-IIa with focal adhesions acts as a regulator of migration and mechanosensing (Pasapera et al, 2015). Thus, impact of substrate elasticity on irregular oscillations of myosin-IIa cortex associations was assessed, using elastomeric surfaces that were kindly gifted by Dr. Bernd Hoffman (FZ Jülich). U2OS cells transfected with EGFP-NMHCIIa were plated on collagen-coated elastomeric substrates with a defined Young´s modulus (force per area unit, needed to compress or stretch solid materials) of 500 or 10 kPa (see section 2.2.3.4). As control cells were plated on collagen-coated glass-bottom dishes (MatTek), representing a surface of infinite stiffness with a very high Young's modulus (~70,000 kPa for soda lime glass (Oliver and Pharr, 1992)). Due to the thickness of the elastomeric layer (approx. 80 µm) that is not compatible with the low z-resolution in TIRF microscopy, the examination of samples was performed via spinning disc microscopy. First, the amplitude and frequency of EGFP-myosin-IIa oscillations was quantified in live-cell measurements. Then, each sample was fixed and stained with rhodamine labeled phalloidin and anti-paxillin antibody to visualize F-actin and focal adhesions, respectively. Based on this staining, circularity and adhesion area of cells plated on the different substrates was measured using the ImageJ Shape descriptors plugin (N > 169 cells for each condition) (see section 2.2.4.4).

A first examination of cellular morphologies in fixed cells suggested an increased number of protrusions on surfaces with a low Young's modulus (Figure 3.1.12a, yellow arrows). In particular, on 10 kPa substrates individual cell protrusions were most prominent. In agreement with this, cell area and circularity were significantly decreased on the 10 kPa elastomer (Figure 3.1.12b-c) as compared to glass and 500 kPa elastomers further supporting the increase of peripheral protrusions on softer substrate.

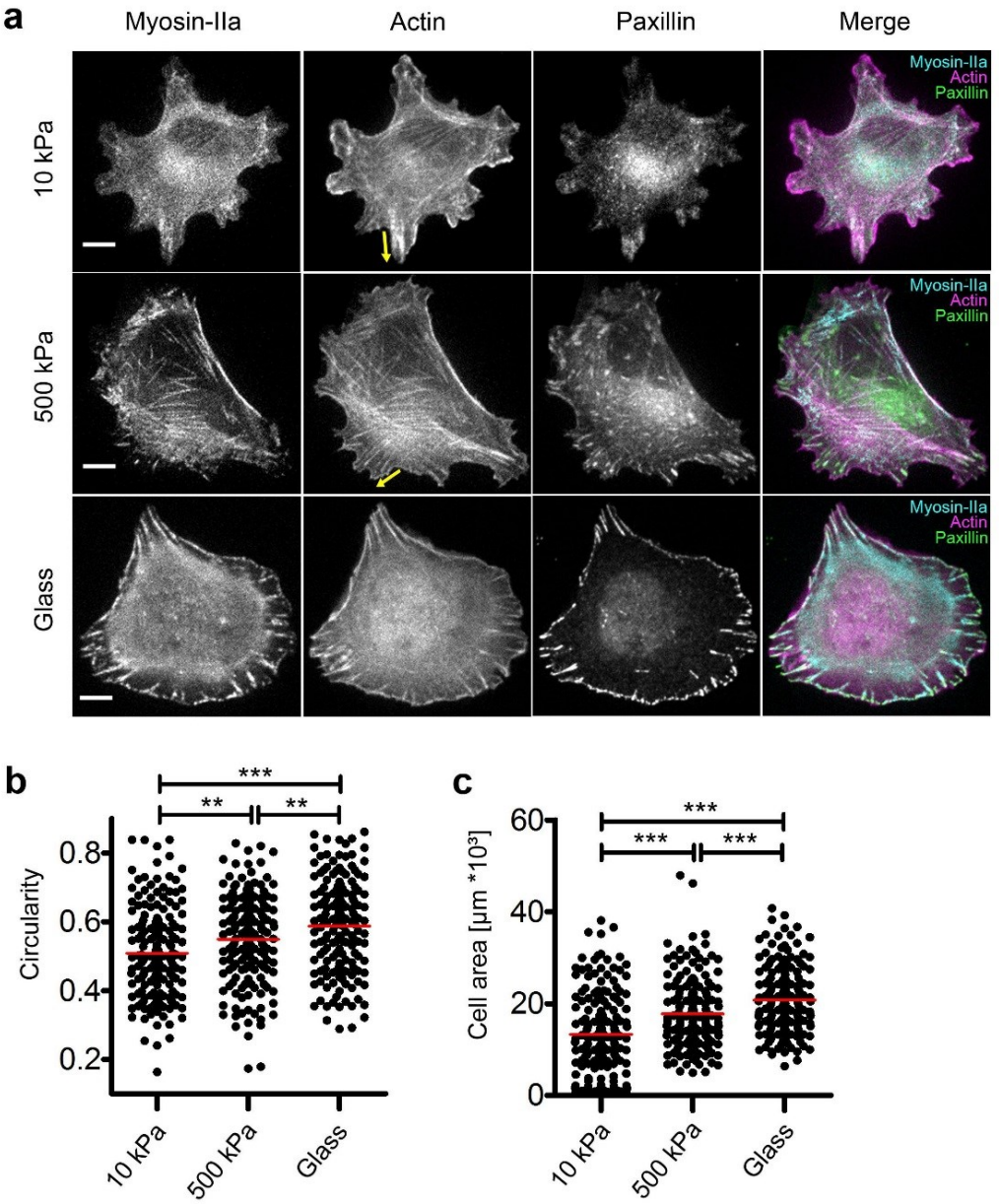

Figure 3.1.12: Morphological analysis of U2OS cells growing on elastomeric substrates of different stiffness.

(a) Confocal images of U2OS cell expressing EGFP-NMHCIIa, treated with 30µM nocodazole 45-90 min and fixed to visualize F-actin (rhodamine-phalloidin) and focal adhesions (anti-paxillin antibody). Scale bars: 10µm, yellow arrows highlight protrusions. **Top Panel**: Cells plated on collagen-coated elastomeric substrate with a defined Young´s modulus of 10 kPa or **mid panel**: 500 kPa. **Bottom panel**: Cell plated on collagen-coated glass-bottom dishes. **(b)** Circularity and **(c)** cell area measured using ImageJ Shape descriptor Plugin. N > 169 cells (for each condition) from 3 experiments. Red lines indicate mean; ***: P<0.001; **: P<0.01 Unpaired t-test).

Figure 3.1.13 shows representative myosin-IIa oscillations (highlighted by yellow arrows) in cells plated on substrates with different elasticities. Oscillation amplitude and frequency were not altered on the firmer gel substrate (Young´s modulus of 500 kPa) relative to glass, whereas decrease of both parameters were measured on the softer substrate (Young´s modulus of 10 kPa) (N > 24 cells from three experiments) (Figure 3.1.13b, c). The decrease in frequency and amplitude of myosin-IIa oscillations on softer substrates coincides with the rise of both protrusion size and number (see Figure 3.1.12a, yellow arrows), indicating that the elastic

extracellular environment modulates the irregular oscillations of myosin-IIa potentially during exploratory processes and thus contributes to determine directionality during migration of U2OS cells.

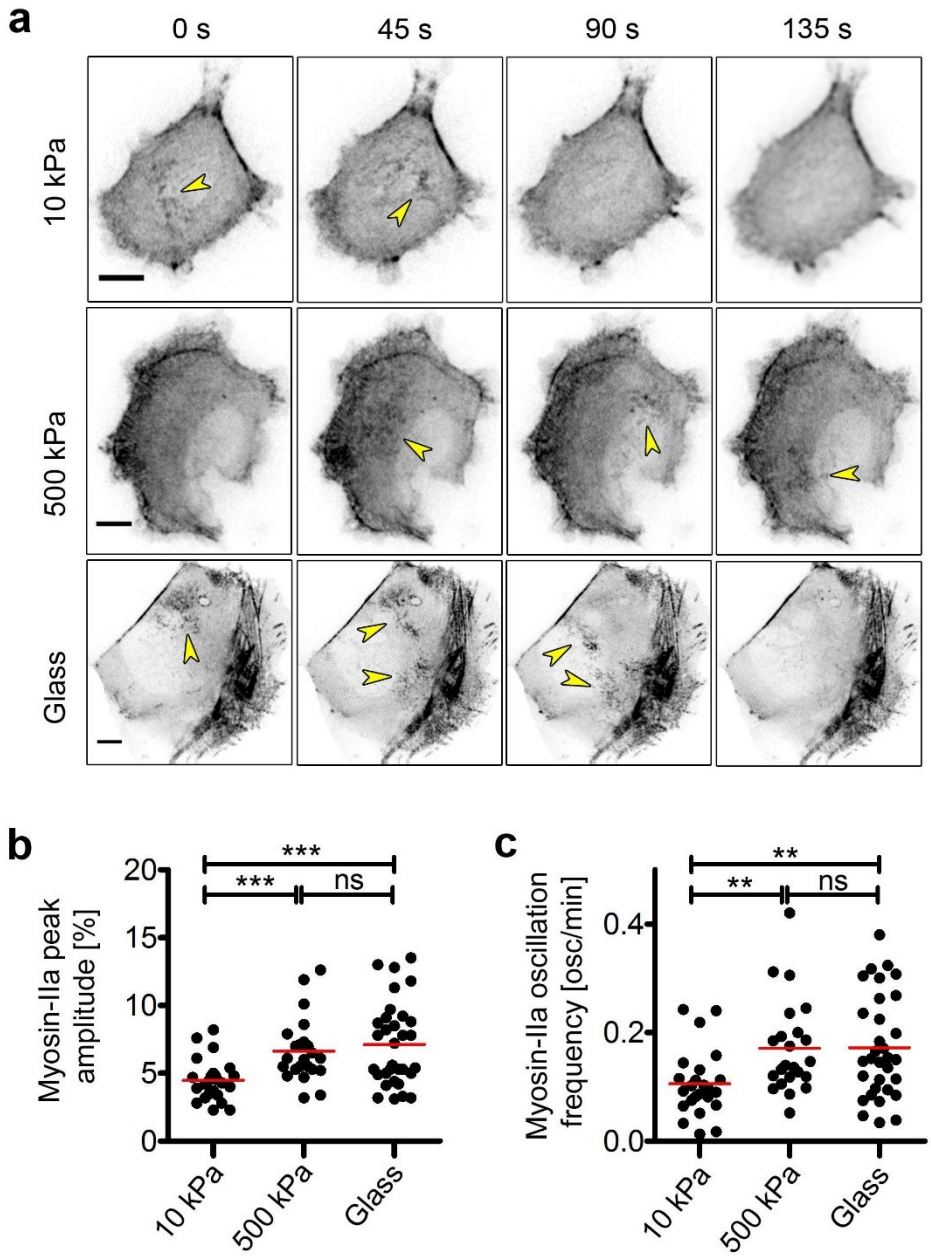

Figure 3.1.13: Irregular myosin-IIa activity oscillations on elastomeric substrates with different stiffness.

(a) Individual frames from confocal spinning disc time-lapse imaging experiments of U2OS cell expressing EGFP-NMHCIIa. Cells were analyzed 45-90 min after treatment with 30 µM nocodazole. To highlight signal oscillations in central regions of the cells, images were presented using inverse LUT. **Top Panel**: Cells plated on collagen-coated gel substrate with a defined Young´s modulus of 10 kPa or **mid panel**: 500 kPa. **Bottom panel**: Cell plated on collagen-coated glass-bottom dishes. **(b)** Myosin-IIa peak amplitude (in percent of mean intensity) and **(c)** oscillation frequency (in oscillations per minute) 45-90 min after nocodazole addition (N >23 cells from 3 experiments). Red lines indicate mean; ***: P<0.001; **: P<0.01, ns: not significant in Unpaired t-test). Frame rate: 3/min. Scale bars: 10µm.

3.2 The formin FHOD1 is not required for Rho, myosin-IIa and actin oscillations

Activated mutants of the formin FHOD1 strongly induce the formation of actin-myosin stress fibers. It has previously been shown that phosphorylation of this formin by the RhoA effector ROCK leads to its full activation and we have recently reported that that this formin and co-localizes with myosin-IIa on contractile stress fibers in U2OS cells. However, spatio-temporal dynamics of FHOD1 localization has not been well understood and the regulatory mechanisms that control dynamic localization of the formin are not known. Here, the dynamic localization of FHOD1 was examined using TIRF live-cell measurements. These studies revealed irregular oscillations of FHOD1 cortex association in U2OS cells that correlate to Rho activity and myosin-IIa dynamics. Similar to Rho activity and myosin-IIa, FHOD1 oscillations are enhanced after pharmacological depolymerization of microtubules with nocodazole (see Supplemental Material, Figure S1). In this part of the work, sub-cellular localization of FHOD1 was crosscorrelated with Rho activity and myosin-IIa localization dynamics (3.2.1 and 3.2.2). Furthermore, the role of FHOD1 in Rho activity and myosin-IIa oscillations was investigated, using RNAi mediated gene silencing of the formin (3.2.3).

3.2.1 Irregular oscillations of Rho activity correlate with FHOD1 oscillations

Oscillations of FHOD1 cortex association and Rho activity dynamics were measured by TIRF microscopy using delCMV-EGFP-FHOD1 and the Rho activity sensor delCMV-mCherry-RBD. The recorded intensity signals were crosscorrelated using the same pixel-based approach as described in section 3.1.5. Thereto, transfected U2OS cells were imaged after global stimulation of Rho activity via the microtubule-depolymerizing drug nocodazole, to monitor the maximal number of oscillations. Figure 3.2.1a-c depict a representative cell with corresponding intensity plots, as well as the mean temporal crosscorrelation plot of N = 11 cells (from four experiments) that was calculated as described in section 2.2.4.1. The time-shifts relative to maximal Rho activity and the frequency distribution of maximal FHOD1-Rho activity crosscorrelation cell were derived from the crosscorrelation plots of each individual cell and are presented in Figure 3.1.2c. The mean temporal delay of FHOD1 oscillations with respect to Rho activity was found to be $\Delta t = 6.3$ s $\pm$ 0.8 s.e.m. with a mean maximal crosscorrelation coefficient of $r = 0.51 \pm 0.07$ s.e.m.. This delay is significantly shorter than the

lag observed between Rho activity and actin or myosin-IIa oscillations (see sections 3.1.5 and 3.1.6).

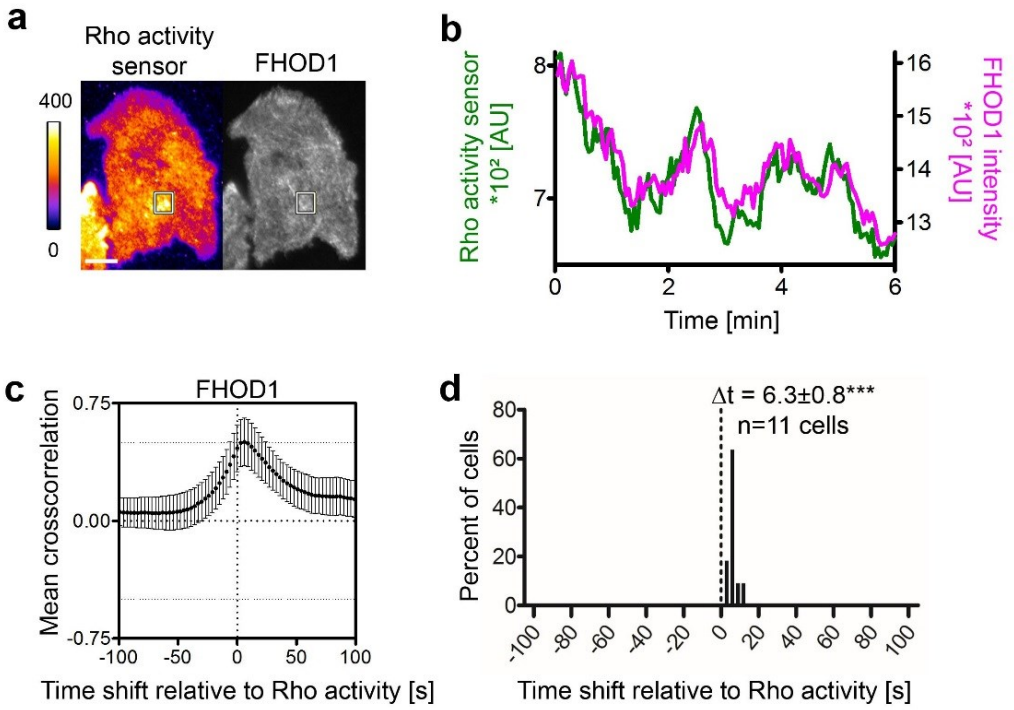

Figure 3.2.1: Crosscorrelation of FHOD1 and Rho activity oscillations.

Temporal crosscorrelation analysis of U2OS cells transfected with the Rho activity sensor delCMV-mCherry-RBD (depicted as Fire LUT) and delCMV-EGFP-FHOD1, 45-90 min after nocodazole treatment (30 µM). Frame rate: 20/min. **(a)** Individual frames of Rho activity and FHOD1 cortex association from time-lapse TIRF measurements. The calibration bar indicates AU. Scale bar: 10 µm. **(b)** Intensity plots of regions marked by white boxes in **a**. **(c)** Mean temporal crosscorrelation function of Rho activity and FHOD1 signal (N = 11 cells from four experiments). Error bars show 95% confidence interval. **(d)** Percent of cells with given time shifts at the point of maximal crosscorrelation relative to Rho activation, derived from **c** (***: P<0.001 in one-sample t test; ±s.e.m.).

3.2.2 Transient FHOD1 localization precedes local myosin-IIa accumulations, but coincides with irregular actin oscillations

To further analyze the apparent temporal sequence of oscillations observed for Rho and its downstream effectors, the temporal crosscorrelation of FHOD1 oscillations was quantified relative to myosin-IIa cortex association dynamics. To this end, U2OS cells were transfected with delCMV-EGFP-FHOD1 and mCherry-NMHCIIa, treated with nocodazole (30 µM, 45-90 min) and examined via time-lapse TIRF microscopy (Figure 3.2.2 a). First, duration of local myosin-IIa intensity maxima was longer as compared to the more transient FHOD1 oscillations, which is reflected in the peak width of the intensity plot in Figure 3.2.2b. Secondly, as evident in the example intensity plot analysis (Figure 3.2.2 b), the maximal myosin-IIa signal was significantly delayed with respect to FHOD1 intensity (Δt = 14.8 s ± 1.3 s.e.m.) and the mean crosscorrelation coefficient between the two signal oscillations was

found as $r = 0.46 \pm 0.03$ s.e.m. (Figure 3.2.2 c and d) (N = 15 cells from four experiments).

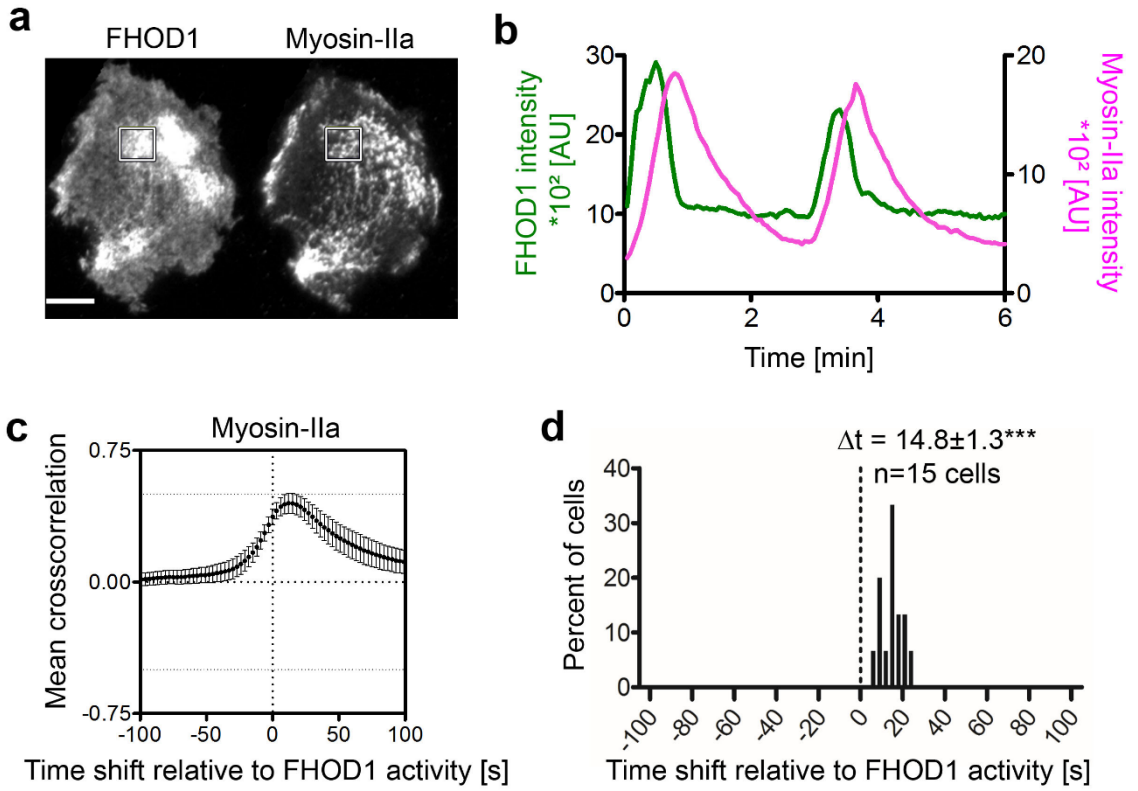

Figure 3.2.2: Quantification of the temporal delay between FHOD1 and myosin-IIa oscillations.

Temporal crosscorrelation analysis of U2OS cells transfected with delCMV-EGFP-FHOD1 and mCherry-NMHCIIa 45-90 min after nocodazole treatment (30 µM). **(a)** Individual frames of FHOD1 and myosin-IIa time-lapse TIRF measurements. **(b)** Intensity plots of regions marked by white boxes in **a**. **(c)** Mean temporal crosscorrelation function (N = 15 cells from four experiments). Error bars show 95% confidence interval. **(d)** Percent of cells with given time shifts at the point of maximal crosscorrelation relative to Rho activation, derived from **c** (***: P<0.001 in one-sample t test; ±s.e.m.). Frame rate: 20/min, scale bar: 10µm.

The high crosscorrelation observed between FHOD1 and myosin-IIa oscillations could indicate a regulatory function of FHOD1 for myosin-IIa activity or vice versa. Alternatively, both signal oscillations could be controlled by their common known upstream regulator ROCK downstream of Rho signaling. Figure 3.2.3 summarizes the mean maximal crosscorrelation coefficients of actin-, FHOD1- and myosin-IIa oscillations relative to Rho activity.

In contrast to the significant delay of FHOD1 oscillations relative to Rho activity and myosin-IIa signals, no substantial time-shift could be detected with respect to actin dynamics at the given frame rate (20 frames / min).

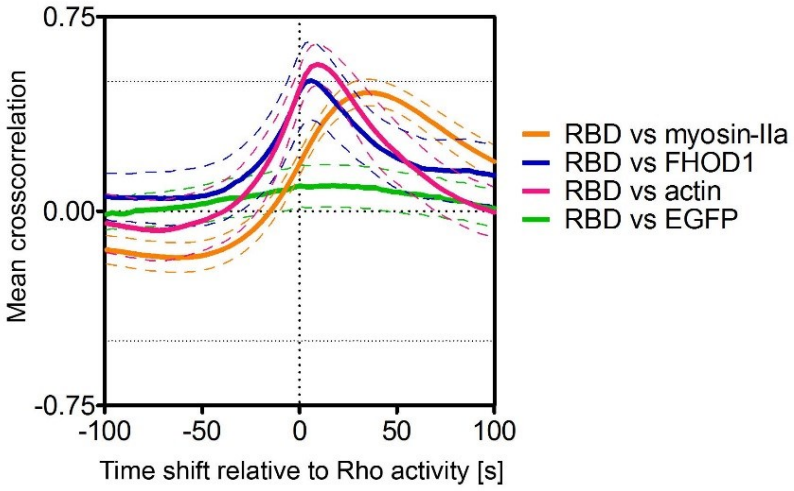

Figure 3.2.3: Summary of mean maximal crosscorrelation between Rho, FHOD1, actin and myosin-IIa activity oscillations.

Mean temporal crosscorrelation functions relative to Rho activity (myosin-IIa: N = 37 cells; FHOD1: N = 11 cells; actin: N = 15 cells; EGFP: N = 31 cells from ≥ 3 experiments). Error bars show 95% confidence interval.

3.2.3 Depletion of FHOD1 reduces actin, but not myosin-IIa and Rho activity oscillations

Next, the impact of FHOD1 activity on actin, myosin-IIa and Rho activity oscillations was validated by depleting the formin using small interfering (si) RNAs, as previously shown in Schulze et al, 2014. To this end, U2OS cells were transfected with a mixture of four different FHOD1siRNAs (siFHOD1 #2, #5, #6, #7) or non-targeting (nt) control siRNA (10 nM). Cells were transfected with the Rho activity sensor delCMV-mCherry-RBD and delCMV-EGFP-actin or EGFP-NMHCIIa, respectively, 48 h after siRNA transfection. At 74 h post siRNA treatment, sufficient depletion of the formin (> 80 %) was verified by SDS-PAGE followed by a western blot analysis (see sections 2.2.2.3 and 2.2.2.4) (Figure 3.2.4 a). Rho, myosin-IIa and actin oscillations were measured by TIRF microscopy in FHOD1 depleted and control cells (Figure 3.2.4 b and c). No significant changes in the mean amplitude and frequency of Rho and myosin-IIa activity oscillations could be observed after FHOD1 depletion (Figure 3.2.4 b and c). In contrast, a significant decrease of actin oscillation amplitude and frequency was detected in cells lacking FHOD1, suggesting that the formin is required for actin oscillations but not for spatio-temporal activity dynamics of neither Rho nor myosin-IIa (Figure 3.2.4 b and c).

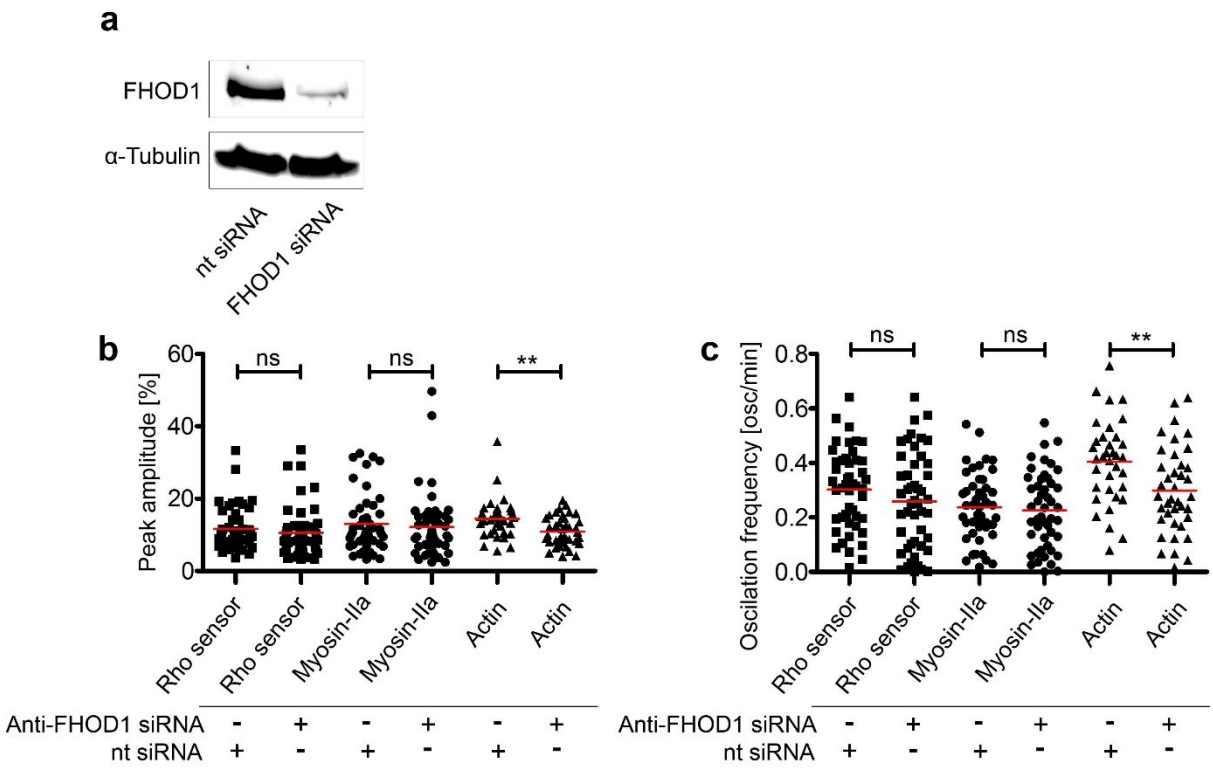

Figure 3.2.4: Oscillation amplitude and frequency of Rho, FHOD1, actin and myosin-IIa activity in FHOD1-depleted and control cells.

U2OS cells were transfected with 10 nM anti-FHOD1 or nt siRNA (control) 78h, and with delCMV-mCherry-RBD, EGFP-NMHCIIa or delCMV-EGFP-actin, 24 h before time-lapse TIRF measurements (frame rate: 3/min). **(a)** Efficiency of FHOD1 protein depletion, performed with 10 nM of a mixture of four different siRNAs against FHOD1 (#2, #5, #6, #7), analyzed by western blot. α-Tubulin was used as a loading control. Representative image of a western blot for two experiments with a depletion efficiency for FHOD1 of > 80 %. **(b)** Peak amplitude (in percent of mean intensity) and **(c)** oscillation frequency (in oscillations per minute), N > 35 cells from 2 experiments. Red lines indicate mean; **: P<0.01, ns: not significant in unpaired t-test).

3.3 ROCK and myosin-IIa activity are required for FHOD1 oscillations

Phosphorylation via ROCK has been described as a crucial part of the molecular mechanism activating FHOD1 (Takeya et al, 2008) and control its localization to stress fibers (Schulze et al, 2014). We therefore tested if inhibition of ROCK by the selective inhibitor Y27632 altered FHOD1 oscillatory behavior. Cells expressing delCMV-EGFP-FHOD1 were treated with nocodazole and FHOD1 oscillations were measured before and after addition of Y27632 (50 µM, 30min) using TIRF microscopy.

The quantification of the detected oscillations, as described in section 3.1.4, confirmed that both oscillation amplitude and frequency of FHOD1 oscillations were significantly decrease after treatment with Y27632 (Figure 3.3.1a-b). This dependence of FHOD1 oscillation dynamics on ROCK activity, together with its strong temporal correlation relative to Rho activity and

myosin-II oscillations (see sections 3.2.1 and 3.2.2) implicate that the formin is regulated by the same signal network, controlling Rho signal oscillations.

To determine whether myosin-IIa activity affects FHOD1 and actin oscillations, the myosin-IIa inhibitor blebbistatin was applied (50 µM, 60 min). The localization dynamics of FHOD1 together with actin oscillations was quantified in cells expressing delCMV-mCherry-actin and delCMV-EGFP-FHOD1 using TIRF microscopy.

As shown in Figure 3.3.1c-d, both peak amplitude and frequency of actin and FHOD1 oscillations were significantly decreased after blebbistatin addition. The drop in FHOD1 oscillations was more prominent than those measured for actin oscillations (peak amplitude: - 33 % for FHOD1, - 28 % for actin; oscillation frequency: - 92 % for FHOD1; - 71 % for actin). This might be due to additional mechanisms in the regulation of actin dynamics compared to FHOD1. Overall, this inhibitor data indicates that the oscillatory behavior of FHOD1 is regulated downstream of ROCK and myosin-IIa activity.

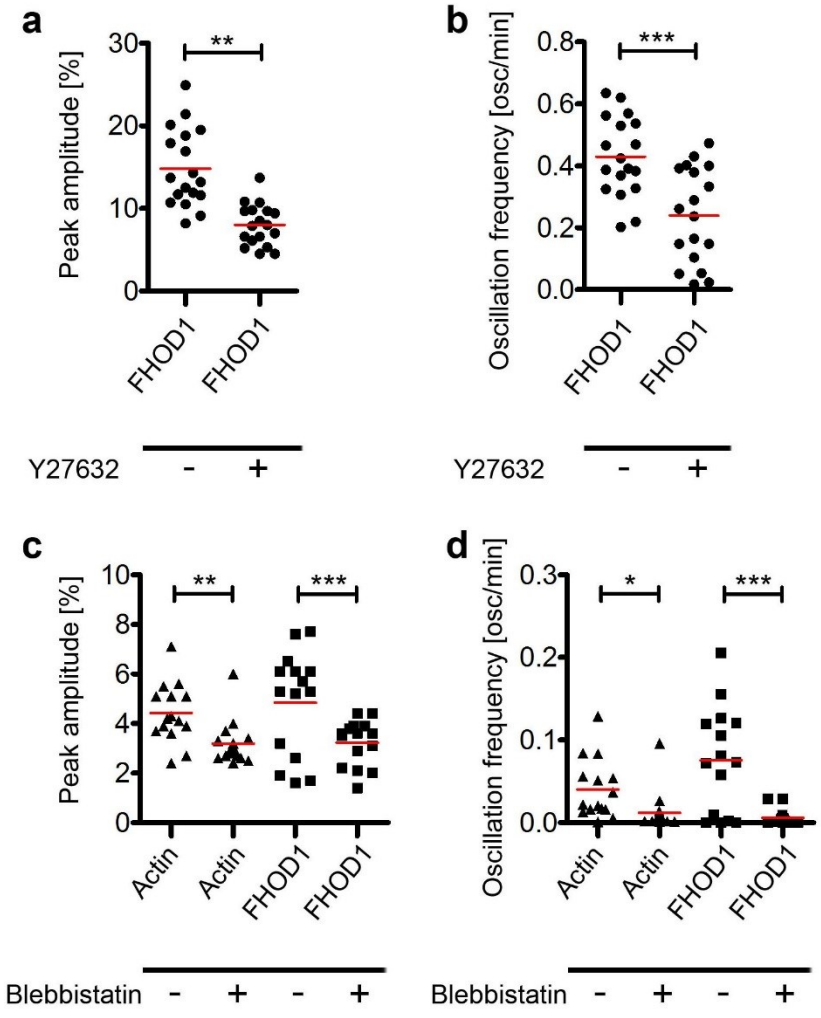

Figure 3.3.1: Inhibition of ROCK and myosin-IIa decreases FHOD1 oscillations.

(a-b) U2OS cell expressing delCMV-EGFP-FHOD1, treated with nocodazole (30 µM, 30-90 min), were examined before and 30 min after addition of 50 µM Y27632. Frame rate: 3/min. **(a)** Peak amplitudes (in percent of mean) and **(b)** oscillation frequencies (in oscillations per minute) before and after incubation with Y27632**,** N = 18 cells from three experiments. Red lines indicate mean; ***: P<0.001; **: P<0.01; ns: not significant in paired t-test). **(c-d)** Oscillations of cells expressing delCMV-mCherry-actin and delCMV-EGFP-FHOD1 were recorded before and 60 min after addition of blebbistatin (50 µM). Frame rate: 3/min. **(c)** Peak amplitudes (in percent of mean) and **(d)** peak frequencies (in oscillations per minute) before and after incubation with blebbistatin**,** N = 15 cells from three experiments. Red lines indicate mean; ***: P<0.001; **: P<0.01; *: P<0.05 in paired t-test).

3.4 Overall integrity of the actin cytoskeleton is not required for FHOD1 oscillations

Based on crosscorrelation analyses, FHOD1 and actin oscillations are detected almost simultaneously (Figure 3.1.8), suggesting a potential interdependence. Thus, the relevance of an intact actin cytoskeleton for the oscillatory cortex association of FHOD1 was investigated by pharmacologically perturbing the organization of actin filaments or the state of actin polymerization.

To understand if a disruption of the actin cytoskeleton alters FHOD1 oscillations, two independent pharmacological treatments were applied that are well established to inhibit actin dynamics. First, Cytochalasin D (CytoD) which binds to the barbed end of actin filaments and thereby inhibits actin polymerization. Over time, this capping of actin filaments leads to the overall degradation of the entire actin meshwork into short filaments (Schliwa, 1982; Cooper, 1987). Latrunculin A on the other hand, disturbs the polymerization of actin by binding to monomeric G-actin (Coue et al, 1987).

First, U2OS cells were transfected with delCMV-mCherry-actin and delCMV-EGFP-FHOD1 and imaged via time-lapse TIRF microscopy before and after addition of 2 µM CytoD. The incubation time of 15 min after CytoD addition was identified to be just the duration when actin oscillations disappear (data not shown).

Peak frequency analysis (Figure 3.4.1a) revealed that number of actin oscillations is significantly reduced under these conditions, whereas of FHOD1 oscillation number was not altered. Interestingly, peak amplitude of FHOD1 oscillations was even enhanced after CytoD treatment (Figure 3.4.1b). FHOD1 was previously suggested to act as an actin filament capping protein. Thus, this increase in mean peak height might be due to competitive elimination of FHOD1 from the barbed end of actin filaments by CytoD. In support of this, large stationary

intracellular accumulations of FHOD1 were detected after CytoD treatment (Figure 3.4.1c, yellow arrows).

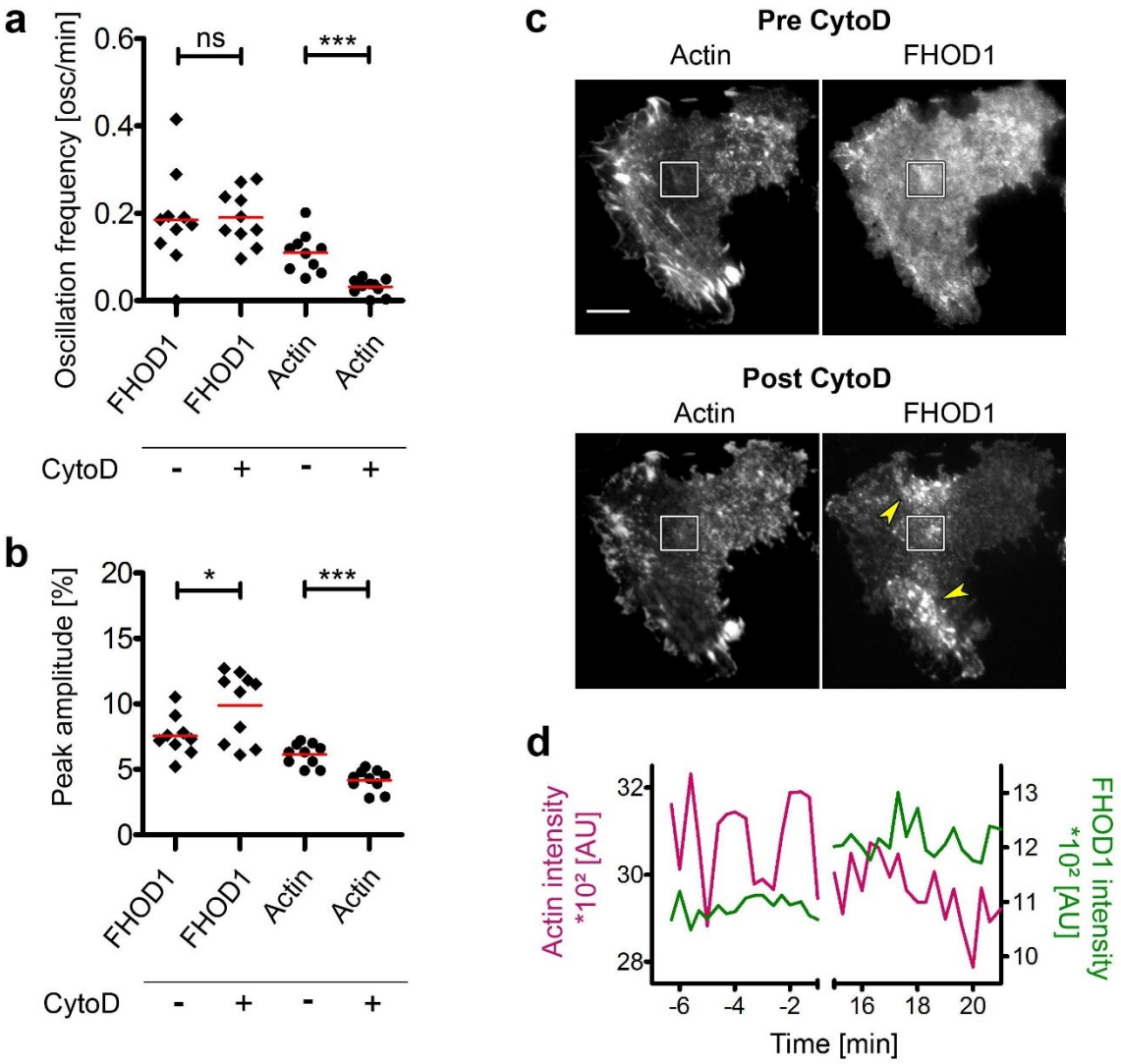

Figure 3.4.1: Degradation of the actin network by CytoD arrests actin, but not FHOD1 oscillations.

(a) Oscillation frequency (in oscillations per minute) and **(b)** peak amplitude (in percent of mean intensity) before and after incubation with CytoD (2µM, 15min) (N = 10 cells from 3 experiments). Red lines indicate mean; ***: P<0.001; *: P<0.05; ns: not significant in paired t-test. Frame rate: 3/min. **(c)** Individual frames of TIRF measurements of a representative U2OS cell expressing delCMV-mCherry-actin and delCMV-EGFP-FHOD1, before and after CytoD treatment. Scale bar 10 µm. **(d)** Intensity plots of regions marked in **c** (white boxes).

To verify the data obtained by CytoD mediated disruption of the actin cytoskeleton, FHOD1 oscillations were measured after treatment with Latrunculin A (LatA). First, treatment conditions were optimized in U2OS cells. For this, different concentrations and incubation times of LatA were tested by fixation, actin-staining (with rhodamine-phalloidin) and evaluation of the actin cytoskeleton and morphology by confocal microscopy (Figure 3.4.2). Those conditions that lead to sufficient disruption of the actin meshwork but without causing

the entire collapse of the cell morphology were chosen for TIRF based analysis of FHOD1 oscillations. Oscillations were measured at a LatA concentration of 600 nM after an incubation time of 25-30 min.

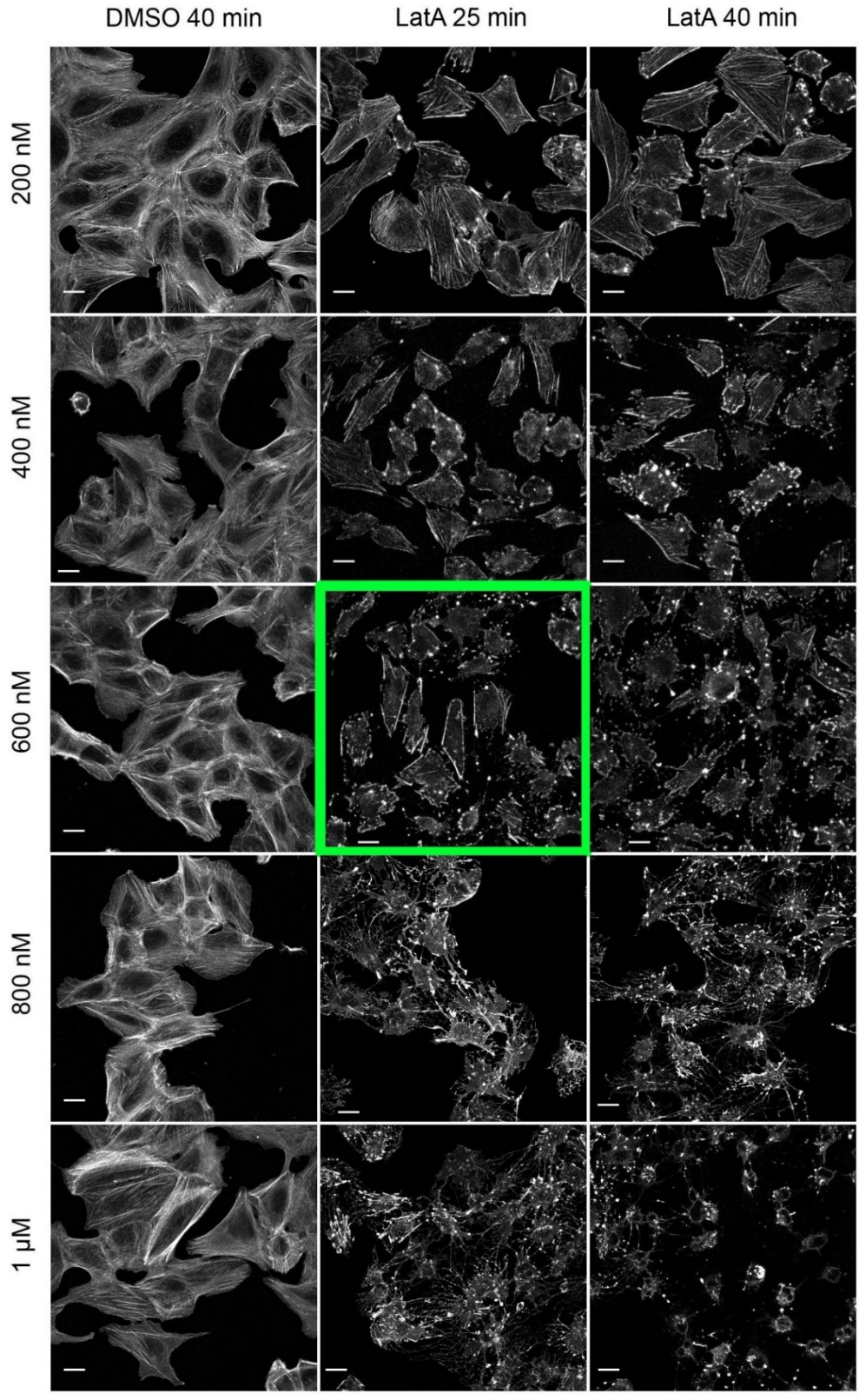

Figure 3.4.2: Optimization of Latrunculin A treatment for U2OS cells.

Confocal images of cells treated with varying concentrations of LatA or DMSO (as a control) for 25 or 40 min, before fixation with 4 % paraformaldehyde and actin staining via rhodamie-phalloidin. The condition highlighted in green (600 nM, 25 min) was chosen for the following live-cell TIRF studies. Scale bars: 20 µm.

Figure 3.4.3a-b display a representative U2OS cell expressing delCMV-mCherry-actin and delCMV-EGFP-FHOD1, before and after treatment with with LatA (600 nM, 25 min), as well as corresponding intensity plots. Similar to CytoD treatment (Figure 3.4.1) actin oscillations under these conditions were significantly reduced, whereas FHOD1 dynamics was not perturbed (Figure 3.4.3c-d). Furthermore, in contrast to the treatment with CytoD, no stationary intracellular FHOD1 accumulations were observed after LatA addition. Taken together, these results suggest that actin oscillations require FHOD1 activity, whereas the integrity of the actin cytoskeleton does not seem to be necessary for formin oscillations.

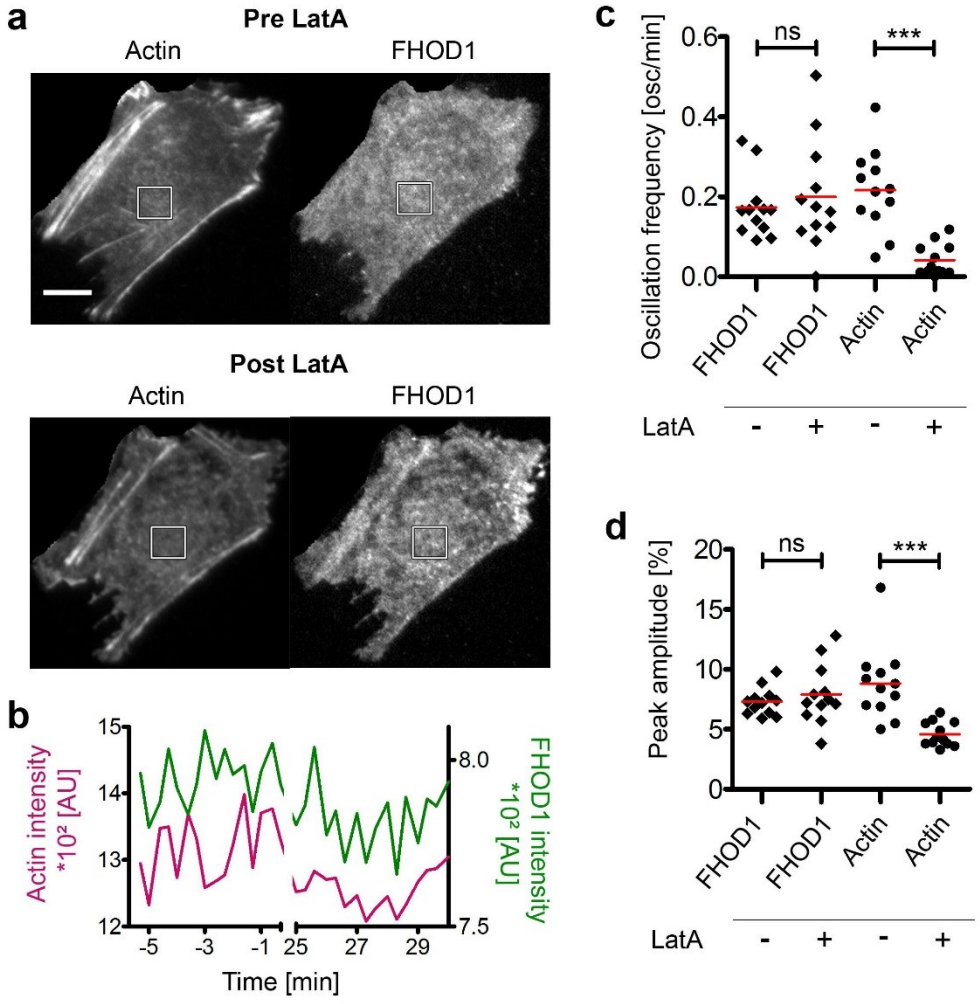

Figure 3.4.3: Degradation of actin filaments by LatA decreases actin, but not FHOD1 oscillations.

(a) Individual frames of TIRF measurements of a representative U2OS cell expressing delCMV-mCherry-actin and delCMV-EGFP-FHOD1, before and 25 min after LatA treatment. Scale bar 10 µm. Frame rate: 3/min. **(b)** Intensity plots of regions marked in **a** (white boxes). **(c)** Oscillation frequency (in oscillations per minute) and **(d)** peak amplitude (in percent of mean intensity) before and after incubation with LatA (600 nM, 25 min), N = 12 cells from 2 experiments. Red lines indicate mean; ***: P<0.001; ns: not significant in paired t-test).

3.5 Myosin-IIa and ROCK act both downstream and upstream of Rho activity oscillations

Unpublished studies performed by Johannes Koch, revealed that expression of the RhoA activator GEF-H1 leads to large propagating Rho activity waves across the plasma membrane in U2OS cells (Graessl et al, submitted). Interestingly, wave-like signal propagation is typical for excitable signal networks, which consist of a self-amplifying component (X) and a time-delayed inhibitory component (Y) (Figure 3.5.1a) (Tian et al, 2009). GEF-H1 was not only found to stimulated Rho activity waves, but also to display coinciding oscillatory behavior, supporting the idea that GEF is involved in the local amplification of Rho activity (Figure 3.5.1b) (unpublished results by Johannes Koch). Myosin-IIa has been shown to inhibit Dbl-like Rho activators including GEF-H1 (Lee et al, 2010). Furthermore, myosin-IIa oscillations emerge with a substantial delay relative to Rho activation (see section 3.1.6). Thus, we hypothesized that ROCK and its downstream effector myosin-IIa might play a role in the control of Rho activity oscillations. This was tested via pharmacological inhibition of both ROCK and myosin-IIa (Figure 3.5.1b).

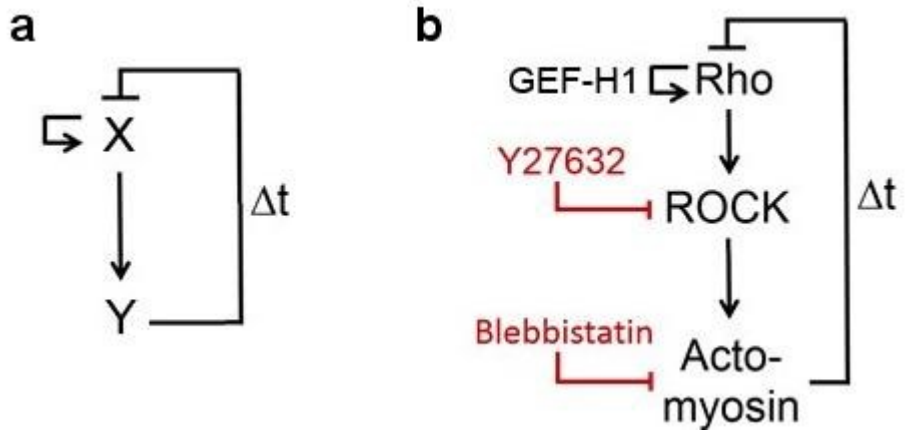

Figure 3.5.1: Schematic of the assumed signal network and the points of attack of the applied inhibitors.

(a) Typical excitable signal networks consists of a fast positive feedback coupled to a slow negative feedback loop. **(b)** Proposed Rho activity based signal network, including ROCK, myosin-IIa and actin as downstream effectors that mediate a temporal delayed feedback to Rho activity. For the selective disturbance of ROCK activity the potent inhibitor Y27632 is applied, a selective inhibition of myosin-IIa is achieved by addition of blebbistatin.

3.5.1 Inhibition of ROCK activity decreases amplitude and frequency of Rho activity oscillations

The Rho-associated kinases (ROCK1/2) are prominent effectors of Rho activity that are known to phosphorylate myosin-IIa (Amano et al, 1996). Phosphorylation by ROCK has been shown to increase the myosin-IIa motor activity and to promote bundling and contractility of actin stress fibers (Ishisaki et al, 1997). The cell permeable pyridine derivate Y27632 specifically inhibits ROCK1 and ROCK2 by binding to their catalytic sites (Ishisaki et al, 2000). Here, Y27632 was used to uncover the proposed feedback of ROCK to Rho activity oscillations in U2OS cells. For this, cells were transfected with the Rho activity sensor (delCMV-mCherry-RBD) and treated with nocodazole to increase the number of oscillations. Afterwards, TIRF measurements of Rho activity were performed before and 30 min after treatment with Y27632 (50 µM).

As depicted in Figure 3.5.2, both Rho activity peak amplitude and oscillation frequency were significantly decreased after Y27532 treatment (50 µM, 30 min; N = 32 cells from four experiments) (Figure 3.5.2c and 3.5.2e), while no changes were observed in H_2O treated control cells (Figure 3.5.2d and 3.5.2f) (N = 35 cells from two experiments).

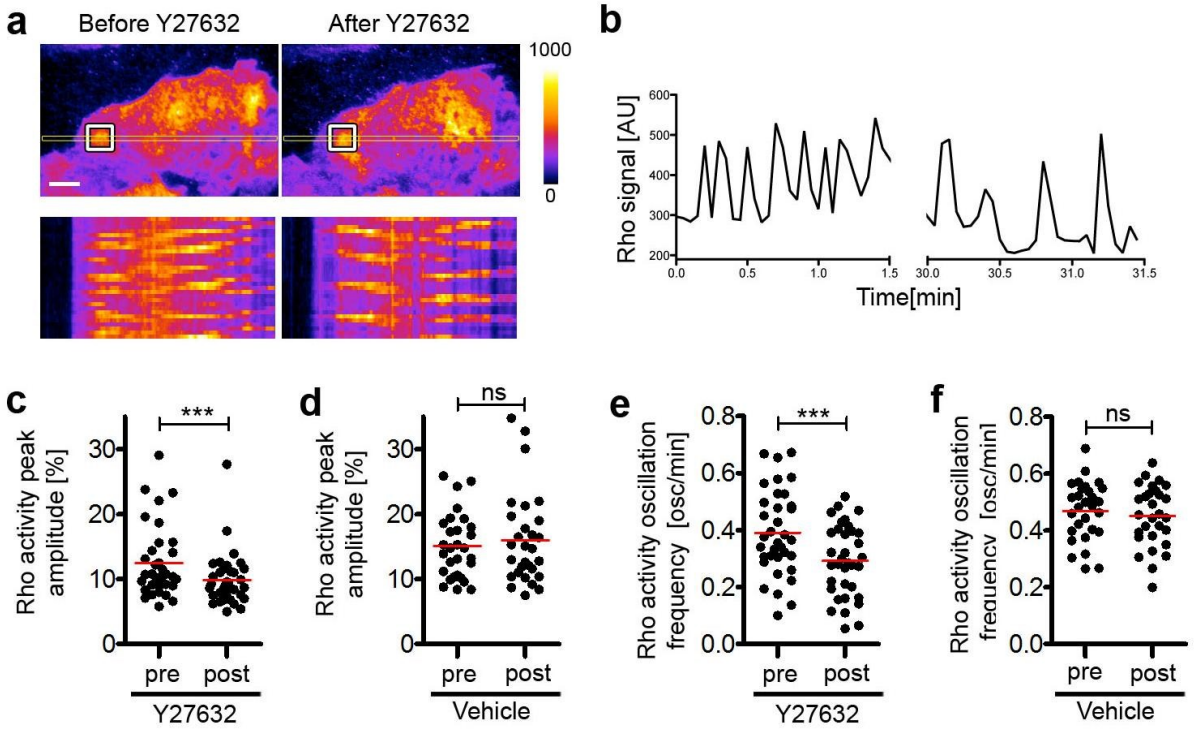

Figure 3.5.2: Inhibition of Rho activity oscillations by its downstream effector ROCK.

(a) Individual TIRF images and kymographs (corresponding to the region indicated by orange rectangle) of a representative U2OS cell expressing delCMV-mCherry-RBD (depicted as Fire LUT) and treated with nocodazole (30 µM, 30-90 min). Cells were analyzed by TIRF before and 30 min after addition of 50 µM Y27632. Scale bar

10 µm. Frame rate: 3/min. Calibration bar indicates AU. **(b)** Intensity plots of regions marked in **a** (white boxes). **(c-d)** Peak amplitude (in percent of mean) and **(e-f)** oscillation frequency (in oscillations per minute) before and after incubation with Y27632 **(c,e)** or H_2O (Vehicle) **(d,f),** N ≥ 32 cells from four experiments and two control experiments (with H_2O as vehicle). Red lines indicate mean; ***: P<0.001; ns: not significant in paired t-test).

3.5.2 Obstruction of myosin-IIa activity with blebbistatin leads to diminished Rho activity oscillations

Blebbistatin is a highly affine inhibitor of myosin-IIa that binds to its actin-detached state and blocks its activity (Kovacs et al, 2004). This was utilized to disable myosin-IIa oscillations and measure the impact of this perturbation on Rho activity oscillations. To this end, U2OS cells were transfected with the Rho activity sensor (delCMV-mCherry-RBD) and myosin-IIa (EGFP-NMHCIIa), treated with nocodazole and imaged with TIRF microscopy before and after treatment with blebbistatin (50 µM, 1h).

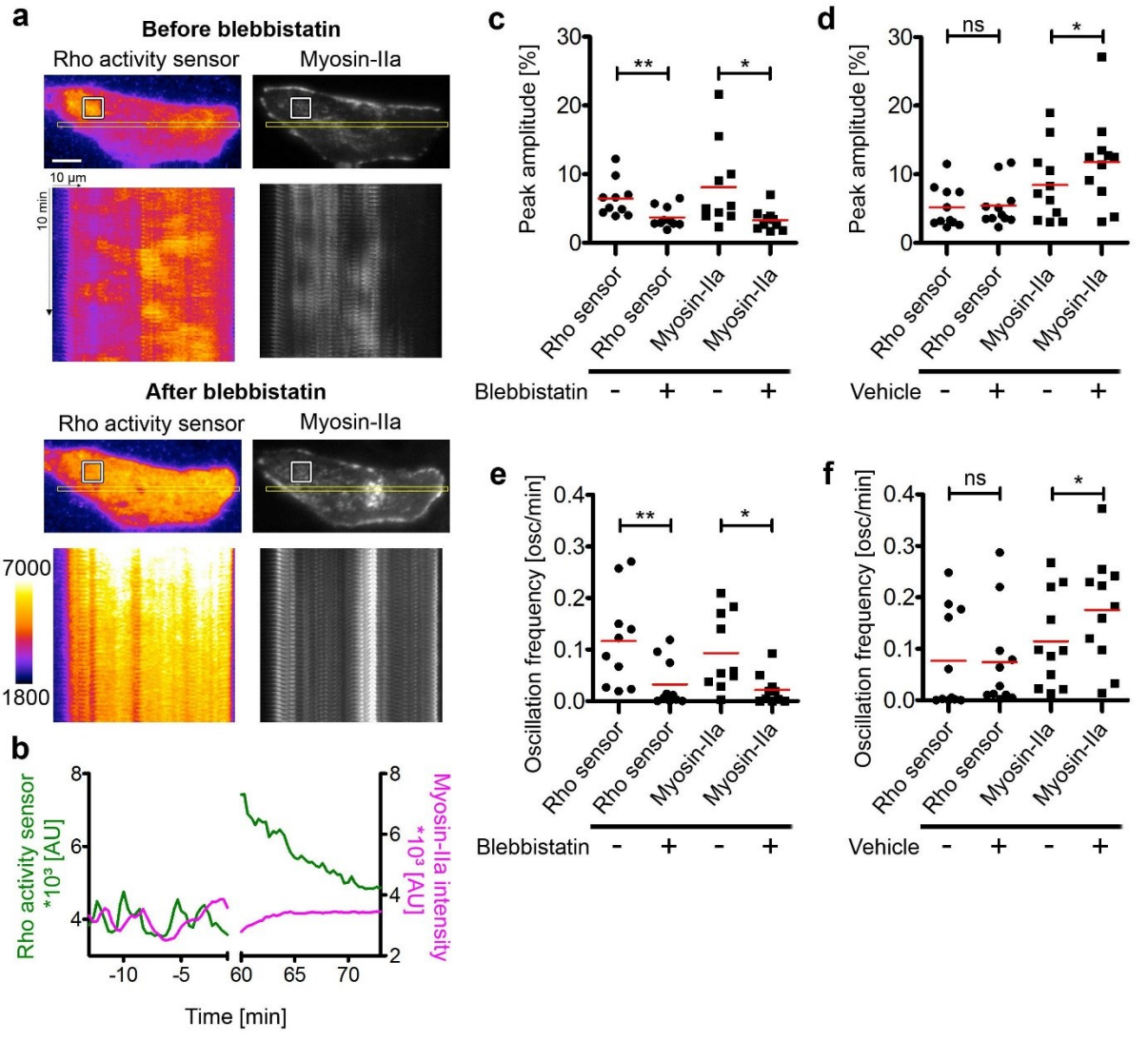

Figure 3.5.3: Inhibition of myosin-IIa oscillations decreases Rho activity oscillations.

(a) Individual frames of TIRF measurements of a representative U2OS cell expressing delCMV-mCherry-RBD (depicted as Fire LUT) and EGFP-NMHCIIa, treated with nocodazole (30 µM, 30-120 min), before and 60 min after addition of blebbistatin (50 µM). Kymographs show regions marked by orange rectangles. Scale bar: 10 µm. Frame rate: 3/min. Calibration bar indicates AU. **(b)** Intensity plots of regions marked in **a** (white boxes). **(c,d)** Peak amplitudes (in percent of mean) and **(e.f)** oscillation frequencies (in oscillations per minute) before and after incubation with blebbistatin (50 µM, 60 min) **(c,e)** or DMSO as vehicle control **(d,f)**. N ≥ 10 from three experiments. Red lines indicate mean; ***: P<0.001; **: P<0.01; *: P<0.05; ns: not significant in paired t-test).

Oscillations of Rho and myosin-IIa activity that were evident in representative kymographs and intensity plots before blebbistatin treatment, are impaired after drug addition (Figure 3.5.3a-b). Quantification of the imaging data confirmed this initial observation, as amplitude and frequency of Rho activity and myosin-IIa oscillations were significantly decreased after inhibition of myosin-IIa (N = 10 cells from three experiments) (Figure 3.5.3c and 3.5.3e). The disturbance of myosin-IIa oscillation amplitude and frequency after blebbistatin treatment was less pronounced as compared to Rho activity changes. This might be due to contrasting effects of the solvent, as myosin-IIa oscillations were slightly enhanced in control cells treated with DMSO (Figure 3.5.3d and 3.5.3f).

Together, these results suggest that myosin-IIa activity is an integral part of the excitable signal network regulating Rho activity oscillations acting as a delayed inhibitory element.

3.6 Role of RhoGAPs in Rho activity oscillations

Myosin-IIa might provide a platform for the recruitment of inhibitory factors such as Rho GAPs (Rho guanosine triphosphatase activating proteins), that mediate the delayed self-inhibition of Rho. In order to find potential regulators of Rho activity oscillations, nine acto-myosin and/or RhoA associated Rho GAPs were investigated (see Supplemental Material Table S1 for an overview). Selected GAPs are presented in the following sections.

3.6.1 ARHGAP18 modulates Rho activity oscillations

ARHGAP18 (or MacGAP) is a recently discovered member of the human GAP family that is known to suppress RhoA activity and disrupt stress fiber formation, when overexpressed in HeLa cells (Li et al, 2008; Maeda et al, 2011). Here, U2OS cells were transfected with the Rho activity sensor, along with either EGFP-ARHGAP18 wild-type or the GAP-deficient mutant EGFP-ARHGAP18 R265A, and treated with nocodazole (30 µM, 45-90 min) to stimulate irregular Rho activity oscillations. Cells were examined via TIRF microscopy and the recorded Rho activity and ARHGAP18 oscillations were analyzed as described in section 2.2.4.1. Interestingly, while no oscillations were observed with the wild-type ARHGAP18 (Figure 3.6.1a-b), pronounced irregular oscillations were detected with the GAP-deficient mutant which were strongly correlated with Rho activity oscillations in time and space (Figure 3.6.1c-d).

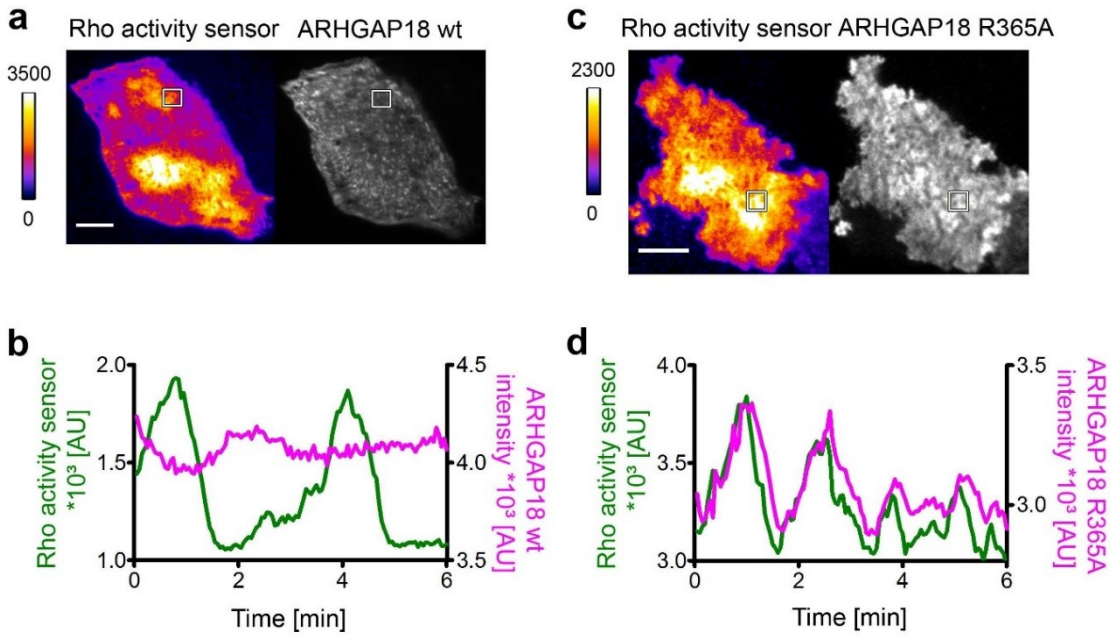

Figure 3.6.1: A GAP-deficient mutant of ARHGAP18, but not its wild-type, correlates with Rho activity oscillations

(a,c) Individual frames of TIRF measurements of a representative U2OS cell expressing delCMV-mCherry-RBD (depicted as Fire LUT) and EGFP-ARHGAP18 wild-type (wt) **(a)** or the GAP-deficient mutant EGFP-

ARHGAP18 R265A **(c)**, treated with nocodazole (30 µM, 45-90 min). Scale bars 10 µm. Frame rates 3/min. Calibration bars indicate AU. **(b,d)** Intensity plots of regions marked in **a** and **c** (white boxes).

The correlation was quantified by Johannes Koch (data not shown) who found a mean crosscorrelation coefficient of $r = 0.59 \pm 0.03$ s.e.m. between the Rho activity sensor and ARHGAP18 R265A, while between Rho activity and ARHGAP18 wt no crosscorrelation could be detected (Graessl et al, submitted). This lack of oscillatory behavior of wild-type ARHGAP18 might be related to its distinct localization patterns as compared to the GAP deficient mutant.

In HeLa cells, wild-type ARHGAP18 was found to be distributed throughout the cell or enriched at the leading edge of migrating or spreading cells (Maeda et al, 2011). Thus, the localization of both constructs was investigated more in detail in U2OS cells. For this, EGFP-fusion constructs encoding ARHGAP18 wt or the GAP-deficient mutant ARHGAP18 R265A were transfected with delCMV-mCherry-actin to analyze the sub-cellular localization in TIRF live-cell measurements. These studies revealed additional localization patterns as compared to previously published data. First, wild-type ARHGAP18 seems to be localized not only to the cell periphery (Figure 3.6.2a, yellow arrow), but also to cellular structures that coincided with linear actin stress fibers (Figure 3.6.2a, blue arrow). The enrichment of ARHGAP18 at stress fibers was quantified by intensity measurements of lines drawn perpendicular to these structures (green and magenta lines). Figure 3.6.2b demonstrates the coherence between signal maxima of the wild-type GAP and actin. In contrast to wild-type ARHGAP18, the GAP-deficient ARHGAP R265A lacked this clear association with actin decorated stress fibers, while prominent localization at the cells periphery was still detected (Figure 3.6.2c, yellow arrow and 3.6.2d).

The ventral side of U2OS cells is majorly decorated with focal adhesions that are associated with the ends of ventral actin stress fibers (Hotulainen and Lappalainen, 2006; Naumanen et al, 2008). Thus, ARHGAP18 constructs were transfected along with mKate-paxillin to investigate their potential enrichment at focal adhesions. Thereto, the localization of ARHGAP18 constructs to adhesions (paxillin) was illustrated with line scans across these structures (green and magenta lines), of which the corresponding intensity (along those lines) was plotted for $N > 30$ cells for each condition.

Together, the distinct localization patterns of ARHGAP18 wild-type as compared to the GAP deficient mutant might bear the underlying reason for the distinct oscillatory behaviors displayed in Figure 3.6.1.

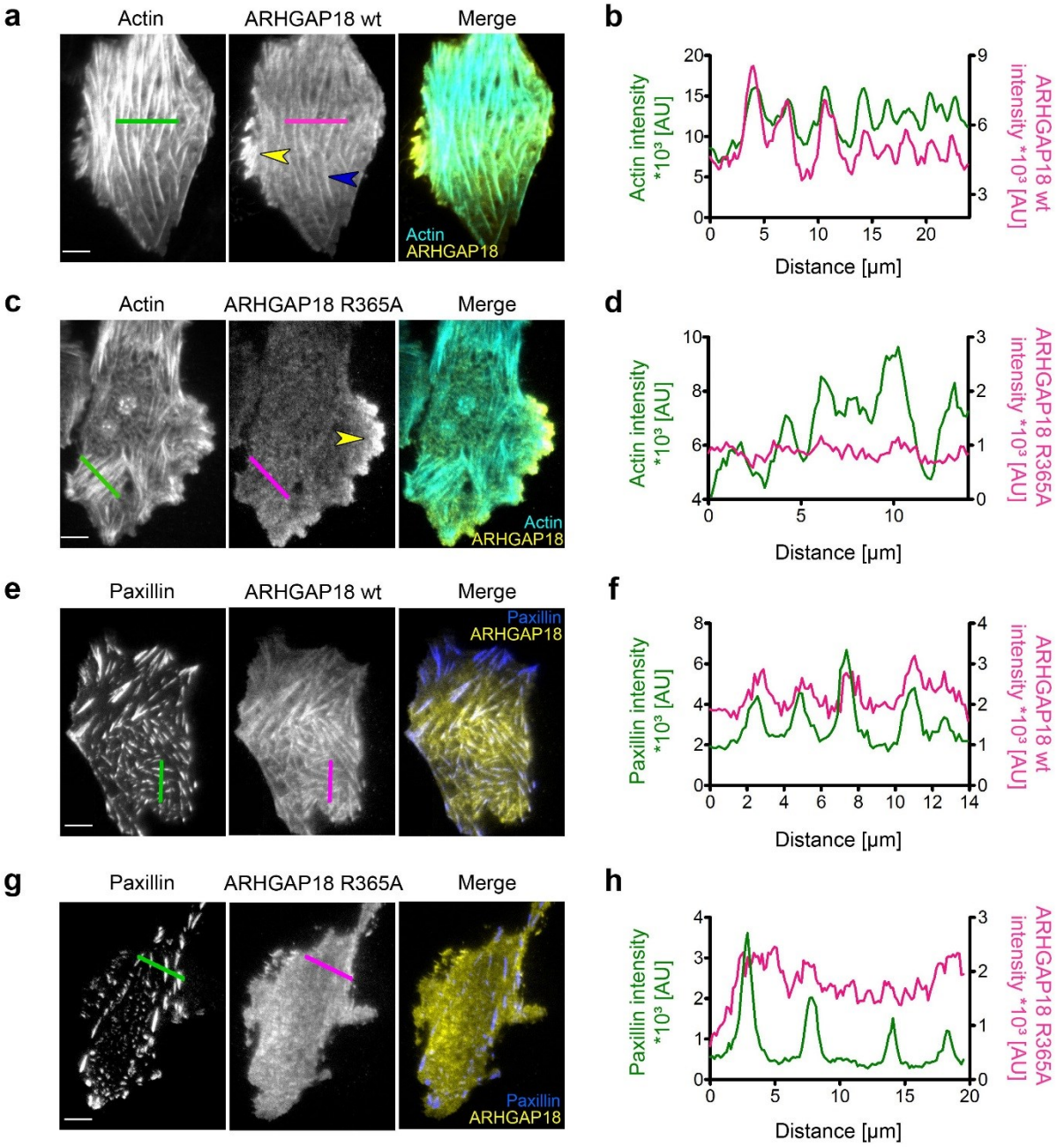

Figure 3.6.2: ARHGAP18 wt, but not its GAP-deficient mutant, colocalizes with actin and focal adhesions.

(a,c,e,g) TIRF micrographs of representative U2OS cells expressing delCMV-mCherry-actin **(a,c)** or mKate-paxillin **(e,g)** and EGFP-ARHGAP18 wild-type (wt) **(a,e)** or the GAP-deficient mutant EGFP-ARHGAP18 R365A **(c,g)**. Scale bars: 10 µm, yellow arrows highlight ARHGAP18 localization to leading edges; blue arrow marks stress fiber localization. **(b,d,f,h)** Intensity plots of regions marked in **a,c,f** and **h** (white boxes).

3.6.2 Quantification of Rho activity oscillation dynamics after in CRISPR/Cas9 mediated depletion of ARHGAP18

The substantial crosscorrelation between Rho activity and ARHGAP18 R365A oscillations suggests that this GAP might be involved in the excitable network regulating Rho activity oscillations. Thus, to investigate a potential role of ARHGAP18 in this process, the GAP was stably knocked out in U2OS cells using the CRISPR/Cas9 method. Clustered (regularly interspaced) short palindromic (DNA) repeats (CRISPR) can be used to modify RNA-guided nucleases such as Caspase 9 (Cas9) to specifically target endogenous genes (Sander and Joung, 2014). Here, this novel technique was utilized to generate a stable cell line with reduced ARHGAP18 expression (see section 2.2.3.3). For this purpose, U2OS cells were transfected with a CRISPR/Cas9 ARHGAP18 knock-out (KO) plasmid along with a homology-directed repair (HDR) plasmid. The ARHGAP18 KO plasmid targets Cas9 to the ARHGAP18 gene loci, via its CRISPR regions and induces its knockdown by sequence-specific double-stranded breaks (DSBs) (Jinek et al, 2012; Gasiunas et al, 2012). The HDR plasmid, which is inserted into the cleavage site, encodes for puromycin resistance and a red fluorescence protein (RFP).

Cells depleted of ARHGAP18 were therefore selected with puromycin-containing growth media for three days and the percentage of ARHGAP18-KO cells was quantified via confocal microscopy by the red fluorescence. The average knock-out efficiency was relatively low (26 % ± 4 % s.e.), but ARHGAP18-KO cells could easily be identified in live-cell experiments, due to the red fluorescence generated by the HDR-plasmid.

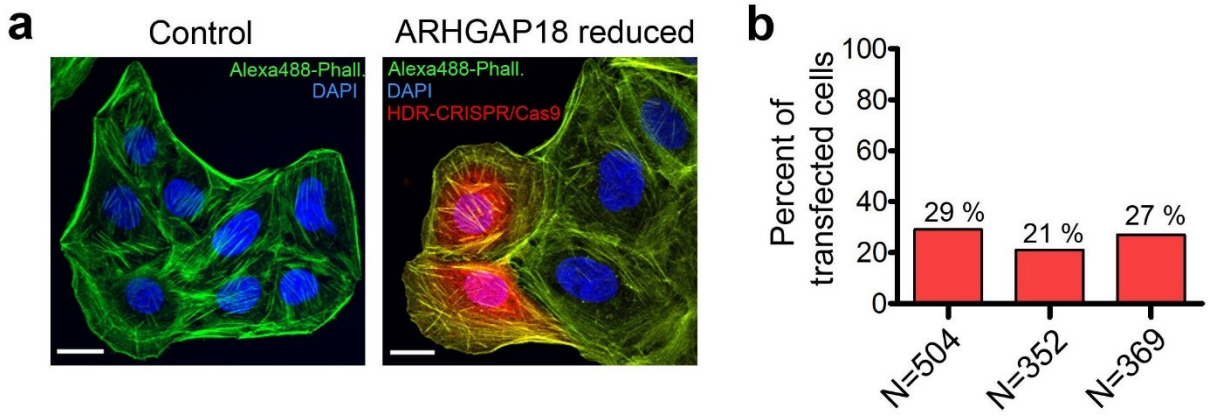

Figure 3.6.3: Validation of the ARHGAP18 depleted U2OS cells.

(a) Average Z-projections of confocal Z-stacks of representative U2OS cells expressing the HDR-CRISPR/Cas9 plasmids. Fluorescence from RFP encoded by the incorporated HDR plasmid indicated successful gene knock-out (highlighted in red). The actin cytoskeleton was stained with Alexa488-phalloidin (depicted in green) and nuclei were visualized with DAPI (illustrated in blue). Scale bar: 20 µm. **(b)** Quantification of ARHGAP18-depleted cells by red fluorescence from three independent experiments. N indicates the number of cells, analyzed in three individual experiments.

In Maeda et al, 2011, siRNA-mediated depletion of ARHGAP18 led to a sustained activation of RhoA. To quantify the effect of ARHGAP18 knock-down on Rho activity oscillations, U2OS cells modified via CRISPR/Cas9 and control cells, expressing mChery-C1, were transfected with the Rho activity sensor (delCMV-EGFP-RBD) and measured with TIRF live-cell imaging. Oscillation amplitude and frequency of Rho activity were quantified as described in section 2.2.4.2 (N > 67 cells from three experiments for each condition) (see Figure 3.6.4).

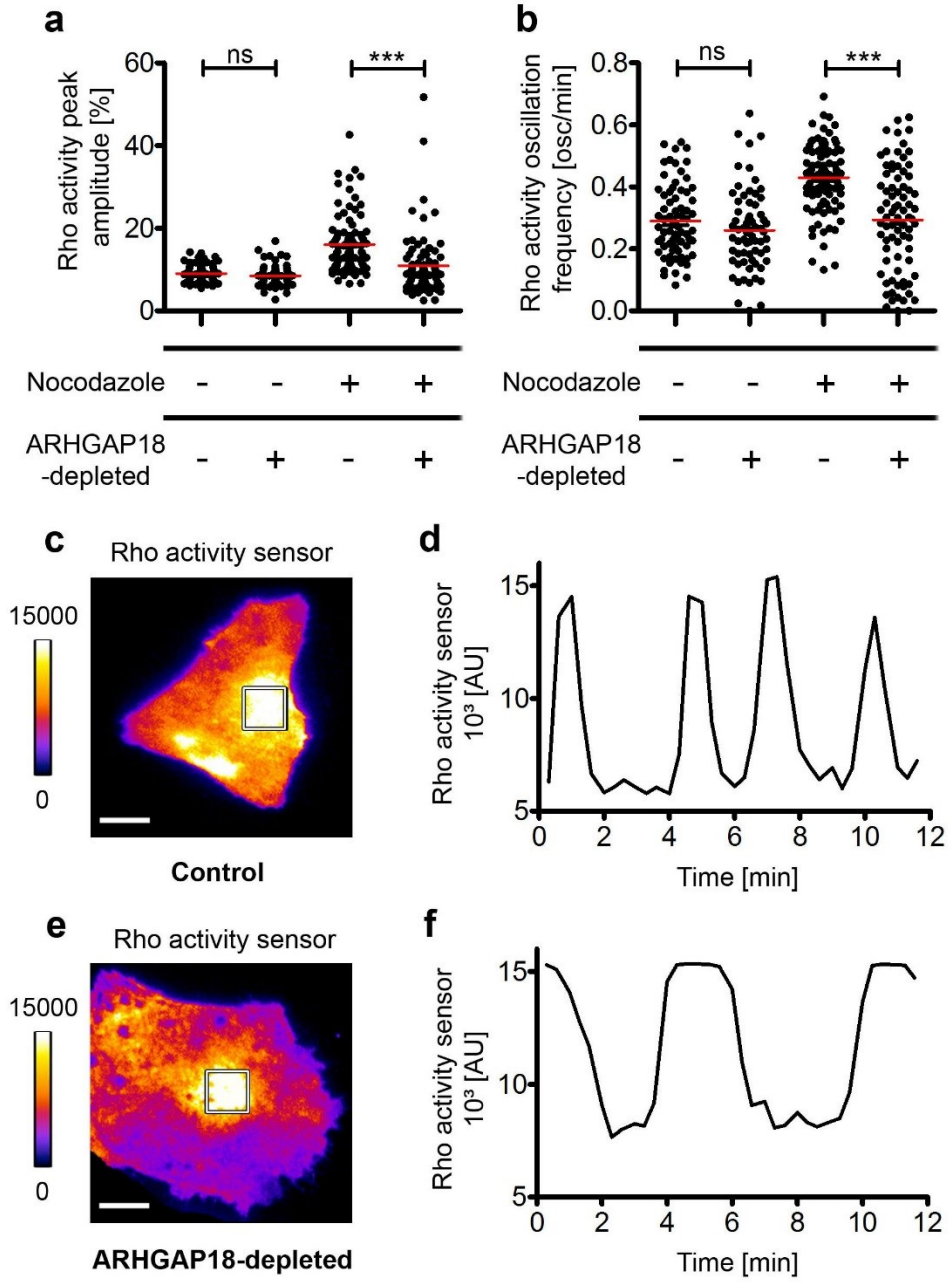

Figure 3.6.4: Rho activity oscillations are modulated by ARHGAP18 activity.

(a) Peak amplitudes (in percent of mean) and **(b)** peak frequencies (in oscillations per minute) of N = 67-93 ARHGAP18-KO or control cells for each condition (with or in absence of 30 µM nocodazole) from three experiments. Red lines indicate mean; ***: P<0.001; ns: not significant in unpaired t-test). **(c,e)** Individual frames of TIRF measurements of a representative ARHGAP18-KO or control U2OS cell, expressing delCMV-mCherry-RBD (depicted as Fire LUT) and treated with nocodazole (30 µM, 45-90 min). Scale bar: 10 µm. Frame rate: 3/min. Calibration bars indicates AU. **(d,f)** Intensity plots of regions marked in **a** (white boxes).

Without nocodazole, Rho activity oscillations were not significantly altered upon depletion of ARHGAP18 as compared to control cells (Figure 3.6.4c and 3.6.4d). However, the increase in both oscillation frequency and peak amplitude after nocodazole addition, observed in control cells, was significantly reduced when ARHGAP18 was depleted (Figure 3.6.4e and 3.6.4f). Notably, depletion of ARHGAP18 led to substantial extension of individual oscillation duration as indicated by the widening of intensity peaks (Figure 3.6.4a and 3.6.4b).

Taken together, these results indicate that ARHGAP18 affects oscillation dynamics by switching off Rho activity. Since Rho oscillations were still observed in ARHGAP18 depleted cells, additional GAPs might contribute to the inhibition of Rho activity oscillations.

3.6.3 Irregular oscillations of p190RhoGAP correlate with Rho activity oscillations

The inhibition of RhoA by p190RhoGAP was shown to enhance migration and spreading in Rat1 fibroblast (Arthur and Burridge, 2001). To investigate the correlation of p190RhoGAP and Rho activity oscillations, U2OS cells were transfected with the Rho activity sensor (delCMV-mCherry-RBD) and either wild-type p190RhoGAP or its GAP-deficient mutant (p190RhoGAP R1283A), fused to EGFP. After treatment with nocodazole, cells were analyzed with TIRF live-cell microscopy.

Representative cells are shown in Figure 3.6.5a. Intensity plots of indicated cell regions reveal pronounced coincidence of signal dynamics both for p190RhoGAP wt (N = 14 cells from four experiments) and for p190RhoGAP R1283A (N = 23 cells from four experiments) (Figure 3.6.5b). For better quantification, the mean temporal crosscorrelation functions, as well as the distribution of the maximal crosscorrelation coefficient were determined. Both the GAP-deficient mutant and wild-type p190RhoGAP exhibit robust mean crosscorrelation ($r = 0.64 \pm 0.05$ s.e.m. for p190RhoGAPwt and $r = 0.76 \pm 0.03$ s.e.m. for p190RhoGAP R1283A). The maximum of crosscorrelation for both proteins was slightly delayed relative to Rho activity ($\Delta t = 2.8$ s $\pm$ 0.9 s.e.m. for the wild-type and $\Delta t = 2.4$ s $\pm$ 0.3 s.e.m. for p190RhoGAP R1283A) implicating that the dynamic increase of Rho activity might recruit its own inhibitor.

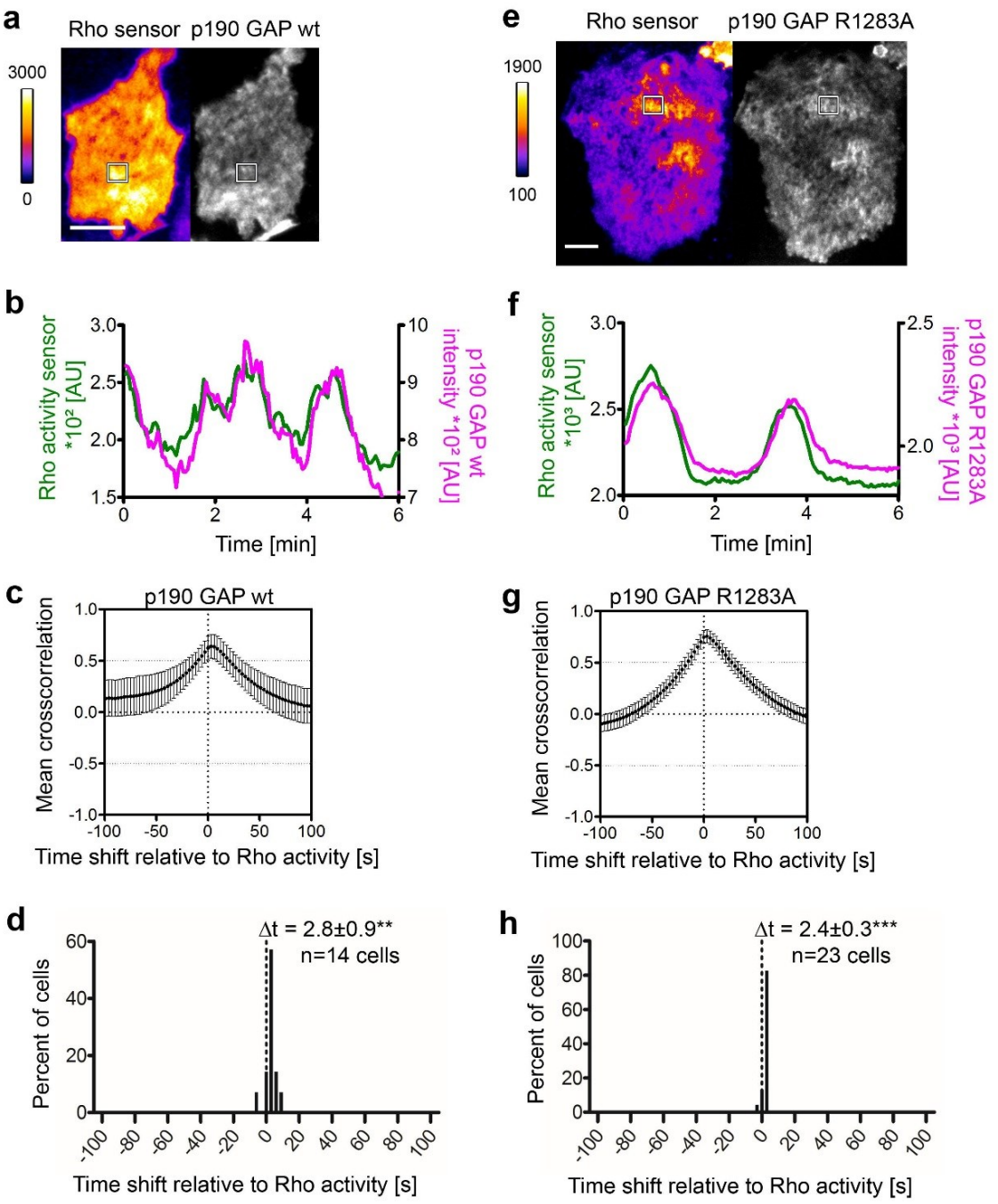

Figure 3.6.5: p190RhoGAP oscillations correlate with Rho activity in space and time.

(a,e) Individual frames of TIRF measurements of a representative U2OS cell expressing delCMV-mCherry-RBD (depicted as Fire LUT) and EGFP-p190RhoGAP wild-type (wt) **(a)** or the GAP-deficient mutant EGFP-p190RhoGAP R1283A **(e)**, treated with nocodazole (30 µM, 45-90 min). Scale bars: 10 µm. Frame rate: 3/min. Calibration bars indicate AU. **(b,f)** Intensity plots of regions marked in **a** and **c** (white boxes). **(c,g)** Mean temporal crosscorrelation functions of Rho activity and p190RhoGAP constructs (N = 14 or 23 cells from four experiments). Error bars show 95% confidence interval. **(d,h)** Percent of cells with given time shifts at the point of maximal crosscorrelation relative to Rho activation, derived from **c** and **h** (***: P<0.001; **: P<0.01 in one-sample t test; ±s.e.m.).

3.6.4 Myosin9b activity modifies Rho activity oscillations

Myosin9b (Myo9b) belongs to the class IX myosins that comprise a RhoGAP domain in addition to the myosin head domain (Reinhard et al, 1995). Myo9b was shown to act as a motorized RhoGAP in cellular regions of actin polymerization (van den Boom et al, 2007). To study a potential role of this RhoGAP in Rho activity oscillations, U2OS cells were transfected with the Rho activity sensor delCMV-mCherry-RBD and either wild-type Myo9b, or its GAP-deficient mutant (Myo9bR1695M). Cells were treated with 30µM nocodazole (45-90 min) and the fluorescence intensity dynamics of both signals were recorded via TIRF microscopy.

Representative cells expressing both, wild-type or mutant GAP are shown in Figure 3.6.6a and 3.6.6e. Intensity profiles of selected regions revealed distinct Rho activity oscillation patterns (Figure 3.6.6b and 3.6.6f). Whereas oscillations with the GAP deficient mutant Myo9b R1695A appears similar to oscillations observed in non-manipulated cells (see Figure 3.1.11) expression of wild-type Myo9b leads to substantially decreased width of the Rho activity oscillations (Figure 3.6.6b and 3.6.6f) (Myo9b wt: N = 21 cells; Myo9b R169M: N = 25 cells from three experiments). Crosscorrelation analyses further supported this difference as in contrast to the GAP deficient mutant, multiple cells displaying a high crosscorrelation coefficient ($r > 0.8$) could be observed with wild-type Myo9b, coinciding with accelerated oscillation dynamics. As these accelerated oscillations were observed in only a sub-set of Myo9b wt expressing cells (32 % ± 7 % s.e. from three experiments), mean maximal crosscorrelation was decreased as compared to Myo9bR1695M (Myo9b wt: $r = 0.22 \pm 0.05$ s.e.m.; Myo9b R1695M*:* $r = 0.42 \pm 0.05$ s.e.m.) (Figure 3.6.6c and 3.6.6g). The slight delay to Rho activity ($\Delta t = 1.1$ s ± 0.5 s.e.m. for the wild-type and $\Delta t = 3.0$ s ± 1.3 s.e.m. for Myo9b R1695M) was similar to those found for p190RhoGAP constructs (Figure 3.6.5d and 3.6.5h).

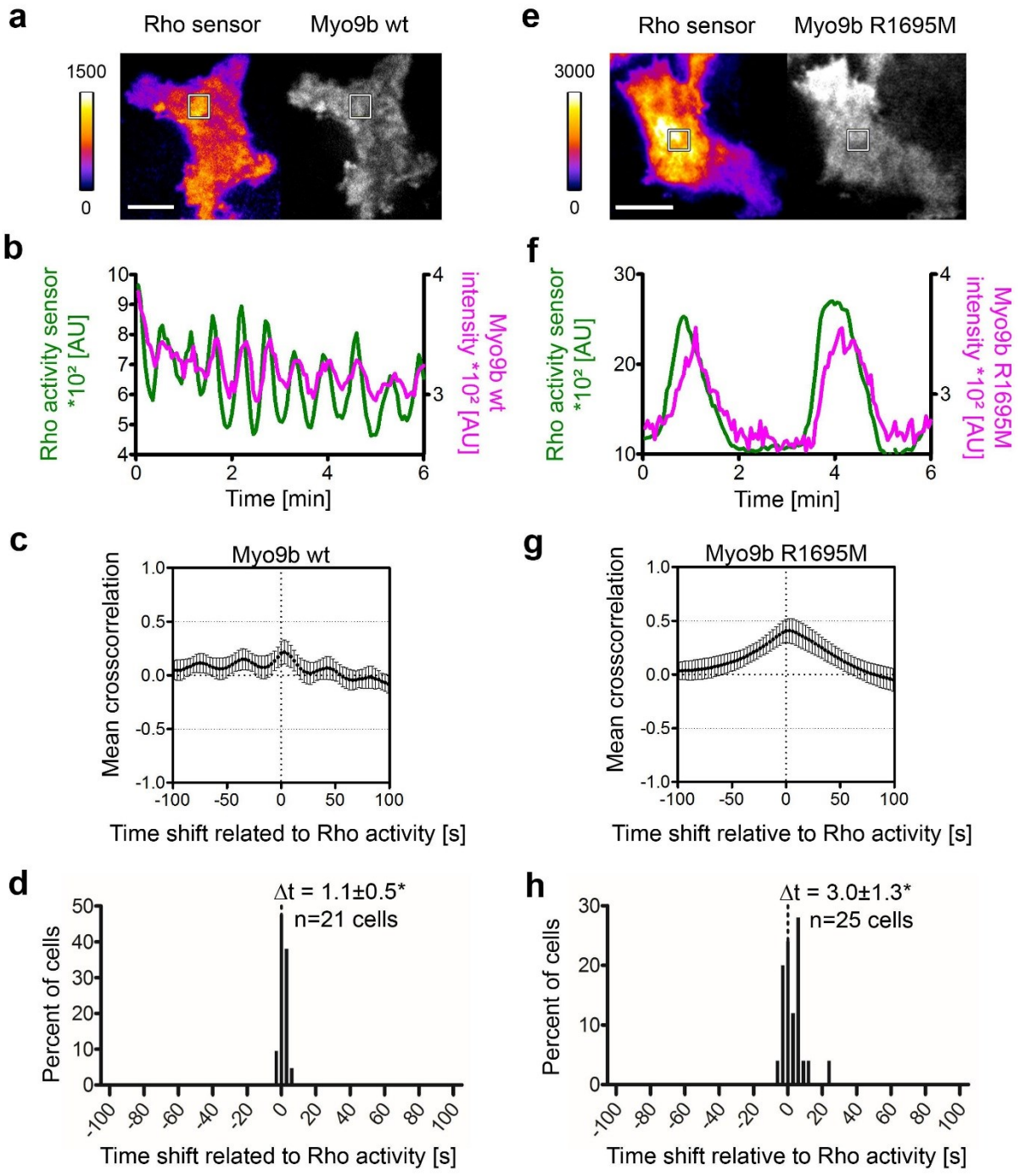

Figure 3.6.6: Myosin9b modulates Rho activity oscillations.

(a,e) Individual frames of TIRF measurements of a representative U2OS cell expressing delCMV-mCherry-RBD (depicted as Fire LUT) and EGFP-Myosin9b wild-type (wt) **(a)** or the GAP-deficient mutant EGFP- Myosin9b R1695A **(e)**, treated with nocodazole (30 µM, 45-90 min). Scale bars: 10 µm. Frame rate: 3/min. Calibration bars indicate AU. **(b,f)** Intensity plots of regions marked in **a** and **c** (white boxes). **(c,g)** Mean temporal crosscorrelation functions of Rho activity and Myosin9b constructs (N = 21 or 25 cells from three experiments). Error bars show 95% confidence interval. **(d,h)** Frequency distribution of the maximal crosscorrelations derived from **c** and **h** (***: P<0.001; **: P<0.01 in one-sample t test; ±s.e.m.).

Based on the progression of the intensity plots and the mean crosscorrelation analyses, overexpression of wild-type Myo9b seems to shorten the duration of individual Rho activity oscillations leading to elevated oscillation frequency.

This observation was further quantified by measurement of the average peak width of Rho activity oscillations. In particular, the peak width was defined as the time difference between two intensity minima. Figure 3.6.7 depicts the significant decrease in oscillation peak width of Rho activity with Myo9b wt as compared to EGFP-C1 plasmid. Interestingly, expression of the GAP deficient mutant did not lead to any change in the peak width suggesting that GAP activity towards Rho is involved in the signal network controlling Rho activity oscillations (EGFP-C1: N = 31, Myo9b wt: N = 21 cells, Myo9b R1695M: N = 25 cells).

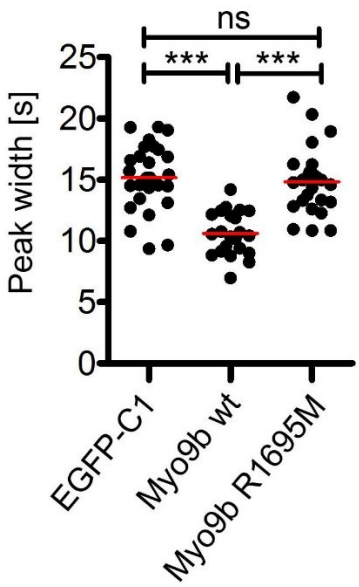

Figure 3.6.7: Wild-type Myo9b alters the peak width of Rho activity oscillations.

Peak width of Rho activity oscillations in U2OS cells was quantified by measuring the time between two intensity minima (in seconds). Cells were transfected with delCMV-mCherry-RBD to measure Rho activity dynamics together with EGFP-C1 (N = 31), EGFP-Myo9b wt (N = 21) or the GAP-deficient mutant EGFP-Myo9b R1695M (N = 25), respectively. Nocodazole treatment was done before TIRF live-cell imaging (30 µM, 45-90 min); frame rate 20/min. Red lines indicate mean; ***: P<0.001; ns: not significant in unpaired t-test).

Together, in this part of the work, three Rho GAPs were identified as potential regulatory modules that are involved in the excitable signal network controlling Rho activity oscillations in U2OS cells.

4. Discussion and Outlook

A hallmark for excitable behavior is the emergence of travelling waves. The presence of wave-like behavior of the actin cytoskeleton was first reported by Vicker and colleagues in *Dictyostelium* (Vicker et al, 1997; Vicker, 2000 and 2002). More recent studies have revealed that these actin waves occur due to actin polymerization, caused by an underlying excitable system that governs amoeboid motility (Naoki et al, 2008; Xiong et al, 2010; Iglesias and Devreotes, 2012; Shi and Iglesias, 2013). Interestingly, in *Dictyostelium* myosin-IB was found to be associated to actin waves, although its depletion had no effect on the ability of cells to form actin waves (Bretschneider et al, 2009; Brzeska et al, 2014). In stationary, mammalian cells actin waves were found to mediate Rac-induced actin polymerization via Arp2/3 (Weiner et al, 2007). In mouse fibroblasts, melanoma B16-F10 cells and U2OS cells, actin waves contained paxillin, vinculin and talin, additionally to ARP2/3, and are thought to facilitate adhesion (Case and Waterman, 2011). Nevertheless, the functional significance of F-actin waves in mammalian cells remains unclear, but it has been hypothesized that they are associated with environmental exploration (Weiner et al, 2007; Allard and Mogilner, 2013). Accordingly, oscillatory behavior could imply a direct link between actin waves and myosin-II, which is a key regulator of mechanosensation, as it mediates the transduction of mechanical information into biochemical information (reviewed by Aguilar-Cuenca et al, 2014). Myosin-II mediated cell contractility was found to be mainly regulated by the RhoA-ROCK pathway (reviewed by Riento and Ridley, 2003). In mammalian cells, cyclic RhoA activity was observed in the leading edge of migrating cells that is subject to protein kinase A (PKA) activity and regulates protrusion retraction cycles of the cell membrane (Tkachenko et al, 2011). Furthermore, two independent recent studies have demonstrated oscillatory behavior of Rho activity during embryogenesis in fruit fly, frogs and star fish (Munjal et al, 2015; Bement et al, 2015). Interestingly, although those Rho oscillations correlated with acto-myosin pulses, pharmacological inhibition of myosin activity did not affect activity dynamics of Rho.

In this thesis, irregular oscillations of Rho activity are described and characterized in detail for the first time in mammalian cells. In particular, the role of Rho in the proposed excitable activator-inhibitor network underlying those oscillations was elucidated. Overall, the findings in this work suggest that Rho oscillations recruit and activate downstream effectors, including myosin-IIa, actin and FHOD1. Furthermore, this oscillatory Rho signal network was found to

respond to external cues and to self-organize by recruiting its own activators and inhibitors that in turn control spatial and temporal activity dynamics of the GTPase.

4.1 Irregular Rho activity oscillations are generated by an excitable system

The Rho GTPase RhoA is a key regulator of numerous cellular functions, each of which is controlled via specialized effectors that switch on distinct downstream signaling pathways. For instance, RhoA can activate multiple kinases, such as citron kinase, protein kinase C-related kinase (PRK1) or Rho-associated coiled-coil kinase (ROCK) (reviewed by Bishop and Hall, 2000; Karnoub et al, 2004). These kinases can phosphorylate several substrates, leading to a broad range of cellular responses downstream of RhoA. For example, ROCK was shown to promote cell motility but also cell-size regulation and centrosome positioning (reviewed by Riento and Ridley, 2003). As for other GTPases, the multitude of effectors alone is not sufficient to explain how RhoA can coordinate complex cellular processes in space and time. During the recent years, several studies revealed the relevance of spatio-temporal regulation of GTPase activity. In particular, the isoprenylation at the C-terminus that mediates the insertion of the active Rho proteins into the plasma membrane was reported to be essential for their correct function (Michaelson et al, 2001). Furthermore, in migrating cells, activation of distinct signal pathways downstream of Rho proteins was suggested to depend on whether the GTPase was activated in the leading edge (Machacek et al, 2009; Nalbant et al, 2009), or in the trailing end (Ridley and Hall, 1992; Nobes and Hall, 1995). However, mechanisms defining sub-cellular Rho recruitment and activation patterns are still not understood.

Here, we report transient oscillations of Rho cortex activity in U2OS cells measured via TIRF microscopy by use of an effector-domain based activity biosensor. This effector domain, Rhotekin, was found to interact strongly with RhoA and RhoC, but only weakly with RhoB, and not at all with Rac1 or Cdc42 (Reid et al, 1996). We provide evidence that the observed oscillations are generated by an excitable activator (X) - inhibitor (Y) network consisting of a fast positive feedback that is coupled to a slow negative feedback (see Figure 4.1) (reviewed by Allard and Mogilner, 2013). In particular, we have observed waves of Rho activity (section 3.1.2) which is in agreement with signal propagation generated by an excitable network (Sinha and Sridhar, 2014). In theory Rho activity could fulfill different functions in this excitable network (Figure 4.1a-b). As a simple downstream “effector” of the network, Rho signal perturbation, such as global increase, should not affect oscillation dynamics (Figure 4.1a). However, global stimulation of RhoA activity by nocodazole, which has been shown to be

mediated by the upstream guanine nucleotide exchange factor GEF-H1, significantly enhanced Rho oscillation amplitude and frequency (section 3.1.4). Secondly, the activator "X" in the model of an activator-inhibitor network can amplify its own activity via a positive feedback. Indeed, data provided by Johannes Koch shows that localization signals of GEF-H1 strongly correlate with Rho activity oscillations with only a short time delay. These findings suggest that Rho recruits its activator to amplify its signal strength during oscillations and comprise an integral part of the oscillation generating network (Figure 4.1b).

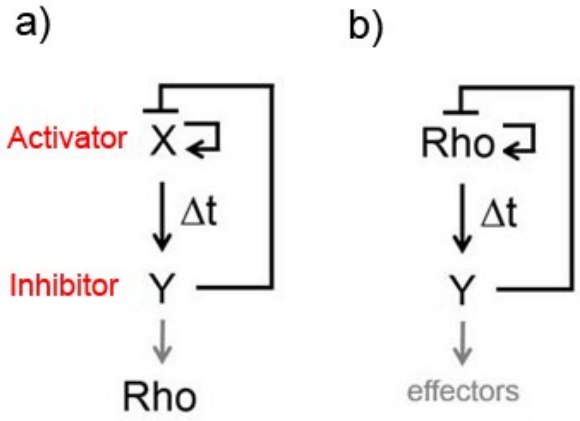

Figure 4.1: Potential roles of Rho in an excitable system, composed of an activator-inhibitor network.

Excitable network composed of a positive feedback loop, controlled by the activator X, and a delayed negative feedback loop, mediated by component Y. Rho activity oscillations can occur if Rho is an effector of the network **(a)**. However, experimental evidence indicates that Rho acts as activating component **(b)**.

4.2 Transient oscillations of cortical actin downstream of Rho might recruit time-delayed inhibitory signals

The dynamic actin cytoskeleton plays a fundamental role in all eukaryotes, mediating various cellular processes. Among those processes the most thoroughly characterized are cell migration and endocytosis that both are driven by actin polymerization and associated with membrane dynamics (reviewed by Pollard and Borisy, 2003; Kaksonen et al, 2006). The precise spatial coordination of actin polymerization was found to depend on membrane curvature via the recruitment of the nucleation-promoting factor neural Wiskott-Aldrich syndrome protein (N-WASP) and the actin nucleator the actin-related protein (Arp) 2/3 complex (Takano et al, 2008; Gallop et al, 2013). Remarkably, this two actin-modulating proteins were reported to display oscillatory behavior in human neutrophils and U2OS cells, coinciding with actin waves, downstream of Rac1 (Weiner et al, 2007; Case and Waterman, 2011).

Here, a new type of irregular actin oscillations downstream of Rho was described for the first time in human cells. These transient patterns of actin cortex localization showed no correlation to the localization of commercial Arp2/3 constructs (Addgene 8462 and 23224; data not shown) and were distinct from ventral F-actin waves reported previously in U2OS cells (section 3.1.2, Figure 3.1.6). Also, this type of oscillatory behavior occurred at the flat membrane/surface interface being independent of membrane curvature changes. Instead, actin waves shown here correlated with Rho activity oscillations (section 3.1.2, Figure 3.1.5) and emerged with a significant temporal delay relative to Rho activity (section 3.1.5; Figure 3.1.9). This temporal delay suggest that actin oscillation are generated downstream of Rho and therefore depend on its activity. In agreement with this conclusion, nocodazole-induced Rho stimulation led to a significant increase in amplitude and frequency of actin oscillations (section 3.1.4; Figure 3.1.8). A recent study has reported waves of Rho activity and F-actin polymerization in oocytes and embryonic cells, derived from frogs and star fish (Bement et al, 2015), indicating that oscillations of actin are indeed relevant for physiological behavior. In particular, the described actin waves have been shown to appear during cytokinesis and were proposed to emerge in regions with dynamic F-actin assembly that follow and inhibit Rho activity waves (Bement et al, 2015). However, these waves were not dependent on contractility, as myosin-II inhibition did not alter wave dynamics (Bement et al, 2015) and thus they are distinct from the actin contractility oscillations reported in this theses.

Contractile actin nodes described here might provide a structural surface to mediate time delayed accumulation of inhibitory signals that temper Rho activity during oscillations. In particular, several potential inhibitor signals such as myosin-IIa and several RhoGAPs have been identified and are discussed below.

4.3 Time-delayed myosin-IIa accumulation as potential mediator of Rho activity inhibition

Non-muscle myosin-II is an actin-binding and crosslinking protein that plays a fundamental role in cell contractility. Its properties are regulated by phosphorylation via myosin light-chain kinase, which in the context of contractility is thought to be promoted by the Rho-ROCK pathway (Totsukawa et al, 2000). Oscillatory nature of acto-myosin systems was first described in an *in vitro* assay composed of single actin filaments and randomly distributed myosin-II motor proteins (Placais et al, 2009). Later, atomic force microscopy used to monitor elasticity

of epithelial cells and confirmed spontaneous oscillation of the cytoskeleton *in vivo* (Schillers et al, 2010). Recent studies further provide evidence that pulsed contractions of myosin drive morphogenesis in mouse and *Drosophila* embryos (Vasquez et al, 2014; Maitre et al, 2015). In COS-7 cells (derived from monkey kidney), propagating aggregates of myosin-XV were observed only recently, forming traveling waves or pulse-trains along cellular protrusions (Yochelis et al, 2015).

Here, transient accumulations of myosin-IIa at the cell cortex were detected for the first time in human cells that correlated with Rho activity oscillations. Myosin-IIa oscillations emerged with a temporal delay of approx. 40 s relative to Rho oscillations (section 3.1.6) suggesting upstream control by the Rho-ROCK signal pathway.

Inhibition of myosin-IIa via blebbistatin (Kovacs et al, 2004) strongly impaired Rho activity oscillations (3.5.2), strongly suggesting a feedback of myosin-IIa to control Rho activity. Such feedback was further verified by pharmacological inhibition of ROCK kinase, which reduced Rho activity dynamics very efficiently (section 3.5.1). To further elaborate on this idea, spatio-temporal myosin-IIa dynamics were correlated to actin contractility in cooperation with Leif Dehmelt (MPI Dortmund / CCB, TU Dortmund). In particular, the spatio-temporal image correlation (STICS) ImageJ (ICS) plugin (measuring the temporal development of the translocation of myosin-IIa flux fields) with a built-in Matlab function (measuring the divergence of the resulting vector field) to separate cellular regions with outward fluxes ("sources") from regions with inward fluxed ("sinks") (Graessl et al, submitted). Notably, we found that maximal cellular contraction not only correlates with maximal myosin-IIa intensity, but precedes it by 35.1 ± 3.4 s. This significant time lag indicates that myosin-driven contractility might self-amplify via enhanced myosin-IIa accumulation to the cell cortex.

Interestingly, myosin-II-mediated contractility might temper Rho activity by multiple potential mechanisms. First, myosin-II-mediated contractility could indirectly inhibit Rho activity by reducing the feedback of Rho self-amplification. Second, the Rho regulators GEF-H1 and LARG were shown to get activated by Src family kinases (Fyn and ERK) in response to tension force (Guilluy et al, 2011). Furthermore, multiple actin and myosin associated RhoGAPs have been identified in this work as potential inhibitors of Rho activity during oscillation generation and are discussed in detail below.

4.4 The inhibitory feedback between Rho and myosin-IIa activity is mediated by RhoGAPs

In order to generate oscillations of a signal X, a precise temporal coordination of activating and inhibitory regulators is required (Figure 4.2). We hypothesize that the activity dynamics revealed in this thesis for Rho and downstream effectors, emerge from an underlying activator-inhibitor network. Accordingly, the transient intensity peaks are caused by signal amplification, coupled to an inhibiting component, decreasing the activity to a basal level, see Figure 4.2.

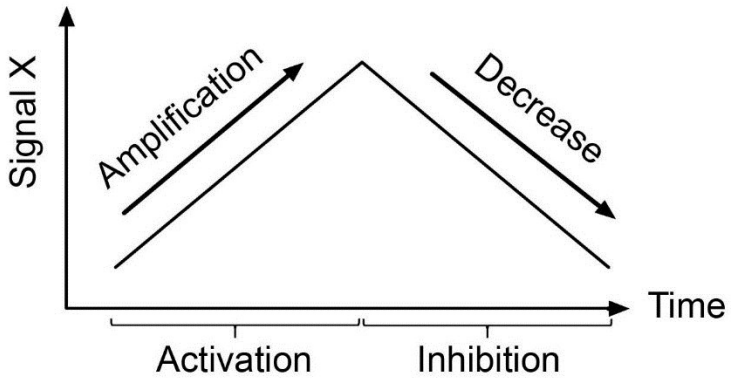

Figure 4.2: Schematic illustration of a transient intensity peak caused by an activator-inhibitor network.

As mentioned above, we suggest that the guanine nucleotide exchange factor GEF-H1 mediates the self-amplification of Rho activity in U2OS cells (Graessl et al, submitted). The inhibitory component in the activator-inhibitor network, on the other hand, could link myosin-IIa with Rho activity. Therefore, oscillatory behavior of several acto-myosin- and Rho-related RhoGAPs was examined (all tested candidates are listed in the Supplemental Material, Table 1). Of the nine RhoGAPs tested, three, ARHGAP18 (collaboration with Johannes Koch), p190RhoGAP and Myosin9b, displayed activity oscillations (Graessl et al, submitted). Interestingly, GAP-deficient mutants showed oscillatory behavior more frequently and had a higher crosscorrelation with Rho oscillations, compared to the corresponding wild-type constructs (section 3.6). This might be due to the inhibitory function of the wild-type GAPs on the oscillatory network, if overexpressed. For all three RhoGAPs, maximal crosscorrelation of oscillations was reached approximately 3s after Rho activity maximum (Figure 3.6.5). This is in agreement with a gradual increase of GAP activity towards Rho that counteracts the Rho self-activation (Figure 4.2).

If a distinct RhoGAP activity is sufficient to temper Rho activity during oscillatory behavior, its overexpression is expected to alter dynamics of activity oscillations. However, expression

of wild-type p190RhoGAP and ARHGAP18 did not alter the duration (peak width) or frequency of Rho activity oscillations (data not shown), suggesting that activity of these two GAPs alone is not sufficient to temper RhoA activity in this context. Interestingly, although Rho activity oscillations were not altered in cells expressing wild-type ARHGAP18 (data not shown), a strong localization of this GAP to stress fibers and focal adhesions was observed suggestive of an indirect regulatory function (Figure 3.6.1). Thus, the role of ARHGAP18 to generate Rho oscillatory behavior was further investigated in ARHGAP18-depleted cells (section 3.6.2). Interestingly, while ARHGAP18 depletion did not affect Rho activity oscillations in unperturbed cells, stimulation of oscillations after nocodazole treatment was significantly tempered in cells lacking the RhoGAP (Figure 3.6.4). These findings imply a regulatory function of ARHGAP18 in the generation of Rho oscillations, albeit only after upon nocodazole mediated GEF-H1 activation, where additional signaling molecules might be activated to potentially facilitate ARHGAP18 function. Thus, the ARHGAP18 knock-out cell line will be a valuable tool to be used in future experiments to further elaborate on the potential interplay between multiple regulatory RhoGAPs.

For the GAP-deficient mutant of Myo9b and a sub-set of Myo9b wt expressing cells (approx. 30 %) oscillatory behavior was observed, correlating with Rho activity oscillations (section 3.6.4). Interestingly, expression of wild-type Myo9b lead to elevated frequency of Rho activity oscillations, as demonstrated by analysis of Rho oscillation peak width (Figure 3.6.7). The fact that neither the expression of the GAP deficient mutant, nor of pEGFP-C1 had this effect on Rho oscillations further confirms that Myosin9b activity is an integral part of the excitable signal network regulating Rho activity oscillations.

Myo9b is a plus-end directed motor protein (O'Connell and Mooseker, 2003) that was shown to be enriched at sites of actin polymerization such as filopodia and retraction fibers (van den Boom et al, 2007; Bähler et al, 2011). Thus, the time-delayed oscillatory formation of contractile acto-myosin fibers might arise from dynamic F-actin assembly. Future experiments using RNAi-mediated knockdown of the RhoGAP and pharmacological perturbation of potential effectors, such as actin filaments and myosin-II, will provide further details of the regulatory function of Myo9b in Rho activity oscillations.

4.5 Irregular oscillations of FHOD1 are downstream of Rho

The human formin FHOD1 might link different signaling pathways, as it has multiple regulators and cellular functions (section 1.3.2.2). Downstream of Src-family of kinases FHOD1 controls gene expression (Koka et al, 2005), while its activation by nesprin-2g is crucial for nuclear movement (Kutscheidt et al, 2014; Antoku et al, 2015). Downstream of RhoA, the formin is thought to regulate stress fiber formation and focal adhesion maturation (Iskratsch et al, 2013; Schulze et al, 2014) via its dual function as actin capping and bundling protein (Schönichen et al, 2013).

In this work, the dynamic localization of FHOD1 was studied in live-cell TIRF measurements and for the first time irregular oscillations of wild-type FHOD1 were observed. They appeared with a temporal delay of approx. 6s after Rho activity oscillations (section 3.2.1) and were enhanced by nocodazole-induced Rho stimulation (Supplemental Material, Figure S1).

The mean maximal crosscorrelation between FHOD1 oscillations and myosin-IIa intensity peaks, on the other hand was found to be shifted approx. 15 s towards FHOD1 activity (section 3.2.2). However siRNA-mediated knock-down of the formin did not alter myosin-IIa oscillations (section 3.2.3), indicating alternative signaling pathways to be involved in myosin-IIa regulation.

Notably, experiments performed with the constitutive active FHOD1 mutants FHOD1 1-1011 (lacking the auto-inhibitory DAD domain) and FHOD1 V228E (this point mutation keeps the protein in its active state) revealed less pronounced oscillations, compared to wild-type FHOD1 (data not shown). This observation suggests that the dynamic change between FHOD1 activity states is required to display oscillatory behavior. In agreement with this, FHOD1 oscillation frequency and peak amplitude were significantly decreased after pharmacological ROCK inhibition (section 3.3), implicating a direct link between FHOD1 oscillatory behavior and its activity cycle regulated by ROCK mediated phosphorylation. In turn, Rho activity oscillations did not seem to be controlled by FHOD1 activity, as siRNA-mediated knock-down of the formin did not alter Rho oscillations (section 3.2.3). In contrast, FHOD1 depletion, distinctively tempered actin oscillations (section 3.2.2), while perturbed actin dynamics after Cytochalasin D or Latrunculin A treatment did not affect FHOD1 oscillations (section 3.4). These findings suggest that localized dynamics of FHOD1 activity might control actin oscillations potentially due to recruiting sub-populations of monomeric actin to polymerization sites and sites of newly formed focal adhesions. Concomitantly, a current study by Iskratsch and colleagues found that FHOD1 is targeted to integrin sites via direct interaction with Src family kinases (Iskratsch et al, 2013). However, the authors also reported that this recruitment is upstream of ROCK

activation in mouse embryonic fibroblast (Iskratsch et al, 2013). Our observations that the inhibition of ROCK impairs FHOD1 oscillations, while its knockdown does not disturb Rho or myosin-II oscillations, contradict this finding and suggest FHOD1 oscillations occur downstream of ROCK (section 3.3 and 3.2.3).

4.6 Biological relevance of Rho activity and acto-myosin oscillations

The internal architecture and fate of cells is long-known to be influenced by their ability to adhere to extracellular matrix (Chen et al, 1997; Folkman and Moscona, 1978; McBeath et al, 2004). During cell adhesion and spreading, tension within the cell is developed that orchestrates the reorganization of the cytoskeleton and polarity (reviewed by Zemel and Safran, 2011). This intracellular force was shown to mediate cell differentiation (McBeath et al, 2004) and growth control (Chen et al, 1997; Tilghman et al, 2010; Mih et al, 2012) by activating major regulatory pathways in integrin-mediated cell-matrix adhesions and other types of adhesion structures (Bershadsky et al, 2006). During cell shape changes, conventional models depict that protrusive forces are generated by Arp2/3 mediated G-actin polymerization, pushing the membrane forward (reviewed by Cramer, 1997; Small et al, 2002; Pollard and Borisy, 2003). However, recent studies using traction force microscopy were able to demonstrate that the increase in spreading area precedes the development of force (Dubin-Thaler et al, 2008; Nisenholz et al, 2014). Also, two independent studies have reported that cells were still able to form protrusions even when Arp2/3 activity was inhibited (Suraneni et al, 2012; Wu et al, 2012), suggesting additional mechanisms to generate protrusive force. Recently, numerous studies have reported the role of myosin-II in cell migration. There, myosin-II is thought to counteract cell spreading by increasing the retrograde F-actin flow (Giannone et al, 2004; Cai et al, 2006). Furthermore myosin-II-mediated contractility, downstream of the RhoA-ROCK pathway, is thought to provide the necessary mechanical integrity and rigidity for cell motility (Koenderink et al, 2009; Cai et al, 2010; Aratyn-Schaus et al, 2011).

Here, we observed two distinct localization patterns for myosin-IIa in spreading cells. First, in agreement with previous findings, myosin-II was robustly localized at the cell periphery, suggesting its association with the actin-retrograde flow and stress fiber formation. Surprisingly, myosin-II localization did not correlate with Rho activity oscillations indicating an alternative regulatory mechanism for this myosin-II population.

In addition, we found highly transient myosin-IIa patterns in the cells center (section 3.1.1) that are strongly correlated with Rho activity oscillations. In adherent cells, those Rho-myosin

oscillations were highly correlated with oscillations of actin (section 3.1.5). Thus, oscillations in the cell center might be relevant for probing the extracellular environment, such as matrix elasticity, and for regulating signal pathways controlling the cellular response during cell fate decisions. However this hypothesis has to be further investigated in live-cell spreading assays to study the spatio-temporal activity dynamics of signaling proteins that are established to mediate cell survival and proliferation during cellular spreading, such as focal adhesion kinase (FAK) or zyxin (Pirone et al, 2006; van der Gaag et al, 2002). Previously, GEF-H1 was shown to control the leading edge activity pattern of RhoA activation (Nalbant et al, 2009) and its depletion was found to reduce the spread area of cells (Vega et al, 2012). Thus, it will be also interesting to investigate the impact of GEF-H1 overexpression or knock-down, in order to dissect how the distinct localization patterns of myosin-II during cell spreading are regulated by this pathway.

Mechanosensing is an integral part of cellular durotaxis that is the directional migration in response to differences in the extracellular matrix elasticity (Lo et al, 2000). A potential role of the identified activator-inhibitor network could constitute the spatio-temporal coordination of processes relevant to mechanosensing. We have shown that local myosin-IIa activity patterns, downstream of Rho activity oscillations facilitate cell contractility (Graessl et al, submitted). This in turn, was previously shown to mediate the intracellular response to extracellular substrate rigidity (Discher et al, 2005). Secondly, we found that the pharmacological inhibition of cell contractility leads to a significant decrease of Rho activity oscillation amplitudes and frequencies (section 3.5.2), implying a feedback between intracellular force and Rho activity oscillations. Interestingly, stiffening caused by internal contractility was reported to induce the same cellular response as stiffening created by external stress (Koenderink et al, 2009; Geiger et al, 2009). Thirdly, the frequency and amplitude of myosin-IIa oscillations was significantly reduced on softer substrates, which coincided with a rise of both protrusion size and number (section 3.1.7). Notably, these long and narrow extensions resemble filopodium-like protrusions, detected in invasive cancer cells (Shibue et al, 2012). The formation of such invadosome-like protrusions that are induced by soft matrices was recently described for primary fibroblasts (Gu et al, 2013). Thus, local oscillations of acto-myosin contractility and Rho activity might play a role in tumor stroma related mechanosensation. Additional experiments using local manipulation of external forces such as via perturbation of matrix elasticity will help to elaborate on the potential role of Rho and myosin-IIa oscillations in mechanosensing.

Taken together, the findings presented in this thesis provide first evidence that extracellular cues modulate the irregular oscillations of myosin-IIa and potentially Rho activity.

In summary, we have identified an excitable activator-inhibitor network (Figure 4.3) that generates oscillatory Rho activity dynamics in U2OS cells. We propose that Rho represents the activator in this network that can self-amplify its activation by a positive feedback via the guanine nucleotide exchange factor GEF-H1. A time-delayed negative feedback is provided by the acto-myosin network that inhibits Rho activity via multiple potential RhoGAP pathways, such as Myo9b and ARHGAP18. We further show evidence that the proposed excitable signal network contributes to exploratory processes mediated by mechanosensing, such as cell spreading and durotaxis, directional migration in response to different matrix elasticities.

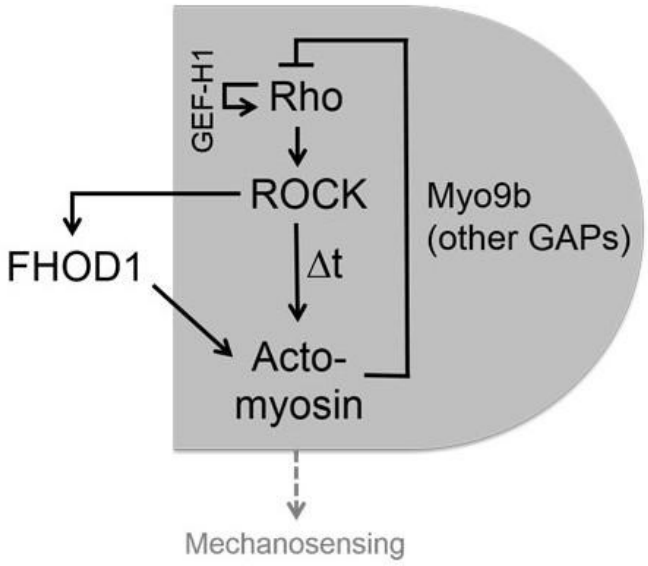

Figure 4.3: Schematic illustration of the proposed excitable network generating Rho oscillations

Proposed excitable network regulating the observed oscillatory behavior in U2OS cells and mediating mechanosensing. Accordingly, Rho activity oscillations self-amplify via GEF-H1 and activate the downstream effector Rho-kinase (ROCK). A delayed inhibitory feedback loop, comprising acto-myosin contractility oscillations, inactivates Rho again. Thus, generating the cycling between transient activation and inactivation, underlying oscillatory behavior and exploratory processes. FHOD1, on the other hand, does not seem to be involved in this excitable network, although it displays oscillatory behavior downstream of ROCK that is involved in the dynamic control of acto-myosin.

References

Abe, K., K. L. Rossman, B. Liu, K. D. Ritola, D. Chiang, S. L. Campbell, K. Burridge and C. J. Der (2000). "Vav2 Is an Activator of Cdc42, Rac1, and RhoA." Journal of Biological Chemistry **275**(14): 10141-10149.

Abercrombie, M., J. E. Heaysman and S. M. Pegrum (1970). "The locomotion of fibroblasts in culture. I. Movements of the leading edge." Exp Cell Res **59**(3): 393-398.

Aguilar-Cuenca, R., A. Juanes-García and M. Vicente-Manzanares (2014). "Myosin II in mechanotransduction: master and commander of cell migration, morphogenesis, and cancer." Cellular and Molecular Life Sciences **71**(3): 479-492.

Alberts, A. S., N. Bouquin, L. H. Johnston and R. Treisman (1998). "Analysis of RhoA-binding Proteins Reveals an Interaction Domain Conserved in Heterotrimeric G Protein β Subunits and the Yeast Response Regulator Protein Skn7." Journal of Biological Chemistry **273**(15): 8616-8622.

Allard, J. and A. Mogilner (2013). "Traveling waves in actin dynamics and cell motility." Curr Opin Cell Biol **25**(1): 107-115.

Alt, W., O. Brosteanu, B. Hinz and H. W. Kaiser (1995). "Patterns of spontaneous motility in videomicrographs of human epidermal keratinocytes (HEK)." Biochem Cell Biol **73**(7-8): 441-459.

Alvarez, D. E. and H. Agaisse (2013). "The formin FHOD1 and the small GTPase Rac1 promote vaccinia virus actin-based motility." J Cell Biol **202**(7): 1075-1090.

Amano, M., K. Chihara, N. Nakamura, T. Kaneko, Y. Matsuura and K. Kaibuchi (1999). "The COOH terminus of Rho-kinase negatively regulates rho-kinase activity." J Biol Chem **274**(45): 32418-32424.

Amano, M., M. Ito, K. Kimura, Y. Fukata, K. Chihara, T. Nakano, Y. Matsuura and K. Kaibuchi (1996). "Phosphorylation and Activation of Myosin by Rho-associated Kinase (Rho-kinase)." Journal of Biological Chemistry **271**(34): 20246-20249.

Ambrose, E. J. (1956). "A Surface Contact Microscope for the study of Cell Movements." Nature **178**(4543): 1194-1194.

Ang, S. F., Z. S. Zhao, L. Lim and E. Manser (2010). "DAAM1 is a formin required for centrosome re-orientation during cell migration." PLoS One **5**(9).

Antoku, S., R. Zhu, S. Kutscheidt, O. T. Fackler and G. G. Gundersen (2015). "Reinforcing the LINC complex connection to actin filaments: the role of FHOD1 in TAN line formation and nuclear movement." Cell Cycle **14**(14): 2200-2205.

Aratyn-Schaus, Y., P. W. Oakes and M. L. Gardel (2011). "Dynamic and structural signatures of lamellar actomyosin force generation." Mol Biol Cell **22**(8): 1330-1339.

Arthur, W. T. and K. Burridge (2001). "RhoA inactivation by p190RhoGAP regulates cell spreading and migration by promoting membrane protrusion and polarity." Mol Biol Cell **12**(9): 2711-2720.

Axelrod, D. (1981). "Cell-substrate contacts illuminated by total internal reflection fluorescence." J Cell Biol **89**(1): 141-145.

Axelrod, D. (2008). "Chapter 7: Total internal reflection fluorescence microscopy." Methods Cell Biol **89**: 169-221.

Axelrod, D., T. P. Burghardt and N. L. Thompson (1984). "Total internal reflection fluorescence." Annu Rev Biophys Bioeng **13**: 247-268.

Azzarelli, R., T. Kerloch and E. Pacary (2015). "Regulation of cerebral cortex development by Rho GTPases: insights from in vivo studies." Frontiers in Cellular Neuroscience **8**.

Bähler, M. (1996). "Myosins on the move to signal transduction." Curr Opin Cell Biol **8**(1): 18-22.

Bähler, M., K. Elfrink, Peter J. Hanley, S. Thelen and Y. Xu (2011). "Cellular functions of class IX myosins in epithelia and immune cells." Biochemical Society Transactions **39**(5): 1166-1168.

Bakolitsa, C., J. M. de Pereda, C. R. Bagshaw, D. R. Critchley and R. C. Liddington (1999). "Crystal structure of the vinculin tail suggests a pathway for activation." Cell **99**(6): 603-613.

Barnhart, E. L., K.-C. Lee, K. Keren, A. Mogilner and J. A. Theriot (2011). "An Adhesion-Dependent Switch between Mechanisms That Determine Motile Cell Shape." PLoS Biol **9**(5): e1001059.

Bechtold, M., J. Schultz and S. Bogdan (2014). "FHOD proteins in actin dynamics--a formin' class of its own." Small GTPases **5**(2): 11.

Bement, W. M., M. Leda, A. M. Moe, A. M. Kita, M. E. Larson, A. E. Golding, C. Pfeuti, K.-C. Su, A. L. Miller, A. B. Goryachev and G. von Dassow (2015). "Activator-inhibitor coupling between Rho signalling and actin assembly makes the cell cortex an excitable medium." Nat Cell Biol *advance online publication*.

Bendix, P. M., G. H. Koenderink, D. Cuvelier, Z. Dogic, B. N. Koeleman, W. M. Brieher, C. M. Field, L. Mahadevan and D. A. Weitz (2008). "A Quantitative Analysis of Contractility in Active Cytoskeletal Protein Networks." Biophysical Journal **94**(8): 3126-3136.

Bernards, A. (2003). "GAPs galore! A survey of putative Ras superfamily GTPase activating proteins in man and Drosophila." Biochim Biophys Acta **1603**(2): 47-82.

Berridge, M. J. (2009). "Inositol trisphosphate and calcium signalling mechanisms." Biochimica et Biophysica Acta (BBA) - Molecular Cell Research **1793**(6): 933-940.

Bershadsky, A., M. Kozlov and B. Geiger (2006). "Adhesion-mediated mechanosensitivity: a time to experiment, and a time to theorize." Curr Opin Cell Biol **18**(5): 472-481.

Billuart, P., C. G. Winter, A. Maresh, X. Zhao and L. Luo (2001). "Regulating axon branch stability: the role of p190 RhoGAP in repressing a retraction signaling pathway." Cell **107**(2): 195-207.

Birkenfeld, J., P. Nalbant, B. P. Bohl, O. Pertz, K. M. Hahn and G. M. Bokoch (2007). "GEF-H1 modulates localized RhoA activation during cytokinesis under the control of mitotic kinases." Developmental cell **12**(5): 699-712.

Bishop, A. L. and A. Hall (2000). "Rho GTPases and their effector proteins." Biochemical Journal **348**(Pt 2): 241-255.

Blanchoin, L., R. Boujemaa-Paterski, C. Sykes and J. Plastino (2014). "Actin dynamics, architecture, and mechanics in cell motility." Physiol Rev **94**(1): 235-263.

Borgon, R. A., C. Vonrhein, G. Bricogne, P. R. Bois and T. Izard (2004). "Crystal structure of human vinculin." Structure **12**(7): 1189-1197.

Bos, J. L., H. Rehmann and A. Wittinghofer "GEFs and GAPs: Critical Elements in the Control of Small G Proteins." Cell **129**(5): 865-877.

Bradford, M. M. (1976). "A rapid and sensitive method for the quantitation of microgram quantities of protein utilizing the principle of protein-dye binding." Anal Biochem **72**: 248-254.

Bravo-Cordero, J. J., V. P. Sharma, M. Roh-Johnson, X. Chen, R. Eddy, J. Condeelis and L. Hodgson (2013). "Spatial regulation of RhoC activity defines protrusion formation in migrating cells." J Cell Sci **126**(Pt 15): 3356-3369.

Breitsprecher, D. and B. L. Goode (2013). "Formins at a glance." J Cell Sci **126**(Pt 1): 1-7.

Bretschneider, T., K. Anderson, M. Ecke, A. Muller-Taubenberger, B. Schroth-Diez, H. C. Ishikawa-Ankerhold and G. Gerisch (2009). "The three-dimensional dynamics of actin waves, a model of cytoskeletal self-organization." Biophys J **96**(7): 2888-2900.

Bretschneider, T., K. Anderson, M. Ecke, A. Müller-Taubenberger, B. Schroth-Diez, H. C. Ishikawa-Ankerhold and G. Gerisch (2009). "The Three-Dimensional Dynamics of Actin Waves, a Model of Cytoskeletal Self-Organization." Biophysical Journal **96**(7): 2888-2900.

Bretschneider, T., S. Diez, K. Anderson, J. Heuser, M. Clarke, A. Muller-Taubenberger, J. Kohler and G. Gerisch (2004). "Dynamic actin patterns and Arp2/3 assembly at the substrate-attached surface of motile cells." Curr Biol **14**(1): 1-10.

Brouns, M. R., S. F. Matheson and J. Settleman (2001). "p190 RhoGAP is the principal Src substrate in brain and regulates axon outgrowth, guidance and fasciculation." Nat Cell Biol **3**(4): 361-367.

Brzeska, H., K. Pridham, G. Chery, M. A. Titus and E. D. Korn (2014). "The Association of Myosin IB with Actin Waves in Dictyostelium Requires Both the Plasma Membrane-Binding Site and Actin-Binding Region in the Myosin Tail." PLoS ONE **9**(4): e94306.

Burbelo, P. D., A. A. Finegold, C. A. Kozak, Y. Yamada and H. Takami (1998). "Cloning, genomic organization and chromosomal assignment of the mouse p190-B gene." Biochim Biophys Acta **1443**(1-2): 203-210.

Burbelo, P. D., S. Miyamoto, A. Utani, S. Brill, K. M. Yamada, A. Hall and Y. Yamada (1995). "p190-B, a new member of the Rho GAP family, and Rho are induced to cluster after integrin cross-linking." J Biol Chem **270**(52): 30919-30926.

Burnette, D. T., S. Manley, P. Sengupta, R. Sougrat, M. W. Davidson, B. Kachar and J. Lippincott-Schwartz (2011). "A role for actin arcs in the leading-edge advance of migrating cells." Nat Cell Biol **13**(4): 371-381.

Burridge, K. and E. S. Wittchen (2013). "The tension mounts: stress fibers as force-generating mechanotransducers." J Cell Biol **200**(1): 9-19.

Cai, Y., N. Biais, G. Giannone, M. Tanase, G. Jiang, J. M. Hofman, C. H. Wiggins, P. Silberzan, A. Buguin, B. Ladoux and M. P. Sheetz (2006). "Nonmuscle Myosin IIA-Dependent Force Inhibits Cell Spreading and Drives F-Actin Flow." Biophysical Journal **91**(10): 3907-3920.

Cai, Y., O. Rossier, N. C. Gauthier, N. Biais, M. A. Fardin, X. Zhang, L. W. Miller, B. Ladoux, V. W. Cornish and M. P. Sheetz (2010). "Cytoskeletal coherence requires myosin-IIA contractility." J Cell Sci **123**(Pt 3): 413-423.

Campellone, K. G. and M. D. Welch (2010). "A nucleator arms race: cellular control of actin assembly." Nat Rev Mol Cell Biol **11**(4): 237-251.

Carisey, A., R. Tsang, Alexandra M. Greiner, N. Nijenhuis, N. Heath, A. Nazgiewicz, R. Kemkemer, B. Derby, J. Spatz and C. Ballestrem (2013). "Vinculin Regulates the Recruitment and Release of Core Focal Adhesion Proteins in a Force-Dependent Manner." Current Biology **23**(4): 271-281.

Carlsson, L., L. E. Nystrom, I. Sundkvist, F. Markey and U. Lindberg (1977). "Actin polymerizability is influenced by profilin, a low molecular weight protein in non-muscle cells." J Mol Biol **115**(3): 465-483.

Case, L. B., M. A. Baird, G. Shtengel, S. L. Campbell, H. F. Hess, M. W. Davidson and C. M. Waterman (2015). "Molecular mechanism of vinculin activation and nanoscale spatial organization in focal adhesions." Nat Cell Biol **17**(7): 880-892.

Case, L. B. and C. M. Waterman (2011). "Adhesive F-actin waves: a novel integrin-mediated adhesion complex coupled to ventral actin polymerization." PLoS One **6**(11): e26631.

Chakravarty, G., D. Roy, M. Gonzales, J. Gay, A. Contreras and J. M. Rosen (2000). "P190-B, a Rho-GTPase-activating protein, is differentially expressed in terminal end buds and breast cancer." Cell Growth Differ **11**(7): 343-354.

Chalkia, D., N. Nikolaidis, W. Makalowski, J. Klein and M. Nei (2008). "Origins and evolution of the formin multigene family that is involved in the formation of actin filaments." Mol Biol Evol **25**(12): 2717-2733.

Chandra, P. and S. J. Lee (2015). "Synthetic Extracellular Microenvironment for Modulating Stem Cell Behaviors." Biomark Insights **10**(Suppl 1): 105-116.

Chang, G. H., A. J. Lay, K. K. Ting, Y. Zhao, P. R. Coleman, E. E. Powter, A. Formaz-Preston, C. J. Jolly, N. I. Bower, B. M. Hogan, S. Rinkwitz, T. S. Becker, M. A. Vadas and J. R. Gamble (2014). "ARHGAP18: an endogenous inhibitor of angiogenesis, limiting tip formation and stabilizing junctions." Small GTPases **5**(3): 1-15.

Chang, Y. C., P. Nalbant, J. Birkenfeld, Z. F. Chang and G. M. Bokoch (2008). "GEF-H1 couples nocodazole-induced microtubule disassembly to cell contractility via RhoA." Mol Biol Cell **19**(5): 2147-2153.

Chen, B. H., J. T. Tzen, A. R. Bresnick and H. C. Chen (2002). "Roles of Rho-associated kinase and myosin light chain kinase in morphological and migratory defects of focal adhesion kinase-null cells." J Biol Chem **277**(37): 33857-33863.

Chen, C. S., M. Mrksich, S. Huang, G. M. Whitesides and D. E. Ingber (1997). "Geometric control of cell life and death." Science **276**(5317): 1425-1428.

Chen, Q., M. S. Kinch, T. H. Lin, K. Burridge and R. L. Juliano (1994). "Integrin-mediated cell adhesion activates mitogen-activated protein kinases." Journal of Biological Chemistry **269**(43): 26602-26605.

Chen, X., L. Guo, J. Kang, Y. Huo, S. Wang and W. Tan (2014). "Calcium waves initiating from the anomalous subdiffusive calcium sparks." J R Soc Interface **11**(91): 20130934.

Cherfils, J. and P. Chardin (1999). "GEFs: structural basis for their activation of small GTP-binding proteins." Trends in Biochemical Sciences **24**(8): 306-311.

Cherfils, J. and M. Zeghouf (2013). "Regulation of small GTPases by GEFs, GAPs, and GDIs." Physiol Rev **93**(1): 269-309.

Chevrier, V., M. Piel, N. Collomb, Y. Saoudi, R. Frank, M. Paintrand, S. Narumiya, M. Bornens and D. Job (2002). "The Rho-associated protein kinase p160ROCK is required for centrosome positioning." The Journal of Cell Biology **157**(5): 807-817.

Chieregatti, E., A. Gartner, H. E. Stoffler and M. Bahler (1998). "Myr 7 is a novel myosin IX-RhoGAP expressed in rat brain." J Cell Sci **111 (Pt 24)**: 3597-3608.

Chowdhury, F., I. T. Li, B. J. Leslie, S. Doganay, R. Singh, X. Wang, J. Seong, S. H. Lee, S. Park, N. Wang and T. Ha (2015). "Single molecular force across single integrins dictates cell spreading." Integr Biol (Camb) **7**(10): 1265-1271.

Chung, C. T., S. L. Niemela and R. H. Miller (1989). "One-step preparation of competent Escherichia coli: transformation and storage of bacterial cells in the same solution." Proceedings of the National Academy of Sciences of the United States of America **86**(7): 2172-2175.

Clapham, D. E. (2007). "Calcium Signaling." Cell **131**(6): 1047-1058.

Cohen, D. M., B. Kutscher, H. Chen, D. B. Murphy and S. W. Craig (2006). "A Conformational Switch in Vinculin Drives Formation and Dynamics of a Talin-Vinculin Complex at Focal Adhesions." Journal of Biological Chemistry **281**(23): 16006-16015.

Coleman, P. R., C. N. Hahn, M. Grimshaw, Y. Lu, X. Li, P. J. Brautigan, K. Beck, R. Stocker, M. A. Vadas and J. R. Gamble (2010). "Stress-induced premature senescence mediated by a novel gene, SENEX, results in an anti-inflammatory phenotype in endothelial cells." Blood **116**(19): 4016-4024.

Colombelli, J., A. Besser, H. Kress, E. G. Reynaud, P. Girard, E. Caussinus, U. Haselmann, J. V. Small, U. S. Schwarz and E. H. Stelzer (2009). "Mechanosensing in actin stress fibers revealed by a close correlation between force and protein localization." J Cell Sci **122**(Pt 10): 1665-1679.

Coue, M., S. L. Brenner, I. Spector and E. D. Korn (1987). "Inhibition of actin polymerization by latrunculin A." FEBS Lett **213**(2): 316-318.

Craig, R., R. Smith and J. Kendrick-Jones (1983). "Light-chain phosphorylation controls the conformation of vertebrate non-muscle and smooth muscle myosin molecules." Nature **302**(5907): 436-439.

Cramer, L. P. (1997). "Molecular mechanism of actin-dependent retrograde flow in lamellipodia of motile cells." Front Biosci **2**: d260-270.

del Rio, A., R. Perez-Jimenez, R. Liu, P. Roca-Cusachs, J. M. Fernandez and M. P. Sheetz (2009). "Stretching single talin rod molecules activates vinculin binding." Science **323**(5914): 638-641.

Denry, I. L. and J. A. Holloway (2004). "Elastic constants, Vickers hardness, and fracture toughness of fluorrichterite-based glass-ceramics." Dent Mater **20**(3): 213-219.

Discher, D. E., P. Janmey and Y. L. Wang (2005). "Tissue cells feel and respond to the stiffness of their substrate." Science **310**(5751): 1139-1143.

Dubin-Thaler, B. J., J. M. Hofman, Y. Cai, H. Xenias, I. Spielman, A. V. Shneidman, L. A. David, H. G. Dobereiner, C. H. Wiggins and M. P. Sheetz (2008). "Quantification of cell edge velocities and traction forces reveals distinct motility modules during cell spreading." PLoS One **3**(11): e3735.

Dulyaninova, N. G., R. P. House, V. Betapudi and A. R. Bresnick (2007). "Myosin-IIA heavy-chain phosphorylation regulates the motility of MDA-MB-231 carcinoma cells." Mol Biol Cell **18**(8): 3144-3155.

Dunlap, J. C. (1999). "Molecular bases for circadian clocks." Cell **96**(2): 271-290.

Elfrink, K., W. Liao, U. Pieper, S. J. Oeding and M. Bähler (2014). "The Loop2 Insertion of Type IX Myosin Acts as an Electrostatic Actin Tether that Permits Processive Movement." PLoS ONE **9**(1): e84874.

Ellis, C., M. Moran, F. McCormick and T. Pawson (1990). "Phosphorylation of GAP and GAP-associated proteins by transforming and mitogenic tyrosine kinases." Nature **343**(6256): 377-381.

Elphick, C., A. Hagberg, B. A. Malomed and E. Meron (1997). "On the origin of traveling pulses in bistable systems." Physics Letters A **230**(1–2): 33-37.

Engler, A. J., S. Sen, H. L. Sweeney and D. E. Discher (2006). "Matrix elasticity directs stem cell lineage specification." Cell **126**(4): 677-689.

Europe-Finner, G. N., B. Gammon, C. A. Wood and P. C. Newell (1989). "Inositol tris- and polyphosphate formation during chemotaxis of Dictyostelium." Journal of Cell Science **93**(4): 585-592.

Fall C, M. E., Wagner J, Tyson J (2005). Computational cell biology. New York u.a., Springer.

Fillingham, I., A. R. Gingras, E. Papagrigoriou, B. Patel, J. Emsley, D. R. Critchley, G. C. Roberts and I. L. Barsukov (2005). "A vinculin binding domain from the talin rod unfolds to form a complex with the vinculin head." Structure **13**(1): 65-74.

Finer, J. T., R. M. Simmons and J. A. Spudich (1994). "Single myosin molecule mechanics: piconewton forces and nanometre steps." Nature **368**(6467): 113-119.

Fiorio Pla, A., D. Maric, S. C. Brazer, P. Giacobini, X. Liu, Y. H. Chang, I. S. Ambudkar and J. L. Barker (2005). "Canonical transient receptor potential 1 plays a role in basic fibroblast growth factor (bFGF)/FGF receptor-1-induced Ca2+ entry and embryonic rat neural stem cell proliferation." J Neurosci **25**(10): 2687-2701.

Fish, K. N. (2009). "Total internal reflection fluorescence (TIRF) microscopy." Curr Protoc Cytom Chapter 12: Unit12 18.

Folkman, J. and A. Moscona (1978). "Role of cell shape in growth control." Nature **273**(5661): 345-349.

Fujisawa, K., A. Fujita, T. Ishizaki, Y. Saito and S. Narumiya (1996). "Identification of the Rho-binding domain of p160ROCK, a Rho-associated coiled-coil containing protein kinase." J Biol Chem **271**(38): 23022-23028.

Galbraith, C. G., K. M. Yamada and M. P. Sheetz (2002). "The relationship between force and focal complex development." The Journal of Cell Biology **159**(4): 695-705.

Gallop, J. L., A. Walrant, L. C. Cantley and M. W. Kirschner (2013). "Phosphoinositides and membrane curvature switch the mode of actin polymerization via selective recruitment of toca-1 and Snx9." Proceedings of the National Academy of Sciences of the United States of America **110**(18): 7193-7198.

Gardberg, M., K. Kaipio, L. Lehtinen, P. Mikkonen, V. D. Heuser, K. Talvinen, K. Iljin, C. Kampf, M. Uhlen, R. Grenman, M. Koivisto and O. Carpen (2013). "FHOD1, a formin upregulated in epithelial-mesenchymal transition, participates in cancer cell migration and invasion." PLoS One **8**(9): e74923.

Garrett, M. D., A. J. Self, C. van Oers and A. Hall (1989). "Identification of distinct cytoplasmic targets for ras/R-ras and rho regulatory proteins." J Biol Chem **264**(1): 10-13.

Gasiunas, G., R. Barrangou, P. Horvath and V. Siksnys (2012). "Cas9–crRNA ribonucleoprotein complex mediates specific DNA cleavage for adaptive immunity in bacteria." Proceedings of the National Academy of Sciences of the United States of America **109**(39): E2579-E2586.

Gasteier, J. E., R. Madrid, E. Krautkramer, S. Schroder, W. Muranyi, S. Benichou and O. T. Fackler (2003). "Activation of the Rac-binding partner FHOD1 induces actin stress fibers via a ROCK-dependent mechanism." J Biol Chem **278**(40): 38902-38912.

Gasteier, J. E., S. Schroeder, W. Muranyi, R. Madrid, S. Benichou and O. T. Fackler (2005). "FHOD1 coordinates actin filament and microtubule alignment to mediate cell elongation." Exp Cell Res **306**(1): 192-202.

Geiger, B., J. P. Spatz and A. D. Bershadsky (2009). "Environmental sensing through focal adhesions." Nat Rev Mol Cell Biol **10**(1): 21-33.

Gelens, L., G. A. Anderson and J. E. Ferrell, Jr. (2014). "Spatial trigger waves: positive feedback gets you a long way." Mol Biol Cell **25**(22): 3486-3493.

Gerisch, G. (2010). "Self-organizing actin waves that simulate phagocytic cup structures." PMC Biophys **3**(1): 7.

Gerisch, G., M. Ecke, B. Schroth-Diez, S. Gerwig, U. Engel, L. Maddera and M. Clarke (2009). "Self-organizing actin waves as planar phagocytic cup structures." Cell Adhesion & Migration **3**(4): 373-382.

Giannone, G., B. J. Dubin-Thaler, H. G. Dobereiner, N. Kieffer, A. R. Bresnick and M. P. Sheetz (2004). "Periodic lamellipodial contractions correlate with rearward actin waves." Cell **116**(3): 431-443.

Giannone, G., B. J. Dubin-Thaler, O. Rossier, Y. Cai, O. Chaga, G. Jiang, W. Beaver, H. G. Dobereiner, Y. Freund, G. Borisy and M. P. Sheetz (2007). "Lamellipodial actin mechanically links myosin activity with adhesion-site formation." Cell **128**(3): 561-575.

Gingras, A. R., W. H. Ziegler, R. Frank, I. L. Barsukov, G. C. Roberts, D. R. Critchley and J. Emsley (2005). "Mapping and consensus sequence identification for multiple vinculin binding sites within the talin rod." J Biol Chem **280**(44): 37217-37224.

Glyn, M. C., J. G. Lawrenson and B. J. Ward (2003). "A Rho-associated kinase mitigates reperfusion-induced change in the shape of cardiac capillary endothelial cells in situ." Cardiovasc Res **57**(1): 195-206.

Goh, W. I. and S. Ahmed (2012). "mDia1-3 in mammalian filopodia." Communicative & Integrative Biology **5**(4): 340-344.

Goh, W. I., K. B. Lim, T. Sudhaharan, K. P. Sem, W. Bu, A. M. Chou and S. Ahmed (2012). "mDia1 and WAVE2 proteins interact directly with IRSp53 in filopodia and are involved in filopodium formation." J Biol Chem **287**(7): 4702-4714.

Goh, W. I., T. Sudhaharan, K. B. Lim, K. P. Sem, C. L. Lau and S. Ahmed (2011). "Rif-mDia1 interaction is involved in filopodium formation independent of Cdc42 and Rac effectors." J Biol Chem **286**(15): 13681-13694.

Goldschmidt-Clermont, P. J., J. W. Kim, L. M. Machesky, S. G. Rhee and T. D. Pollard (1991). "Regulation of phospholipase C-gamma 1 by profilin and tyrosine phosphorylation." Science **251**(4998): 1231-1233.

Goode, B. L. and M. J. Eck (2007). "Mechanism and function of formins in the control of actin assembly." Annu Rev Biochem **76**: 593-627.

Gould, C. J., S. Maiti, A. Michelot, B. R. Graziano, L. Blanchoin and B. L. Goode (2011). "The formin DAD domain plays dual roles in autoinhibition and actin nucleation." Curr Biol **21**(5): 384-390.

Gu, X. and N. C. Spitzer (1995). "Distinct aspects of neuronal differentiation encoded by frequency of spontaneous Ca2+ transients." Nature **375**(6534): 784-787.

Gu, Z., F. Liu, E. A. Tonkova, S. Y. Lee, D. J. Tschumperlin and M. B. Brenner (2014). "Soft matrix is a natural stimulator for cellular invasiveness." Molecular Biology of the Cell **25**(4): 457-469.

Guilluy, C., R. Garcia-Mata and K. Burridge (2011). "Rho protein crosstalk: another social network?" Trends in Cell Biology **21**(12): 718-726.

Guilluy, C., V. Swaminathan, R. Garcia-Mata, E. Timothy O/'Brien, R. Superfine and K. Burridge (2011). "The Rho GEFs LARG and GEF-H1 regulate the mechanical response to force on integrins." Nat Cell Biol **13**(6): 722-727.

Hagren, O. I. and A. Tengholm (2006). "Glucose and Insulin Synergistically Activate Phosphatidylinositol 3-Kinase to Trigger Oscillations of Phosphatidylinositol 3,4,5-Trisphosphate in β-Cells." Journal of Biological Chemistry **281**(51): 39121-39127.

Hakoshima, T., T. Shimizu and R. Maesaki (2003). "Structural Basis of the Rho GTPase Signaling." Journal of Biochemistry **134**(3): 327-331.

Hall, A. (1998). "Rho GTPases and the Actin Cytoskeleton." Science **279**(5350): 509-514.

Hall, A. (2012). Rho family GTPases. Biochemical Society Transactions, **40**(6) 1378-1382;

Hanley, P. J., Y. Xu, M. Kronlage, K. Grobe, P. Schön, J. Song, L. Sorokin, A. Schwab and M. Bähler (2010). "Motorized RhoGAP myosin IXb (Myo9b) controls cell shape and motility." Proceedings of the National Academy of Sciences of the United States of America **107**(27): 12145-12150.

Hannemann, S., R. Madrid, J. Stastna, T. Kitzing, J. Gasteier, A. Schonichen, J. Bouchet, A. Jimenez, M. Geyer, R. Grosse, S. Benichou and O. T. Fackler (2008). "The Diaphanous-related Formin FHOD1 associates with ROCK1 and promotes Src-dependent plasma membrane blebbing." J Biol Chem **283**(41): 27891-27903.

Hansen, S. D. and R. D. Mullins (2010). "VASP is a processive actin polymerase that requires monomeric actin for barbed end association." J Cell Biol **191**(3): 571-584.

Harootunian, A. T., J. P. Kao, S. Paranjape and R. Y. Tsien (1991). "Generation of calcium oscillations in fibroblasts by positive feedback between calcium and IP3." Science **251**(4989): 75-78.

Harris, E. S., F. Li and H. N. Higgs (2004). "The mouse formin, FRLalpha, slows actin filament barbed end elongation, competes with capping protein, accelerates polymerization from monomers, and severs filaments." J Biol Chem **279**(19): 20076-20087.

Harris, E. S., I. Rouiller, D. Hanein and H. N. Higgs (2006). "Mechanistic differences in actin bundling activity of two mammalian formins, FRL1 and mDia2." J Biol Chem **281**(20): 14383-14392.

Haskell, M. D., A. L. Nickles, J. M. Agati, L. Su, B. D. Dukes and S. J. Parsons (2001). "Phosphorylation of p190 on Tyr1105 by c-Src is necessary but not sufficient for EGF-induced actin disassembly in C3H10T1/2 fibroblasts." J Cell Sci **114**(Pt 9): 1699-1708.

He, L., X. Wang, H. L. Tang and D. J. Montell (2010). "Tissue elongation requires oscillating contractions of a basal actomyosin network." Nat Cell Biol **12**(12): 1133-1142.

Heasman, S. J. and A. J. Ridley (2008). "Mammalian Rho GTPases: new insights into their functions from in vivo studies." Nat Rev Mol Cell Biol **9**(9): 690-701.

Heath, J. P. (1983). "Behaviour and structure of the leading lamella in moving fibroblasts. I. Occurrence and centripetal movement of arc-shaped microfilament bundles beneath the dorsal cell surface." J Cell Sci **60**: 331-354.

Heath, J. P. and G. A. Dunn (1978). "Cell to substratum contacts of chick fibroblasts and their relation to the microfilament system. A correlated interference-reflexion and high-voltage electron-microscope study." J Cell Sci **29**: 197-212.

Heck, J. N., S. M. Ponik, M. G. Garcia-Mendoza, C. A. Pehlke, D. R. Inman, K. W. Eliceiri and P. J. Keely (2012). "Microtubules regulate GEF-H1 in response to extracellular matrix stiffness." Molecular Biology of the Cell **23**(13): 2583-2592.

Hoffmann, J.-E., Y. Fermin, R. L. O. Stricker, K. Ickstadt and E. Zamir (2014). "Symmetric exchange of multi-protein building blocks between stationary focal adhesions and the cytosol." eLife **3**: e02257.

Hohendanner, F., A. D. McCulloch, L. A. Blatter and A. P. Michailova (2014). "Calcium and IP3 dynamics in cardiac myocytes: Experimental and computational perspectives and approaches." Frontiers in Pharmacology **5**.

Hotulainen, P. and P. Lappalainen (2006). "Stress fibers are generated by two distinct actin assembly mechanisms in motile cells." J Cell Biol **173**(3): 383-394.

Hu, K., L. Ji, K. T. Applegate, G. Danuser and C. M. Waterman-Storer (2007). "Differential Transmission of Actin Motion Within Focal Adhesions." Science **315**(5808): 111-115.

Hudspeth, A. (1997). "Mechanical amplification of stimuli by hair cells." Curr Opin Neurobiol **7**(4): 480-486.

Hussain, N. K., S. Jenna, M. Glogauer, C. C. Quinn, S. Wasiak, M. Guipponi, S. E. Antonarakis, B. K. Kay, T. P. Stossel, N. Lamarche-Vane and P. S. McPherson (2001). "Endocytic protein intersectin-l regulates actin assembly via Cdc42 and N-WASP." Nat Cell Biol **3**(10): 927-932.

Huxley, H. E. (1971). "The structural basis of muscular contraction." Proc R Soc Lond B Biol Sci **178**(1051): 131-149.

Hytönen, V. P. and V. Vogel (2008). "How Force Might Activate Talin's Vinculin Binding Sites: SMD Reveals a Structural Mechanism." PLoS Computational Biology **4**(2): e24.

Iglesias, P. A. and P. N. Devreotes (2012). "Biased excitable networks: how cells direct motion in response to gradients." Curr Opin Cell Biol **24**(2): 245-253.

Ishizaki, T., M. Maekawa, K. Fujisawa, K. Okawa, A. Iwamatsu, A. Fujita, N. Watanabe, Y. Saito, A. Kakizuka, N. Morii and S. Narumiya (1996). "The small GTP-binding protein Rho binds to and activates a 160 kDa Ser/Thr protein kinase homologous to myotonic dystrophy kinase." The EMBO Journal **15**(8): 1885-1893.

Ishizaki, T., M. Naito, K. Fujisawa, M. Maekawa, N. Watanabe, Y. Saito and S. Narumiya (1997). "p160ROCK, a Rho-associated coiled-coil forming protein kinase, works downstream of Rho and induces focal adhesions." FEBS Lett **404**(2-3): 118-124.

Ishizaki, T., M. Uehata, I. Tamechika, J. Keel, K. Nonomura, M. Maekawa and S. Narumiya (2000). "Pharmacological properties of Y-27632, a specific inhibitor of rho-associated kinases." Mol Pharmacol **57**(5): 976-983.

Iskratsch, T., C. H. Yu, A. Mathur, S. Liu, V. Stevenin, J. Dwyer, J. Hone, E. Ehler and M. Sheetz (2013). "FHOD1 is needed for directed forces and adhesion maturation during cell spreading and migration." Dev Cell **27**(5): 545-559.

Jacobs, M., K. Hayakawa, L. Swenson, S. Bellon, M. Fleming, P. Taslimi and J. Doran (2006). "The structure of dimeric ROCK I reveals the mechanism for ligand selectivity." J Biol Chem **281**(1): 260-268.

Jaffe, A. B. and A. Hall (2005). "RHO GTPASES: Biochemistry and Biology." Annual Review of Cell and Developmental Biology **21**(1): 247-269.

Jaffe, L. F. (1991). "The path of calcium in cytosolic calcium oscillations: a unifying hypothesis." Proc Natl Acad Sci U S A **88**(21): 9883-9887.

Janmey, P. A. and C. A. McCulloch (2007). "Cell mechanics: integrating cell responses to mechanical stimuli." Annu Rev Biomed Eng **9**: 1-34.

Jannie, K. M., S. M. Ellerbroek, D. W. Zhou, S. Chen, D. J. Crompton, A. J. García and K. A. DeMali (2015). "Vinculin-dependent actin bundling regulates cell migration and traction forces." The Biochemical journal **465**(3): 383-393.

Jegou, A., M. F. Carlier and G. Romet-Lemonne (2013). "Formin mDia1 senses and generates mechanical forces on actin filaments." Nat Commun **4**: 1883.

Jinek, M., K. Chylinski, I. Fonfara, M. Hauer, J. A. Doudna and E. Charpentier (2012). "A programmable dual-RNA-guided DNA endonuclease in adaptive bacterial immunity." Science **337**(6096): 816-821.

Johnson, H. E., S. J. King, S. B. Asokan, J. D. Rotty, J. E. Bear and J. M. Haugh (2015). "F-actin bundles direct the initiation and orientation of lamellipodia through adhesion-based signaling." J Cell Biol **208**(4): 443-455.

Johnson, R. P. and S. W. Craig (1994). "An intramolecular association between the head and tail domains of vinculin modulates talin binding." J Biol Chem **269**(17): 12611-12619.

Johnson, R. P. and S. W. Craig (1995). "F-actin binding site masked by the intramolecular association of vinculin head and tail domains." Nature **373**(6511): 261-264.

Julian, L. and M. F. Olson (2014). "Rho-associated coiled-coil containing kinases (ROCK)." Small GTPases **5**(2): e29846.

Jung, H. S., S. Komatsu, M. Ikebe and R. Craig (2008). "Head-head and head-tail interaction: a general mechanism for switching off myosin II activity in cells." Mol Biol Cell **19**(8): 3234-3242.

Junttila, M. R., S.-P. Li and J. Westermarck (2008). "Phosphatase-mediated crosstalk between MAPK signaling pathways in the regulation of cell survival." The FASEB Journal **22**(4): 954-965.

Jurmeister, S., M. Baumann, A. Balwierz, I. Keklikoglou, A. Ward, S. Uhlmann, J. D. Zhang, S. Wiemann and O. Sahin (2012). "MicroRNA-200c represses migration and invasion of breast cancer cells by targeting actin-regulatory proteins FHOD1 and PPM1F." Mol Cell Biol **32**(3): 633-651.

Kaksonen, M., C. P. Toret and D. G. Drubin (2006). "Harnessing actin dynamics for clathrin-mediated endocytosis." Nat Rev Mol Cell Biol **7**(6): 404-414.

Kambara, T. and M. Ikebe (2006). "A unique ATP hydrolysis mechanism of single-headed processive myosin, myosin IX." J Biol Chem **281**(8): 4949-4957.

Kanai, M., M. S. Crowe, Y. Zheng, G. F. Vande Woude and K. Fukasawa (2010). "RhoA and RhoC are both required for the ROCK II-dependent promotion of centrosome duplication." Oncogene **29**(45): 6040-6050.

Kanchanawong, P., G. Shtengel, A. M. Pasapera, E. B. Ramko, M. W. Davidson, H. F. Hess and C. M. Waterman (2010). "Nanoscale architecture of integrin-based cell adhesions." Nature **468**(7323): 580-584.

Kaneuchi, T., C. V. Sartain, S. Takeo, V. L. Horner, N. A. Buehner, T. Aigaki and M. F. Wolfner (2015). "Calcium waves occur as Drosophila oocytes activate." Proceedings of the National Academy of Sciences **112**(3): 791-796.

Karnoub, A., M. Symons, S. Campbell and C. Der (2004). "Molecular Basis for Rho GTPase Signaling Specificity." Breast Cancer Research and Treatment **84**(1): 61-71.

Katoh, K., Y. Kano, M. Amano, H. Onishi, K. Kaibuchi and K. Fujiwara (2001). "Rho-Kinase–Mediated Contraction of Isolated Stress Fibers." The Journal of Cell Biology **153**(3): 569-584.

Kawabata, S., J. Usukura, N. Morone, M. Ito, A. Iwamatsu, K. Kaibuchi and M. Amano (2004). "Interaction of Rho-kinase with myosin II at stress fibres." Genes to Cells **9**(7): 653-660.

Kerkhoff, E. (2006). "Cellular functions of the Spir actin-nucleation factors." Trends Cell Biol **16**(9): 477-483.

Kim, D.-H., A. B. Chambliss and D. Wirtz (2013). "The multi-faceted role of the actin cap in cellular mechanosensation and mechanotransduction." Soft matter **9**(23): 5516-5523.

Kitayama, C. and T. Q. Uyeda (2003). "ForC, a novel type of formin family protein lacking an FH1 domain, is involved in multicellular development in Dictyostelium discoideum." J Cell Sci **116**(Pt 4): 711-723.

Koenderink, G. H., Z. Dogic, F. Nakamura, P. M. Bendix, F. C. MacKintosh, J. H. Hartwig, T. P. Stossel and D. A. Weitz (2009). "An active biopolymer network controlled by molecular motors." Proc Natl Acad Sci U S A **106**(36): 15192-15197.

Koka, S., G. T. Minick, Y. Zhou, J. J. Westendorf and M. B. Boehm (2005). "Src regulates the activity of the mammalian formin protein FHOD1." Biochem Biophys Res Commun **336**(4): 1285-1291.

Koka, S., C. L. Neudauer, X. Li, R. E. Lewis, J. B. McCarthy and J. J. Westendorf (2003). "The formin-homology-domain-containing protein FHOD1 enhances cell migration." J Cell Sci **116**(Pt 9): 1745-1755.

Kosako, H., H. Goto, M. Yanagida, K. Matsuzawa, M. Fujita, Y. Tomono, T. Okigaki, H. Odai, K. Kaibuchi and M. Inagaki (1999). "Specific accumulation of Rho-associated kinase at the cleavage furrow during cytokinesis: cleavage furrow-specific phosphorylation of intermediate filaments." Oncogene **18**(17): 2783-2788.

Kovac, B., J. L. Teo, T. P. Makela and T. Vallenius (2013). "Assembly of non-contractile dorsal stress fibers requires alpha-actinin-1 and Rac1 in migrating and spreading cells." J Cell Sci **126**(Pt 1): 263-273.

Kovacs, M., J. Toth, C. Hetenyi, A. Malnasi-Csizmadia and J. R. Sellers (2004). "Mechanism of blebbistatin inhibition of myosin II." J Biol Chem **279**(34): 35557-35563.

Krendel, M., F. T. Zenke and G. M. Bokoch (2002). "Nucleotide exchange factor GEF-H1 mediates cross-talk between microtubules and the actin cytoskeleton." Nat Cell Biol **4**(4): 294-301.

Kruse, K. and F. Jülicher (2005). "Oscillations in cell biology." Curr Opin Cell Biol **17**(1): 20-26.

Kuhn, S. and M. Geyer (2014). "Formins as effector proteins of Rho GTPases." Small GTPases **5**: e29513.

Kumano, M., D. J. Carroll, J. M. Denu and K. R. Foltz (2001). "Calcium-Mediated Inactivation of the MAP Kinase Pathway in Sea Urchin Eggs at Fertilization." Developmental Biology **236**(1): 244-257.

Kumar, S., I. Z. Maxwell, A. Heisterkamp, T. R. Polte, T. P. Lele, M. Salanga, E. Mazur and D. E. Ingber (2006). "Viscoelastic retraction of single living stress fibers and its impact on cell shape, cytoskeletal organization, and extracellular matrix mechanics." Biophys J **90**(10): 3762-3773.

Kurokawa, K. and M. Matsuda (2005). "Localized RhoA activation as a requirement for the induction of membrane ruffling." Mol Biol Cell **16**(9): 4294-4303.

Kusama, T., M. Mukai, H. Endo, O. Ishikawa, M. Tatsuta, H. Nakamura and M. Inoue (2006). "Inactivation of Rho GTPases by p190 RhoGAP reduces human pancreatic cancer cell invasion and metastasis." Cancer Sci **97**(9): 848-853.

Kutscheidt, S., R. Zhu, S. Antoku, G. W. Luxton, I. Stagljar, O. T. Fackler and G. G. Gundersen (2014). "FHOD1 interaction with nesprin-2G mediates TAN line formation and nuclear movement." Nat Cell Biol **16**(7): 708-715.

Laemmli, U. K. (1970). "Cleavage of structural proteins during the assembly of the head of bacteriophage T4." Nature **227**(5259): 680-685.

Lammel, U., M. Bechtold, B. Risse, D. Berh, A. Fleige, I. Bunse, X. Jiang, C. Klambt and S. Bogdan (2014). "The Drosophila FHOD1-like formin Knittrig acts through Rok to promote stress fiber formation and directed macrophage migration during the cellular immune response." Development **141**(6): 1366-1380.

Lammers, M., R. Rose, A. Scrima and A. Wittinghofer (2005). "The regulation of mDia1 by autoinhibition and its release by Rho*GTP." EMBO J **24**(23): 4176-4187.

Lanniel, M., E. Huq, S. Allen, L. Buttery, P. M. Williams and M. R. Alexander (2011). "Substrate induced differentiation of human mesenchymal stem cells on hydrogels with modified surface chemistry and controlled modulus." Soft Matter **7**(14): 6501-6514.

Lauffenburger, D. A. and A. F. Horwitz (1996). "Cell migration: a physically integrated molecular process." Cell **84**(3): 359-369.

Lazarides, E. and K. Burridge (1975). "Alpha-actinin: immunofluorescent localization of a muscle structural protein in nonmuscle cells." Cell **6**(3): 289-298.
Le Clainche, C. and M. F. Carlier (2008). "Regulation of actin assembly associated with protrusion and adhesion in cell migration." Physiol Rev **88**(2): 489-513.

Lee, C.-S., C.-K. Choi, E.-Y. Shin, M. A. Schwartz and E.-G. Kim (2010). "Myosin II directly binds and inhibits Dbl family guanine nucleotide exchange factors: a possible link to Rho family GTPases." The Journal of Cell Biology **190**(4): 663-674.

Leung, T., X. Q. Chen, E. Manser and L. Lim (1996). "The p160 RhoA-binding kinase ROK alpha is a member of a kinase family and is involved in the reorganization of the cytoskeleton." Molecular and Cellular Biology **16**(10): 5313-5327.

Leung, T., E. Manser, L. Tan and L. Lim (1995). "A novel serine/threonine kinase binding the Ras-related RhoA GTPase which translocates the kinase to peripheral membranes." J Biol Chem **270**(49): 29051-29054.

Levayer, R. and T. Lecuit (2012). "Biomechanical regulation of contractility: spatial control and dynamics." Trends Cell Biol **22**(2): 61-81.

Li, F. and H. N. Higgs (2003). "The mouse Formin mDia1 is a potent actin nucleation factor regulated by autoinhibition." Curr Biol **13**(15): 1335-1340.

Li, F. and H. N. Higgs (2005). "Dissecting requirements for auto-inhibition of actin nucleation by the formin, mDia1." J Biol Chem **280**(8): 6986-6992.

Li, X., Q. Liu, S. Liu, J. Zhang and Y. Zhang (2008). "New member of the guanosine triphosphatase activating protein family in the human epididymis." Acta Biochim Biophys Sin (Shanghai) **40**(10): 855-863.

Littlefield, R. and V. M. Fowler (2002). "A minor actin catastrophe." Nat Cell Biol **4**(9): E209-211.

Lo, C. M., H. B. Wang, M. Dembo and Y. L. Wang (2000). "Cell movement is guided by the rigidity of the substrate." Biophysical Journal **79**(1): 144-152.

Ma, Z., M. Kanai, K. Kawamura, K. Kaibuchi, K. Ye and K. Fukasawa (2006). "Interaction between ROCK II and Nucleophosmin/B23 in the Regulation of Centrosome Duplication." Molecular and Cellular Biology **26**(23): 9016-9034.

Machacek, M., L. Hodgson, C. Welch, H. Elliott, O. Pertz, P. Nalbant, A. Abell, G. L. Johnson, K. M. Hahn and G. Danuser (2009). "Coordination of Rho GTPase activities during cell protrusion." Nature **461**(7260): 99-103.

Maddox, A. S. and K. Burridge (2003). "RhoA is required for cortical retraction and rigidity during mitotic cell rounding." J Cell Biol **160**(2): 255-265.

Maeda, M., H. Hasegawa, T. Hyodo, S. Ito, E. Asano, H. Yuang, K. Funasaka, K. Shimokata, Y. Hasegawa, M. Hamaguchi and T. Senga (2011). "ARHGAP18, a GTPase-activating protein for RhoA, controls cell shape, spreading, and motility." Mol Biol Cell **22**(20): 3840-3852.

Maitre, J. L., R. Niwayama, H. Turlier, F. Nedelec and T. Hiiragi (2015). "Pulsatile cell-autonomous contractility drives compaction in the mouse embryo." Nat Cell Biol **17**(7): 849-855.

Malmersjö, S., P. Rebellato, E. Smedler, H. Planert, S. Kanatani, I. Liste, E. Nanou, H. Sunner, S. Abdelhady, S. Zhang, M. Andang, A. El Manira, G. Silberberg, E. Arenas and P. Uhlen (2013). "Neural progenitors organize in small-world networks to promote cell proliferation." Proc Natl Acad Sci U S A **110**(16): E1524-1532.

Matsumura, F. (2005). "Regulation of myosin II during cytokinesis in higher eukaryotes." Trends Cell Biol **15**(7): 371-377.

Matsumura, F. and D. J. Hartshorne (2008). "Myosin phosphatase target subunit: Many roles in cell function." Biochem Biophys Res Commun **369**(1): 149-156.

McBeath, R., D. M. Pirone, C. M. Nelson, K. Bhadriraju and C. S. Chen "Cell Shape, Cytoskeletal Tension, and RhoA Regulate Stem Cell Lineage Commitment." Developmental Cell **6**(4): 483-495.

McGough, A., B. Pope, W. Chiu and A. Weeds (1997). "Cofilin changes the twist of F-actin: implications for actin filament dynamics and cellular function." J Cell Biol **138**(4): 771-781.

Michaelson, D., J. Silletti, G. Murphy, P. D'Eustachio, M. Rush and M. R. Philips (2001). "Differential Localization of Rho Gtpases in Live Cells: Regulation by Hypervariable Regions and Rhogdi Binding." The Journal of Cell Biology **152**(1): 111-126.

Mih, J. D., A. Marinkovic, F. Liu, A. S. Sharif and D. J. Tschumperlin (2012). "Matrix stiffness reverses the effect of actomyosin tension on cell proliferation." J Cell Sci **125**(Pt 24): 5974-5983.

Mitsushima, M., K. Aoki, M. Ebisuya, S. Matsumura, T. Yamamoto, M. Matsuda, F. Toyoshima and E. Nishida (2010). "Revolving movement of a dynamic cluster of actin filaments during mitosis." J Cell Biol **191**(3): 453-462.

Miyazaki, S., H. Shirakawa, K. Nakada and Y. Honda (1993). "Essential role of the inositol 1,4,5-trisphosphate receptor/Ca2+ release channel in Ca2+ waves and Ca2+ oscillations at fertilization of mammalian eggs." Dev Biol **158**(1): 62-78.

Mohl, C., N. Kirchgessner, C. Schafer, B. Hoffmann and R. Merkel (2012). "Quantitative mapping of averaged focal adhesion dynamics in migrating cells by shape normalization." J Cell Sci **125**(Pt 1): 155-165.

Moran, M. F., P. Polakis, F. McCormick, T. Pawson and C. Ellis (1991). "Protein-tyrosine kinases regulate the phosphorylation, protein interactions, subcellular distribution, and activity of p21ras GTPase-activating protein." Mol Cell Biol **11**(4): 1804-1812.

Morris, C. E. (1990). "Mechanosensitive ion channels." J Membr Biol **113**(2): 93-107.

Moseley, J. B., S. Maiti and B. L. Goode (2006). "Formin proteins: purification and measurement of effects on actin assembly." Methods Enzymol **406**: 215-234.

Moseley, J. B., I. Sagot, A. L. Manning, Y. Xu, M. J. Eck, D. Pellman and B. L. Goode (2004). "A conserved mechanism for Bni1- and mDia1-induced actin assembly and dual regulation of Bni1 by Bud6 and profilin." Mol Biol Cell **15**(2): 896-907.

Müller, R. T., U. Honnert, J. Reinhard and M. Bähler (1997). "The rat myosin myr 5 is a GTPase-activating protein for Rho in vivo: essential role of arginine 1695." Mol Biol Cell **8**(10): 2039-2053.

Munjal, A., J.-M. Philippe, E. Munro and T. Lecuit (2015). "A self-organized biomechanical network drives shape changes during tissue morphogenesis." Nature **524**(7565): 351-355.

Murray, J. D. (2011). Mathematical Biology: I. An Introduction, Springer New York.

Nakagawa, O., K. Fujisawa, T. Ishizaki, Y. Saito, K. Nakao and S. Narumiya (1996). "ROCK-I and ROCK-II, two isoforms of Rho-associated coiled-coil forming protein serine/threonine kinase in mice." FEBS Lett **392**(2): 189-193.

Nalbant, P., Y.-C. Chang, J. Birkenfeld, Z.-F. Chang and G. M. Bokoch (2009). "Guanine Nucleotide Exchange Factor-H1 Regulates Cell Migration via Localized Activation of RhoA at the Leading Edge." Molecular Biology of the Cell **20**(18): 4070-4082.

Nalbant, P., L. Hodgson, V. Kraynov, A. Toutchkine and K. M. Hahn (2004). "Activation of endogenous Cdc42 visualized in living cells." Science **305**(5690): 1615-1619.

Naoki, H., Y. Sakumura and S. Ishii (2008). "Stochastic control of spontaneous signal generation for gradient sensing in chemotaxis." J Theor Biol **255**(2): 259-266.

Narumiya, S. and S. Yasuda (2006). "Rho GTPases in animal cell mitosis." Current Opinion in Cell Biology **18**(2): 199-205.

Naumanen, P., P. Lappalainen and P. Hotulainen (2008). "Mechanisms of actin stress fibre assembly." J Microsc **231**(3): 446-454.

Niederman, R. and T. D. Pollard (1975). "Human platelet myosin. II. In vitro assembly and structure of myosin filaments." J Cell Biol **67**(1): 72-92.

Niforou, K. M., A. K. Anagnostopoulos, K. Vougas, C. Kittas, V. G. Gorgoulis and G. T. Tsangaris (2008). "The proteome profile of the human osteosarcoma U2OS cell line." Cancer Genomics Proteomics **5**(1): 63-78.

Nisenholz, N., K. Rajendran, Q. Dang, H. Chen, R. Kemkemer, R. Krishnan and A. Zemel (2014). "Active mechanics and dynamics of cell spreading on elastic substrates." Soft Matter **10**(37): 7234-7246.

Nishikawa, M., S. Nishikawa, A. Inoue, A. H. Iwane, T. Yanagida and M. Ikebe (2006). "A unique mechanism for the processive movement of single-headed myosin-IX." Biochem Biophys Res Commun **343**(4): 1159-1164.

Nobes, C. D. and A. Hall (1995). "Rho, rac, and cdc42 GTPases regulate the assembly of multimolecular focal complexes associated with actin stress fibers, lamellipodia, and filopodia." Cell **81**(1): 53-62.

Oakes, P. W., Y. Beckham, J. Stricker and M. L. Gardel (2012). "Tension is required but not sufficient for focal adhesion maturation without a stress fiber template." The Journal of Cell Biology **196**(3): 363-374.

O'Connell, C. B. and M. S. Mooseker (2003). "Native Myosin-IXb is a plus-, not a minus-end-directed motor." Nat Cell Biol **5**(2): 171-172.

Oliver, W. C. and G. M. Pharr (1992). "An improved technique for determining hardness and elastic modulus using load and displacement sensing indentation experiments." Journal of Materials Research **7**(06): 1564-1583.

Omelchenko, T. and A. Hall (2012). "Myosin-IXA Regulates Collective Epithelial Cell Migration by Targeting RhoGAP Activity to Cell-Cell Junctions." Current Biology **22**(4): 278-288.

Orrenius, S., B. Zhivotovsky and P. Nicotera (2003). "Regulation of cell death: the calcium-apoptosis link." Nat Rev Mol Cell Biol **4**(7): 552-565.

Pantaloni, D. and M. F. Carlier (1993). "How profilin promotes actin filament assembly in the presence of thymosin beta 4." Cell **75**(5): 1007-1014.

Papagrigoriou, E., A. R. Gingras, I. L. Barsukov, N. Bate, I. J. Fillingham, B. Patel, R. Frank, W. H. Ziegler, G. C. Roberts, D. R. Critchley and J. Emsley (2004). "Activation of a vinculin-binding site in the talin rod involves rearrangement of a five-helix bundle." EMBO J **23**(15): 2942-2951.

Pasapera, A. M., S. V. Plotnikov, R. S. Fischer, L. B. Case, T. T. Egelhoff and C. M. Waterman (2015). "Rac1-dependent phosphorylation and focal adhesion recruitment of myosin IIA regulates migration and mechanosensing." Curr Biol **25**(2): 175-186.

Pasapera, A. M., I. C. Schneider, E. Rericha, D. D. Schlaepfer and C. M. Waterman (2010). "Myosin II activity regulates vinculin recruitment to focal adhesions through FAK-mediated paxillin phosphorylation." The Journal of Cell Biology **188**(6): 877-890.

Patla, I., T. Volberg, N. Elad, V. Hirschfeld-Warneken, C. Grashoff, R. Fassler, J. P. Spatz, B. Geiger and O. Medalia (2010). "Dissecting the molecular architecture of integrin adhesion sites by cryo-electron tomography." Nat Cell Biol **12**(9): 909-915.

Paul, A. S. and T. D. Pollard (2008). "The role of the FH1 domain and profilin in formin-mediated actin-filament elongation and nucleation." Curr Biol **18**(1): 9-19.

Peck, J., G. t. Douglas, C. H. Wu and P. D. Burbelo (2002). "Human RhoGAP domain-containing proteins: structure, function and evolutionary relationships." FEBS Lett **528**(1-3): 27-34.

Pellegrin, S. and H. Mellor (2007). "Actin stress fibres." J Cell Sci **120**(Pt 20): 3491-3499.

Pertz, O., L. Hodgson, R. L. Klemke and K. M. Hahn (2006). "Spatiotemporal dynamics of RhoA activity in migrating cells." Nature **440**(7087): 1069-1072.

Placais, P. Y., M. Balland, T. Guerin, J. F. Joanny and P. Martin (2009). "Spontaneous oscillations of a minimal actomyosin system under elastic loading." Phys Rev Lett **103**(15): 158102.

Pollard, T. D. and G. G. Borisy (2003). "Cellular motility driven by assembly and disassembly of actin filaments." Cell **112**(4): 453-465.

Ponti, A., M. Machacek, S. L. Gupton, C. M. Waterman-Storer and G. Danuser (2004). "Two distinct actin networks drive the protrusion of migrating cells." Science **305**(5691): 1782-1786.

Post, P. L., M. J. Tyska, C. B. O'Connell, K. Johung, A. Hayward and M. S. Mooseker (2002). "Myosin-IXb is a single-headed and processive motor." J Biol Chem **277**(14): 11679-11683.

Rajakylä, E. K. and M. K. Vartiainen (2014). "Rho, nuclear actin, and actin-binding proteins in the regulation of transcription and gene expression." Small GTPases **5**(1): e27539.

Ran, F. A., P. D. Hsu, J. Wright, V. Agarwala, D. A. Scott and F. Zhang (2013). "Genome engineering using the CRISPR-Cas9 system." Nature protocols **8**(11): 2281-2308.

Rayment, I., H. M. Holden, M. Whittaker, C. B. Yohn, M. Lorenz, K. C. Holmes and R. A. Milligan (1993). "Structure of the actin-myosin complex and its implications for muscle contraction." Science **261**(5117): 58-65.

Reid, T., T. Furuyashiki, T. Ishizaki, G. Watanabe, N. Watanabe, K. Fujisawa, N. Morii, P. Madaule and S. Narumiya (1996). "Rhotekin, a new putative target for Rho bearing homology to a serine/threonine kinase, PKN, and rhophilin in the rho-binding domain." J Biol Chem **271**(23): 13556-13560.

Reinhard, J., A. A. Scheel, D. Diekmann, A. Hall, C. Ruppert and M. Bahler (1995). "A novel type of myosin implicated in signalling by rho family GTPases." EMBO J **14**(4): 697-704.

Ren, Y., R. Li, Y. Zheng and H. Busch (1998). "Cloning and Characterization of GEF-H1, a Microtubule-associated Guanine Nucleotide Exchange Factor for Rac and Rho GTPases." Journal of Biological Chemistry **273**(52): 34954-34960.

Ridley, A. J. and A. Hall (1992). "The small GTP-binding protein rho regulates the assembly of focal adhesions and actin stress fibers in response to growth factors." Cell **70**(3): 389-399.

Ridley, A. J., A. J. Self, F. Kasmi, H. F. Paterson, A. Hall, C. J. Marshall and C. Ellis (1993). "rho family GTPase activating proteins p190, bcr and rhoGAP show distinct specificities in vitro and in vivo." EMBO J **12**(13): 5151-5160.

Riento, K. and A. J. Ridley (2003). "ROCKs: multifunctional kinases in cell behaviour." Nat Rev Mol Cell Biol **4**(6): 446-456.

Rinzel, J. and D. Terman (1982). "Propagation Phenomena in a Bistable Reaction-Diffusion System." SIAM Journal on Applied Mathematics **42**(5): 1111-1137.

Riveline, D., E. Zamir, N. Q. Balaban, U. S. Schwarz, T. Ishizaki, S. Narumiya, Z. Kam, B. Geiger and A. D. Bershadsky (2001). "Focal Contacts as Mechanosensors: Externally Applied Local Mechanical Force Induces Growth of Focal Contacts by an Mdia1-Dependent and Rock-Independent Mechanism." The Journal of Cell Biology **153**(6): 1175-1186.

Romero, S., C. Le Clainche, D. Didry, C. Egile, D. Pantaloni and M. F. Carlier (2004). "Formin is a processive motor that requires profilin to accelerate actin assembly and associated ATP hydrolysis." Cell **119**(3): 419-429.

Roof, R. W., M. D. Haskell, B. D. Dukes, N. Sherman, M. Kinter and S. J. Parsons (1998). "Phosphotyrosine (p-Tyr)-dependent and -independent mechanisms of p190 RhoGAP-p120 RasGAP interaction: Tyr 1105 of p190, a substrate for c-Src, is the sole p-Tyr mediator of complex formation." Mol Cell Biol **18**(12): 7052-7063.

Ryan, Gillian L., Heather M. Petroccia, N. Watanabe and D. Vavylonis (2012). "Excitable Actin Dynamics in Lamellipodial Protrusion and Retraction." Biophysical Journal **102**(7): 1493-1502.

Sadok, A. and C. J. Marshall (2014). "Rho GTPases: Masters of cell migration." Small GTPases **5**: e29710.

Sagot, I., A. A. Rodal, J. Moseley, B. L. Goode and D. Pellman (2002). "An actin nucleation mechanism mediated by Bni1 and profilin." Nat Cell Biol **4**(8): 626-631.

Sander, J. D. and J. K. Joung (2014). "CRISPR-Cas systems for editing, regulating and targeting genomes." Nat Biotech **32**(4): 347-355.

Schillers, H., M. Walte, K. Urbanova and H. Oberleithner (2010). "Real-time monitoring of cell elasticity reveals oscillating myosin activity." Biophys J **99**(11): 3639-3646.

Schlaepfer, D. D., S. K. Hanks, T. Hunter and P. v. d. Geer (1994). "Integrin-mediated signal transduction linked to Ras pathway by GRB2 binding to focal adhesion kinase." Nature **372**(6508): 786-791.

Schliwa, M. (1982). "Action of cytochalasin D on cytoskeletal networks." J Cell Biol **92**(1): 79-91.

Schönichen, A., M. Alexander, J. E. Gasteier, F. E. Cuesta, O. T. Fackler and M. Geyer (2006). "Biochemical characterization of the diaphanous autoregulatory interaction in the formin homology protein FHOD1." J Biol Chem **281**(8): 5084-5093.

Schönichen, A. and M. Geyer (2010). "Fifteen formins for an actin filament: a molecular view on the regulation of human formins." Biochim Biophys Acta **1803**(2): 152-163.

Schönichen, A., H. G. Mannherz, E. Behrmann, A. J. Mazur, S. Kuhn, U. Silvan, C. A. Schoenenberger, O. T. Fackler, S. Raunser, L. Dehmelt and M. Geyer (2013). "FHOD1 is a combined actin filament capping and bundling factor that selectively associates with actin arcs and stress fibers." J Cell Sci **126**(Pt 8): 1891-1901.

Schroth-Diez, B., S. Gerwig, M. Ecke, R. Hegerl, S. Diez and G. Gerisch (2009). "Propagating waves separate two states of actin organization in living cells." HFSP J **3**(6): 412-427.

Schulte, A., B. Stolp, A. Schonichen, O. Pylypenko, A. Rak, O. T. Fackler and M. Geyer (2008). "The human formin FHOD1 contains a bipartite structure of FH3 and GTPase-binding domains required for activation." Structure **16**(9): 1313-1323.

Schulze, N., M. Graessl, A. Blancke Soares, M. Geyer, L. Dehmelt and P. Nalbant (2014). "FHOD1 regulates stress fiber organization by controlling the dynamics of transverse arcs and dorsal fibers." J Cell Sci **127**(Pt 7): 1379-1393.

Sellers, J. R. (2000). "Myosins: a diverse superfamily." Biochimica et Biophysica Acta (BBA) - Molecular Cell Research **1496**(1): 3-22.

Settleman, J., V. Narasimhan, L. C. Foster and R. A. Weinberg (1992). "Molecular cloning of cDNAs encoding the GAP-associated protein p190: implications for a signaling pathway from ras to the nucleus." Cell **69**(3): 539-549.

Shen, C. H., H. Y. Chen, M. S. Lin, F. Y. Li, C. C. Chang, M. L. Kuo, J. Settleman and R. H. Chen (2008). "Breast tumor kinase phosphorylates p190RhoGAP to regulate rho and ras and promote breast carcinoma growth, migration, and invasion." Cancer Res **68**(19): 7779-7787.

Shi, C. and P. A. Iglesias (2013). "Excitable behavior in amoeboid chemotaxis." Wiley Interdiscip Rev Syst Biol Med **5**(5): 631-642.

Shibue, T., M. W. Brooks, M. F. Inan, F. Reinhardt and R. A. Weinberg (2012). "The Outgrowth of Micrometastases Is Enabled by the Formation of Filopodium-like Protrusions." Cancer Discovery **2**(8): 706-721.

Sinha, S. and S. Sridhar (2014). Patterns in Excitable Media: Genesis, Dynamics, and Control, Taylor & Francis.

Skubiszak, L. and L. Kowalczyk (2002). "Myosin molecule packing within the vertebrate skeletal muscle thick filaments. A complete bipolar model." Acta Biochim Pol **49**(4): 829-840.
Small, J. V. (1988). "The actin cytoskeleton." Electron Microsc Rev **1**(1): 155-174.

Small, J. V., T. Stradal, E. Vignal and K. Rottner "The lamellipodium: where motility begins." Trends in Cell Biology **12**(3): 112-120.

Smedler, E. and P. Uhlén (2014). "Frequency decoding of calcium oscillations." Biochimica et Biophysica Acta (BBA) - General Subjects **1840**(3): 964-969.

Smith, M. A., E. Blankman, M. L. Gardel, L. Luettjohann, C. M. Waterman and M. C. Beckerle (2010). "A Zyxin-Mediated Mechanism for Actin Stress Fiber Maintenance and Repair." Developmental cell **19**(3): 365-376.

Soiné, J. R. D., C. A. Brand, J. Stricker, P. W. Oakes, M. L. Gardel and U. S. Schwarz (2015). "Model-based Traction Force Microscopy Reveals Differential Tension in Cellular Actin Bundles." PLoS Comput Biol **11**(3): e1004076.

Straight, A. F., A. Cheung, J. Limouze, I. Chen, N. J. Westwood, J. R. Sellers and T. J. Mitchison (2003). "Dissecting temporal and spatial control of cytokinesis with a myosin II Inhibitor." Science **299**(5613): 1743-1747.

Stricker, S. A. (1999). "Comparative biology of calcium signaling during fertilization and egg activation in animals." Dev Biol **211**(2): 157-176.

Stroeken, P. J., B. Alvarez, J. Van Rheenen, Y. M. Wijnands, D. Geerts, K. Jalink and E. Roos (2006). "Integrin cytoplasmic domain-associated protein-1 (ICAP-1) interacts with the ROCK-I kinase at the plasma membrane." J Cell Physiol **208**(3): 620-628.

Struchholz, S., K. Elfrink, U. Pieper, G. Kalhammer, U. Honnert, A. Grutzner, W. A. Linke, W. Liao and M. Bahler (2009). "Functional role of the extended loop 2 in the myosin 9b head for binding F-actin." J Biol Chem **284**(6): 3663-3671.

Sun, S. X. and S. Walcott (2010). "Actin crosslinkers: repairing the sense of touch." Curr Biol **20**(20): R895-896.

Suraneni, P., B. Rubinstein, J. R. Unruh, M. Durnin, D. Hanein and R. Li (2012). "The Arp2/3 complex is required for lamellipodia extension and directional fibroblast cell migration." The Journal of Cell Biology **197**(2): 239-251.
Tai, Y., S. Feng, W. Du and Y. Wang (2009). "Functional roles of TRPC channels in the developing brain." Pflugers Arch **458**(2): 283-289.

Takano, K., K. Toyooka and S. Suetsugu (2008). "EFC/F-BAR proteins and the N-WASP–WIP complex induce membrane curvature-dependent actin polymerization." The EMBO Journal **27**(21): 2817-2828.

Takeya, R. and H. Sumimoto (2003). "Fhos, a mammalian formin, directly binds to F-actin via a region N-terminal to the FH1 domain and forms a homotypic complex via the FH2 domain to promote actin fiber formation." J Cell Sci **116**(Pt 22): 4567-4575.

Takeya, R., K. Taniguchi, S. Narumiya and H. Sumimoto (2008). "The mammalian formin FHOD1 is activated through phosphorylation by ROCK and mediates thrombin-induced stress fibre formation in endothelial cells." EMBO J **27**(4): 618-628.

Tanaka, K. (2000). "Formin family proteins in cytoskeletal control." Biochem Biophys Res Commun **267**(2): 479-481.

Tcherkezian, J. and N. Lamarche-Vane (2007). "Current knowledge of the large RhoGAP family of proteins." Biol Cell **99**(2): 67-86.

Tian, X.-J., X.-P. Zhang, F. Liu and W. Wang (2009). "Interlinking positive and negative feedback loops creates a tunable motif in gene regulatory networks." Physical Review E **80**(1): 011926.

Tikoo, A., S. Czekay, C. Viars, S. White, J. K. Heath, K. Arden and H. Maruta (2000). "p190-A, a human tumor suppressor gene, maps to the chromosomal region 19q13.3 that is reportedly deleted in some gliomas." Gene **257**(1): 23-31.

Tilghman, R. W., C. R. Cowan, J. D. Mih, Y. Koryakina, D. Gioeli, J. K. Slack-Davis, B. R. Blackman, D. J. Tschumperlin and J. T. Parsons (2010). "Matrix rigidity regulates cancer cell growth and cellular phenotype." PLoS One **5**(9): e12905.

Tkachenko, E., M. Sabouri-Ghomi, O. Pertz, C. Kim, E. Gutierrez, M. Machacek, A. Groisman, G. Danuser and M. H. Ginsberg (2011). "Protein Kinase A Governs a RhoA-RhoGDI Protrusion-Retraction Pacemaker in Migrating Cells." Nature cell biology **13**(6): 660-667.

Tojkander, S., G. Gateva, G. Schevzov, P. Hotulainen, P. Naumanen, C. Martin, P. W. Gunning and P. Lappalainen (2011). "A molecular pathway for myosin II recruitment to stress fibers." Curr Biol **21**(7): 539-550.

Totsukawa, G., Y. Yamakita, S. Yamashiro, D. J. Hartshorne, Y. Sasaki and F. Matsumura (2000). "Distinct Roles of Rock (Rho-Kinase) and Mlck in Spatial Regulation of Mlc Phosphorylation for Assembly of Stress Fibers and Focal Adhesions in 3t3 Fibroblasts." The Journal of Cell Biology **150**(4): 797-806.

Trappmann, B., J. E. Gautrot, J. T. Connelly, D. G. Strange, Y. Li, M. L. Oyen, M. A. Cohen Stuart, H. Boehm, B. Li, V. Vogel, J. P. Spatz, F. M. Watt and W. T. Huck (2012). "Extracellular-matrix tethering regulates stem-cell fate." Nat Mater **11**(7): 642-649.

Truong, D., D. Brabant, M. Bashkurov, L. C. Wan, V. Braun, W. D. Heo, T. Meyer, L. Pelletier, J. Copeland and J. H. Brumell (2013). "Formin-mediated actin polymerization promotes Salmonella invasion." Cell Microbiol **15**(12): 2051-2063.

Tyson, J. J., K. Chen and B. Novak (2001). "Network dynamics and cell physiology." Nat Rev Mol Cell Biol **2**(12): 908-916.

Tyson, J. J. and J. D. Murray (1989). "Cyclic AMP waves during aggregation of Dictyostelium amoebae." Development **106**(3): 421-426.

Vallenius, T. (2013). "Actin stress fibre subtypes in mesenchymal-migrating cells." Open Biol **3**(6): 130001.

van Buul, J. D., D. Geerts and S. Huveneers (2014). "Rho GAPs and GEFs: Controling switches in endothelial cell adhesion." Cell Adhesion & Migration **8**(2): 108-124.

van den Boom, F., H. Dussmann, K. Uhlenbrock, M. Abouhamed and M. Bahler (2007). "The Myosin IXb motor activity targets the myosin IXb RhoGAP domain as cargo to sites of actin polymerization." Mol Biol Cell **18**(4): 1507-1518.

van der Gaag, E. J., M.-T. Leccia, S. K. Dekker, N. L. Jalbert, D. M. Amodeo and H. R. Byers (2002). "Role of Zyxin in Differential Cell Spreading and Proliferation of Melanoma Cells and Melanocytes." **118**(2): 246-254.

Vandenabeele, P., L. Galluzzi, T. Vanden Berghe and G. Kroemer (2010). "Molecular mechanisms of necroptosis: an ordered cellular explosion." Nat Rev Mol Cell Biol **11**(10): 700-714.

Vasquez, C. G., M. Tworoger and A. C. Martin (2014). "Dynamic myosin phosphorylation regulates contractile pulses and tissue integrity during epithelial morphogenesis." J Cell Biol **206**(3): 435-450.

Vega, F. M., A. Colomba, N. Reymond, M. Thomas and A. J. Ridley (2012). "RhoB regulates cell migration through altered focal adhesion dynamics." Open Biology **2**(5).

Venter, J. C., M. D. Adams, E. W. Myers, P. W. Li, R. J. Mural, et al. (2001). "The sequence of the human genome." Science **291**(5507): 1304-1351.

Vetter, I. R. and A. Wittinghofer (2001). "The Guanine Nucleotide-Binding Switch in Three Dimensions." Science **294**(5545): 1299-1304.

Vicente-Manzanares, M., C. K. Choi and A. R. Horwitz (2009). "Integrins in cell migration – the actin connection." Journal of Cell Science **122**(2): 199-206.

Vicente-Manzanares, M., M. A. Koach, L. Whitmore, M. L. Lamers and A. F. Horwitz (2008). "Segregation and activation of myosin IIB creates a rear in migrating cells." J Cell Biol **183**(3): 543-554.

Vicker, M. G. (2000). "Reaction-diffusion waves of actin filament polymerization /depolymerization in Dictyostelium pseudopodium extension and cell locomotion." Biophys Chem **84**(2): 87-98.

Vicker, M. G. (2002). "Eukaryotic cell locomotion depends on the propagation of self-organized reaction-diffusion waves and oscillations of actin filament assembly." Exp Cell Res **275**(1): 54-66.

Vicker, M. G., W. Xiang, P. J. Plath and W. Wosniok (1997). "Pseudopodium extension and amoeboid locomotion in Dictyostelium discoideum: Possible autowave behaviour of F-actin." Physica D: Nonlinear Phenomena **101**(3–4): 317-332.

Vogel, V. and M. P. Sheetz (2009). "Cell fate regulation by coupling mechanical cycles to biochemical signaling pathways." Current opinion in cell biology **21**(1): 38-46.

Wallar, B. J. and A. S. Alberts (2003). "The formins: active scaffolds that remodel the cytoskeleton." Trends Cell Biol **13**(8): 435-446.

Wallar, B. J., B. N. Stropich, J. A. Schoenherr, H. A. Holman, S. M. Kitchen and A. S. Alberts (2006). "The basic region of the diaphanous-autoregulatory domain (DAD) is required for autoregulatory interactions with the diaphanous-related formin inhibitory domain." J Biol Chem **281**(7): 4300-4307.

Wang, D. Z., E. K. M. S. Nur, A. Tikoo, W. Montague and H. Maruta (1997). "The GTPase and Rho GAP domains of p190, a tumor suppressor protein that binds the M(r) 120,000 Ras GAP, independently function as anti-Ras tumor suppressors." Cancer Res **57**(12): 2478-2484.

Wang, J. G., M. Miyazu, E. Matsushita, M. Sokabe and K. Naruse (2001). "Uniaxial cyclic stretch induces focal adhesion kinase (FAK) tyrosine phosphorylation followed by mitogen-activated protein kinase (MAPK) activation." Biochem Biophys Res Commun **288**(2): 356-361.

Wang, J. G., M. Miyazu, P. Xiang, S. N. Li, M. Sokabe and K. Naruse (2005). "Stretch-induced cell proliferation is mediated by FAK-MAPK pathway." Life Sciences **76**(24): 2817-2825.

Wang, N., J. P. Butler and D. E. Ingber (1993). "Mechanotransduction across the cell surface and through the cytoskeleton." Science **260**(5111): 1124-1127.

Watanabe, N., T. Kato, A. Fujita, T. Ishizaki and S. Narumiya (1999). "Cooperation between mDia1 and ROCK in Rho-induced actin reorganization." Nat Cell Biol **1**(3): 136-143.

Watanabe, N., P. Madaule, T. Reid, T. Ishizaki, G. Watanabe, A. Kakizuka, Y. Saito, K. Nakao, B. M. Jockusch and S. Narumiya (1997). "p140mDia, a mammalian homolog of Drosophila diaphanous,is a target protein for Rho small GTPase and is a ligand for profilin." The EMBO Journal **16**(11): 3044-3056.

Watanabe, N. and T. J. Mitchison (2002). "Single-molecule speckle analysis of actin filament turnover in lamellipodia." Science **295**(5557): 1083-1086.

Watanabe-Nakayama, T., M. Saito, S. i. Machida, K. Kishimoto, R. Afrin and A. Ikai (2013). "Requirement of LIM domains for the transient accumulation of paxillin at damaged stress fibres." Biology Open **2**(7): 667-674.

Wegner, A. (1976). "Head to tail polymerization of actin." J Mol Biol **108**(1): 139-150.

Wei, Q. and R. S. Adelstein (2000). "Conditional expression of a truncated fragment of nonmuscle myosin II-A alters cell shape but not cytokinesis in HeLa cells." Mol Biol Cell **11**(10): 3617-3627.

Weiner, O. D., W. A. Marganski, L. F. Wu, S. J. Altschuler and M. W. Kirschner (2007). "An actin-based wave generator organizes cell motility." PLoS Biol **5**(9): e221.

Wen, K. K., P. A. Rubenstein and K. A. DeMali (2009). "Vinculin nucleates actin polymerization and modifies actin filament structure." J Biol Chem **284**(44): 30463-30473.

Wen, W., W. Liu, J. Yan and M. Zhang (2008). "Structure Basis and Unconventional Lipid Membrane Binding Properties of the PH-C1 Tandem of Rho Kinases." The Journal of Biological Chemistry **283**(38): 26263-26273.

Westendorf, J. J. (2001). "The formin/diaphanous-related protein, FHOS, interacts with Rac1 and activates transcription from the serum response element." J Biol Chem **276**(49): 46453-46459.

Winkelman, J. D., C. G. Bilancia, M. Peifer and D. R. Kovar (2014). "Ena/VASP Enabled is a highly processive actin polymerase tailored to self-assemble parallel-bundled F-actin networks with Fascin." Proc Natl Acad Sci U S A **111**(11): 4121-4126.

Wirth, J. A., K. A. Jensen, P. L. Post, W. M. Bement and M. S. Mooseker (1996). "Human myosin-IXb, an unconventional myosin with a chimerin-like rho/rac GTPase-activating protein domain in its tail." J Cell Sci **109 (Pt 3)**: 653-661.

Wollman, R. and T. Meyer (2012). "Coordinated oscillations in cortical actin and Ca2+ correlate with cycles of vesicle secretion." Nat Cell Biol **14**(12): 1261-1269.

Woods, N. M., K. S. Cuthbertson and P. H. Cobbold (1986). "Repetitive transient rises in cytoplasmic free calcium in hormone-stimulated hepatocytes." Nature **319**(6054): 600-602.

Wu, C., S. B. Asokan, M. E. Berginski, E. M. Haynes, N. E. Sharpless, J. D. Griffith, S. M. Gomez and J. E. Bear (2012). "Arp2/3 is critical for lamellipodia and response to extracellular matrix cues but is dispensable for chemotaxis." Cell **148**(5): 973-987.

Wu, M., X. Wu and P. De Camilli (2013). "Calcium oscillations-coupled conversion of actin travelling waves to standing oscillations." Proc Natl Acad Sci U S A **110**(4): 1339-1344.

Xiong, Y., C. H. Huang, P. A. Iglesias and P. N. Devreotes (2010). "Cells navigate with a local-excitation, global-inhibition-biased excitable network." Proc Natl Acad Sci U S A **107**(40): 17079-17086.

Xu, Y., J. B. Moseley, I. Sagot, F. Poy, D. Pellman, B. L. Goode and M. J. Eck (2004). "Crystal structures of a Formin Homology-2 domain reveal a tethered dimer architecture." Cell **116**(5): 711-723.

Xu, Y., S. Pektor, S. Balkow, S. A. Hemkemeyer, Z. Liu, K. Grobe, P. J. Hanley, L. Shen, M. Bros, T. Schmidt, M. Bähler and S. Grabbe (2014). "Dendritic Cell Motility and T Cell Activation Requires Regulation of Rho-Cofilin Signaling by the Rho-GTPase Activating Protein Myosin IXb." The Journal of Immunology **192**(8): 3559-3568.

Yamaguchi, H., M. Kasa, M. Amano, K. Kaibuchi and T. Hakoshima (2006). "Molecular mechanism for the regulation of rho-kinase by dimerization and its inhibition by fasudil." Structure **14**(3): 589-600.

Yamana, N., Y. Arakawa, T. Nishino, K. Kurokawa, M. Tanji, R. E. Itoh, J. Monypenny, T. Ishizaki, H. Bito, K. Nozaki, N. Hashimoto, M. Matsuda and S. Narumiya (2006). "The Rho-mDia1 pathway regulates cell polarity and focal adhesion turnover in migrating cells through mobilizing Apc and c-Src." Mol Cell Biol **26**(18): 6844-6858.

Yang, C., L. Czech, S. Gerboth, S. Kojima, G. Scita and T. Svitkina (2007). "Novel roles of formin mDia2 in lamellipodia and filopodia formation in motile cells." PLoS Biol **5**(11): e317.

Yeung, C.-Y. C., S. H. Taylor, R. Garva, D. F. Holmes, L. A. Zeef, R. Soininen, R. P. Boot-Handford and K. E. Kadler (2014). "Arhgap28 Is a RhoGAP that Inactivates RhoA and Downregulates Stress Fibers." PLoS ONE **9**(9): e107036.

Yochelis, A., S. Ebrahim, B. Millis, R. Cui, B. Kachar, M. Naoz and N. S. Gov (2015). "Self-organization of waves and pulse trains by molecular motors in cellular protrusions." Sci Rep **5**: 13521.

Zaidel-Bar, R., C. Ballestrem, Z. Kam and B. Geiger (2003). "Early molecular events in the assembly of matrix adhesions at the leading edge of migrating cells." J Cell Sci **116**(Pt 22): 4605-4613.
Zaoui, K., S. Honore, D. Isnardon, D. Braguer and A. Badache (2008). "Memo-RhoA-mDia1 signaling controls microtubules, the actin network, and adhesion site formation in migrating cells." J Cell Biol **183**(3): 401-408.

Zemel, A., R. De and S. A. Safran (2011). "Mechanical consequences of cellular force generation." Current Opinion in Solid State and Materials Science **15**(5): 169-176.

Zhang, W. and H. T. Liu (2002). "MAPK signal pathways in the regulation of cell proliferation in mammalian cells." Cell Res **12**(1): 9-18.

Zhang, Y., F. Wang, Y. J. Niu, H. L. Liu, R. Rui, X. S. Cui, N. H. Kim and S. C. Sun (2015). "Formin mDia1, a downstream molecule of FMNL1, regulates Profilin1 for actin assembly and spindle organization during mouse oocyte meiosis." Biochim Biophys Acta **1853**(2): 317-327.

Zheng, Y. (2001). "Dbl family guanine nucleotide exchange factors." Trends in Biochemical Sciences **26**(12): 724-732.

Zigmond, S. H., M. Evangelista, C. Boone, C. Yang, A. C. Dar, F. Sicheri, J. Forkey and M. Pring (2003). "Formin leaky cap allows elongation in the presence of tight capping proteins." Curr Biol **13**(20): 1820-1823.

Supplemental Material

Figure S1: FHOD1 oscillations are enhanced by Rho activation.

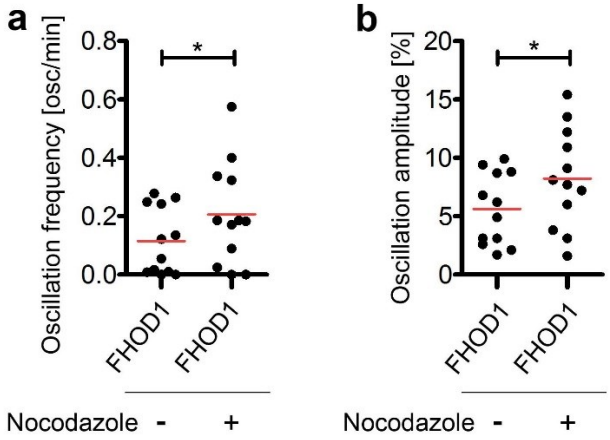

Figure S1: (a) Oscillation frequencies (in oscillations per min) and **(b)** peak amplitudes (in percent of mean) of N = 12 U2OS cells (from three experiments) expressing delCMV-EGFP-FHOD1 imaged with 3 frames per min, before and 45 min after treatment with 30 µM nocodazole. Red lines indicate mean; *: P<0.05; ns in paired t-test).

Table S1: RhoGAPs screened for oscillatory behavior

Table S1: Specified are the investigated GAPs, numbers of cells and experiments performed by Johannes Koch (JK) or Melanie Gräßl (MG)

RhoGAP	cells (n)	experiments	done by
Myo9b wt	21	3	MG
Myo9b R1695M	25	3	MG
DLC3α wt	4	1	MG
DLC3α K725A	5	1	MG
DLC3β wt	4	1	MG
DLC3β K625A	4	1	MG
p190RhoGAP wt	14	4	MG
p190RhoGAP RD	23	4	MG
ARHGAP28 wt	5	1	MG
ARHGAP28 R425A	10	1	MG
Graf1 wt	13	2	JK
GRAF1 RD	23	2	JK
ARHGAP6wt	12	1	JK
ARHGAP18 wt	28	4	JK
ARHGAP18 RA	22	3	JK
Ect2 1-414	20	1	JK
Ect2 414-882	20	1	JK
Ect2 ΔN5	20	1	JK
Ect2 wt	20	1	JK

Acknowledgement

I express my deep sense of gratitude to all the people who contributed to this thesis.

First of all, I would like to thank Dr. Perihan Nalbant for giving me the opportunity to become a part of her great group and to work on this exciting project.You gave me the freedom to explore my own ideas, but your door was literally always open for me. You and shared my joy when I was successful, held me back when I was heading in the wrong direction and motivated me when I was down. Thank you for your trust and guidance!

Thank you as well to Dr. Michael Ehrmann for agreeing to review this thesis and to participate in my defense.

Furthermore, I would like to thank Dr. Leif Dehmelt for putting a lot of time, resources and personal efford into this project. You reminded me to always keep my mind open for the bigger picture and gave me an understanding of computational analysis of biochemical systems. Thank you for your patience and inspiration!

I thank profusely all the former and current members of the AG Nalbant, for providing me with coffee, cake and most important of all fun! You guys always had my back! Thank you for your spontaneous helpfulness and for offering a sympathetic ear and encouraging words, at all times. In particular, I would like to thank Dr. Nina Schulze for sharing your knowledge and experience and Johannes Koch for your excellent and fruitful cooperation, as well as for proofreading this work.

Also, I would like to thank all members of the AG Dehmelt, especially Dr. Tomáš Mazel, who made a decisive contribution to the development of the analyses applied in this thesis.

I acknowledge with thanks the kind gift of Dr. Bernd Hoffmann and Nico Hampe, who provided us with elastomeric surfaces.

Most of all, I owe a deep sense of gratitude to my friends and family, who give me strength and great support. Thank you for your unshakable faith in me, for welcome distractions and for a great deal of understanding for my often busy schedule. In particular, I am very much thankful to my parents for their encouragement and to Cihan for his love!

Der Lebenslauf ist in der Online-Version aus Gründen des Datenschutzes nicht enthalten.